The Selective Hydrogenation of octanal in the presence of octene using γ-alumina supported copper-silver bimetallic catalysts

by

Letisha Deeplal

School of Chemistry and Physics

University of KwaZulu-Natal

Westville

Durban

4000

The Selective Hydrogenation of octanal in the presence of octene using γ-alumina supported copper-silver bimetallic catalysts

by

Letisha Deeplal

School of Chemistry and Physics

University of KwaZulu-Natal

Westville

Durban

4000

Submitted in fulfillment of the academic

requirements, for the degree

Masters of Science in the

School of Chemistry and Physics

University of KwaZulu-Natal,

November 2014

Abstract

This work pertains to the selective hydrogenation of octanal in the presence of octene, which has applications in the hydroformylation process. The octanal should be hydrogenated to the desired product, octanol, while avoiding or inhibiting the hydrogenation of octene. Since octene is more thermodynamically favoured to hydrogenate, complete octene hydrogenation inhibition is difficult.

This study aims to obtain a deeper understanding of the surface chemistry, which occurs on γ-alumina supported copper-silver bimetallic catalysts. This was done by first investigated monometallic copper catalyst at different weight loadings (5 and 15 wt%), then extending this to different weight loadings of the CuAg bimetallic catalysts, while maintaining the total metal loading. Additionally, the effect of the Cu-Ag metal ratios and impregnation sequence were investigated. Seven CuAg bimetallic catalysts and two Cu monometallic catalysts were synthesized via wet impregnation, and characterized using various techniques to determine surface morphology and the metal-metal and metal-support interaction on the catalyst surface.

The characterization showed higher copper loadings (15 wt%) formed agglomerates. The 5 wt% catalysts showed the metals to be well dispersed, with the effect of impregnation sequence showed significant differences simultaneous impregnation and the sequential bimetallic catalysts resulting in changes to the metal dispersion and catalyst acidity.

The feed used consisted of 2% octene, 10% octanal and 88% octanol. All reactions were temperature and pressure dependent, with optimum conditions of 50 bar and 160 °C. The overall result from catalytic testing showed silver to play a significant role in the selective hydrogenation of octanal in the presence of octene. The effect of impregnation sequence showed the simultaneous impregnation to give higher octanal and octene conversions, compared to the sequential impregnation catalysts, due to the synergistic effect between two metals in close contact with each other. Sequential impregnation showed that when the copper was impregnated first followed by silver, produced lower octene conversions, and hence was a more suitable catalyst system for selective hydrogenation. This research showed that γ-alumina supported

CuAg catalysts are beneficial for the selective hydrogenation of octanal while in the presence of octene in a competitive reaction environment.

Preface

I hereby declare that the work conducted in this research effort and presented in this thesis, is my own work conduced from February 2013 to November 2014, at the Catalysis Research Group at the University of KwaZulu-Natal, Westville, Durban, under the supervision of Prof. Holger B. Friedrich.

This work has not been submitted at this or any other university or tertiary institution. Where the work of others have been used, it has been duly recognized in this text.

Declaration

I, Letisha Deeplal, declare that:

1. The research reported in this thesis , except where otherwise indicated, is my own work
2. This thesis has not been submitted for any degree or examination at any other university or tertiary institution
3. This thesis does not contain any other person's data, pictures, graphs, or any other information unless specifically acknowledged as being sourced from other persons
4. This thesis does not contain other person's writing unless specifically acknowledged as being sourced from other researchers. Where other written sources have been quoted, then:
   (a) Their words have been re-written but the general information attributed to them has been referenced
   (b) Where exact words have been used, then their writing has been placed in italics and inside quotation marks, and referenced
5. This thesis does not contain text, graphics or tables copied and pasted from the internet, unless specifically acknowledged, and the source being detailed in the thesis and in the Reference sections

Signed

Letisha Deeplal

Conference Contributions

Parts of this work have been presented at conferences and is detailed below:

1. Poster presentation, Catalysis Society of South Africa (CATSA) conference, Port Edward, RSA, November 2013, titled Copper-Silver bimetallic catalysts for the selective hydrogenation of octanal in the presence of octene

2. Oral presentation, Particle technology workshop, Cape Town, RSA, November 2014, titled An understanding of surface characterization for Copper-Silver bimetallic catalysts for selective hydrogenation: Effect of Impregnation

Acknowledgements

I would like to sincerely acknowledge and extend my gratitude to the following people for their assistance throughout my Masters study.

- I would like to thank the NRF, THRIP and Sasol as this work would not have been possible without their financial support

- To Prof Holger Friedrich, my supervisor, thank you for the guidance and expertise. I will treasure the knowledge I have gained in my Masters study.

- To my mentor, Dr Nico Prinsloo from Sasol, thank you for the valuable advice and contribution.

- To my family, thank you for all the love, support, and strength throughout my academic life. I am grateful for all the time and effort you all have put it to ensure I succeed.

- I express a warm thanks to Phillip and Vishaal, from the EM Unit at UKZN, for the assistance and help with the electron microscopy instruments. In addition, I would like to thank the technical staff at UKZN for the assistance and help with the completion of my research.

- Thanks to the following people that assisted with the instrumentation analysis and interpretation, reactor building and troubleshooting, Dr Abdul. S. Mahomed, Dr Venkat Dasireddy, Drushan, Jignesh, Mo, Samkelo, Thashini, and Ziyaad.

- To the friends I have made throughout my academic career- Chrisanne, Kershen, Mzamo, Sandeeran, Shirveen, Shivania, Terelle, Veresha, and the Catalysis Research Group at UKZN– Thanks for the help, be it for assistance with research or just providing good

memories. Your support has helped me to overcome the many setbacks and frustrations that come with completing a postgrad degree.

- Lastly, I would like to thank Triven for being my rock, my sounding board, and my biggest supporter.

Dedication

To my loved ones: Mum, Dad, Candice, Triven, and the newest addition – Aiden

"And whatever you do, whether in word or deed, do it all in the name of the Lord Jesus Christ, giving thanks to God the Father through him" – Colossians 3:17

Contents

List of Figures

List of Tables

Abbreviations

%	Percent
Å	Angstrom
AL	Octanal
ATR	Attenuated Total Reflectance
BET	Brunauer-Emmet-Teller
cm	Centimeter
° C	Degree Celsius
EDX	Energy Dispersive X-ray spectroscopy
ENE	Octene
ESCA	Energy Spectroscopy for Chemical Analysis
FID	Flame Ionization Detector
GC	Gas chromatograh
GHSV	Gas Hourly Space Velocity
H	Hour
HR TEM	High Resolution Transmission Electron Microscopy
ICP-OES	Inductively Coupled Plasma-Optical Emission Spectroscopy
IR	Infrared Spectroscopy
JCPDS	Joint committee on powder diffraction
LEISS	Low Energy Ion Scattering Spectroscopy
LHSV	Liquid Hourly Space Velocity
m^2/g	Square meter per gram
mg/g	milligram per gram
Mass %	mass percent

ml	milliliters
ml/min	milliliters per minute
mmol	millimole
μm	micrometer
μmol	micromole
Mol %	Mole percent
MS	Mass spectrometer
OL	Octanol
ppm	Parts Per Million
s	second
SILP	Solid ionic liquid phase
SCIL	Solid catalyst with ionic layer
SEM	Scanning Electron Microscopy
STEM	Scanning Transmission Electron Microscopy
TCD	Thermal Conductivity Detector
TEM	Transmission Electron Microscopy
T_d	Thermal decomposition
TOF	Turn Over Frequency
TON	Turn Over Number
TPR	Temperature Programmed Reduction
TPD	Temperature Programmed Desorption
Wt %	Weight percent
XRD	X-ray Diffraction

Equations

BET equation for specific surface area

W: weight of gas adsorbed

P/Po: relative pressure

Wm: weight of adsorbate as monolayer

C: BET constant

$$\frac{1}{W\left(\left(\frac{Po}{P}\right)-1\right)} = \frac{1}{W_m+c} + \frac{c-1}{W_{mC}}\left(\frac{p}{Po}\right)$$

r_k = pore radius

σ = surface tension

V_m = molar volume of gas adsorbed in the pore

$$\text{Pore radius: } \mathbf{r_k} = \frac{2\sigma \text{ x } V_m}{RT \; x \; ln\frac{p}{Po}}$$

Chemisorption parameters

V_{chem} (mol g^{-1}): chemisorption volume

MW: supported metal atomic weight

σ_m (nm^2): supported metal cross sectional area

SF: stoichiometry factor

c (wt%): supported metal weight percent

ρ (g cm^{-3}): supported metal density

Metal dispersion (%): $\frac{\text{Vchem x SF x MW}}{c/100}$ x 100

Metal surface area (per catalyst) = V_{chem} x 6.02 x 10^{23} x SF x σ_m x 10^{-18}

Metal surface area (per supported metal)/ $A_m = \frac{V_{chem} \text{ x } 6.02 \text{ x } 10^{23} \text{ x SF x } \sigma_m \text{ x } 10^{-18} \text{ x } 100}{c}$

Mean particle diameter = $\frac{60c}{A_m \, x\rho}$

X-ray diffraction

d_c: average size of crystallite

k: constant

λ: wavelength of x-rays

Θ: Bragg diffraction angle

β: is at full width at half maximum

$$\mathbf{d_c = \frac{k\lambda}{\beta \cos \Theta}}$$

Catalytic equations

FR_g: Gas flow rate

moles of octanal: AL_m (m0: initial moles, m1: moles of octanal after)

moles of octanol: OL_m

V_c: volume of catalyst

$$\text{GHSV: } \frac{FR_g \, x \, 60}{V_c}$$

$$\text{LHSV: } \frac{AL_m \, x \, 60}{V_c}$$

$$\text{Conversion: } \frac{AL_{m1}}{AL_{m0}} \text{ x } 100$$

$$\text{Selectivity: } \frac{OL_m}{total \; products \; formed} \text{ x } 100$$

Yield = Conversion x selectivity

$$\text{TOF: } \frac{TON}{time \; of \; reaction}$$

$$\text{TON: } \frac{moles \; of \; octanal \; converted}{moles \; of \; active \; centers \; per \; gram \; catalyst}$$

Chapter 1
Introduction and Literature Review

1.1. Catalysis

Catalysis describes the use of a material to speed up the rate of reaction, by lowering the activation energy, without being consumed by the reaction [1-3]. A more in depth understanding of catalysis proves the catalyst does react with the reactants temporarily allowing the products to form on the catalytic surface [1-3]. Essentially the reaction only occurs if there is sufficient activation energy to allow the reactants to undergo the reaction. The catalyst provides an alternate route whereby lower activation energy is required to allow the substrates to react as shown in Figure 1.1. It is important to note that the catalyst only affects the rate of reaction and not the chemical equilibrium. It has been well documented that over time, in some cases, that the catalyst may deactivate [4, 5]. The time taken to deactivate is dependent on the type of catalyst, and other factors like coking, leaching, agglomeration of metal particles on the catalyst surface, and poisoning of active sites [5].

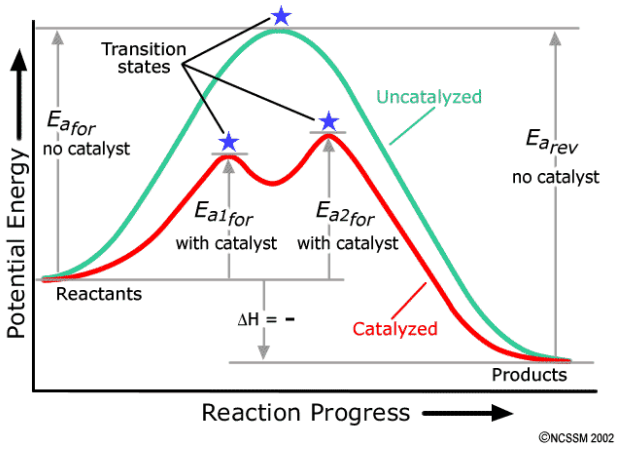

Figure 1.1. Potential energy diagram depicting the reaction pathway comparing a catalyzed vs uncatalyzed reaction [6].

In 1835, Jöns Jacob Berzelius was the first to coin the term ‘catalysis’ which was used to identify an entity which was able to speed up the rate of reaction without being consumed in the process [7]. Catalysis was used as early as 1522 when Valerius Cordus used sulfuric acid to catalyze the conversion of alcohol to ether [7]. This began the first era of catalysis whereby other notable discoveries were reported such as: [7-10]

1. The Lead chamber process (1746), describes the production of sulfuric acid, which is one of the first industrial processes.

2. Kirschoff (1812) reporting on the use of dilute acids to hydrolyze starch to sugar.

3. Humpfry Davy (1817) used heated platinum to assist in the combustion of gases below their ignition temperature.

4. The oxidation of alcohol to acetic acid using platinum, which was demonstrated by Edmund Davy in 1820.

5. The deactivation of platinum-based catalysts, which was first observed by Henry in 1825, in his work regarding the combustion of methane and ethylene.

6. The first commercial process which was developed by Phillips for the oxidation of sulfur dioxide (1831) over platinum-based catalysts.

The second era marked a greater interest in the understanding of how reactions are influenced by catalysis. This lead to breakthroughs regarding the rates of reactions by Wilhemy (1850), who proved the effect of the concentration of reactants, and by Willamson (1851), who showed that esters could be reversed back to alcohol. In 1877, Lemoine showed that a catalyst can be used to increase the rate of reaction, speeding up the time it takes for a reaction to reach equilibrium [7, 10].

The third era of catalysis marked the beginning of an industrial chemical revolution. One of the most notable industrial processes began in 1898 with the ‘contact process’ involving the production of sulfuric acid using vanadium pentoxide as a catalyst. Other important process which began in this time period were: [7]

1. The Ostwald process, in 1902, allowed for the production of nitric acid from a multi-step oxidation of ammonia.

2. The Haber process which uses an iron-based catalyst for the production of ammonia on an industrial scale in 1913

Other major catalytic advances since then are presented in Table 1.1: [7-14]

Table 1.1. A few notable catalytic advances from 1920's till 1990's.

Company/Process	Year	Description
Standard Oil Company	1920	Isoproponal from petroleum [7]
Fischer-Tropsch	1922	Hydrocarbons from CO and H_2 [11]
Dupont	1926	Synthetic methanol production [7]
Eugene Houdry	1936	Catalytic cracking [7]
Karl Zieglar	1953	Ethylene polymerization [7]
Sohio	1960's	Industrial production of acrylonitrile [9, 10]
Monsanto	1966	Carbonylation of methanol [9, 10]
Mobil Oil	1977	Methanol to olefins [12]
Phillips petroleum Co.	1983	Hydroisomerization [7, 10]
Exxon Research and Engineering	1990	Wax isomerization [13]

In recent times, the focus in industry was to innovate and improve existing catalytic processes, in terms of catalyst lifetime, activity, selectivity, as well as becoming more environmentally friendly. This led to chemistry fields such as green chemistry and photocatalysis. There are three main categories of catalysis, which are heterogeneous, homogenous, and biocatalysis.

Biocatalysis or Enzymatic catalysis uses enzymes with processes such as fermentation [1, 2]. Enzymatic catalysis is used in a wide variety of processes and is applied in pharmaceuticals, paper and pulp production, agriculture and the food industry. Enzymatic catalysis aims to use enzymes or cells similar to those found in nature; meaning that biocatalysts are active under mild reaction conditions and well-controlled temperature and pH. These reactions are also preferred in aqueous media which is in correlation with many 'green' and 'environmentally-friendly'

initiatives [15, 16]. Enzymatic catalysis has shown to be effective in enantioselective and stereospecific reactions [17-19].

Zhang *et al.* [20] reported on the effectiveness of enone/enoate reductases for the reduction of a wide variety of substrates including α, β-unsaturated alkenes, ketones, nitriles, and carboxylic acids. These enzymes showed to have high activity at temperatures below 50 °C; however, it was also shown that pH plays a major role on the activity, which varies according to the enzyme used.

Lam *et al.* [21] reported on trans-esterification of biodiesel using three major fields of catalysis namely; homogenous, heterogeneous, and enzymatic catalysis. Each of these fields showed to contribute in different ways toward the overall aim of the study. In the homogeneous system, catalysts are relatively cheap but a major drawback was the susceptibility to soap formation in the presence of excess free fatty acids (FFA). Heterogeneous catalysis offered reusability and recyclability; however leaching lead to contamination of the product feed. Enzymatic catalysts have high cost but they are also insensitive to FFA and water in the reactant feed. The advantages and disadvantages for the types of catalysts used and explained in this study could also be extended into other types of chemical reactions such as alkylation, isomerization, oxidation and hydrogenation [16].

1.2. Homogeneous catalysis

Homogenous catalysis applies when both reactants and catalyst are in the same phase. Homogeneous catalysis is used in approximately 25 % of catalytic industrial processes [22]. Homogeneous catalysis, in some cases, proves superior to heterogeneous catalysis due to its ability to operate in relatively milder conditions and providing high selectivity [22, 23]. The main drawback from this type of catalysis is the difficulty in separation of the reactants, products and catalyst. A homogeneous catalyst is mainly comprised of a metal center with ligands. The interaction between the ligand and metal defines the way the catalyst will behave in terms of activity and selectivity. The factors which govern the behavior of the catalyst include electronic and steric effects [24].

The most well-known homogeneous catalyst is a rhodium based organometallic complex also known as the Wilkinson's catalyst which is a used for the hydrogenation of unsaturated organic molecules such as alkenes and alkynes [25]. Zakzeski *et al.* [26] reported on the use of rhodium- and ruthenium-based catalysts to obtain high yields in hydroformylation. Other metals such as platinum, when combined with various ligands, have proven to be effective homogeneous catalysts for hydroformylation, hydrogenation, hydration, oxidation and carbonylation reactions [27]. Palladium has also been used for functionalizing aryl halides with yields ranging from 40 – 95 % depending on the ligand used [28]. A few well known palladium catalyzed reactions include the Heck, Buchwald, and Hartwig reactions [28].

Some of the elementary steps in homogeneous catalysis involve ligand association and dissociation, which allows a vacant site to be produced in which the reactant can interact with the metal center. Insertion occurs when the reactant bonds to the metal center, in some cases the R-group on the reactant can migrate to form a single bond with the metal. Types of migration such as hydride and methyl migration can also be promoted by the other ligands on the metal. β-elimination, oxidative addition and reductive elimination are all examples of catalytic steps which occur in homogenous catalysis [29].

1.3. Heterogeneous catalysis

Heterogeneous catalysis comprises of 75 % of the world's industrial catalytic processes and is defined as the reactant and catalyst being in different phases i.e. gas-solid, liquid-solid, or gas-liquid [22]. Heterogeneous catalysis usually consists of a solid catalyst containing a porous inorganic material as the support and a metal as the active component. The common types of supports used are; alumina, ceria, silica, manganese oxide, zeolites, and hydrotalcite [30]. The reaction between the reactant and active metal usually takes place at the interface between the catalyst surface and molecule which is depicted in Figure 1.2 [31].

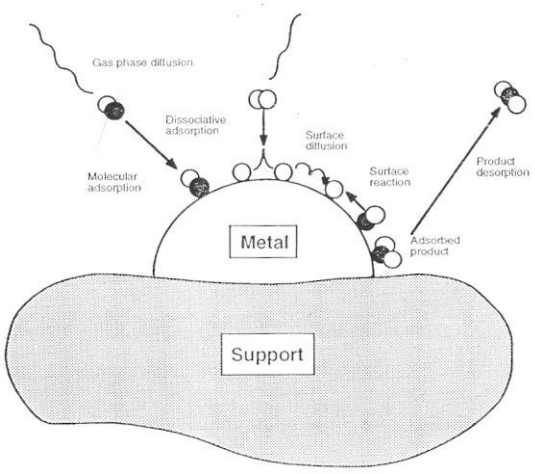

Figure 1.2. Illustrating of a reaction on a heterogeneous catalyst.

A catalyst is effective in decreasing the activation energy of a reaction. This allows the thermodynamically favoured reaction to occur at an enhanced rate. This enhanced rate also increases the formation of by-products via side reactions. It is of great importance to have some control of the catalyst in terms of the selectivity to the desired products, as well as the activity of the catalyst, which depends on the catalyst stability. The activity and selectivity in heterogeneous catalysis is dependent on many factors such as the support, metal, method of preparation, reaction conditions, etc. The electronic and steric properties of the catalyst can be modified with the use of promoters, or a secondary metal. These catalysts are able to have a long life span; however, it does depend on its susceptibility to deactivation caused by poisoning, leaching, coking, and sintering. It has been noted that a major advantage of heterogeneous catalysis is the ease of the catalyst to be recycled and regenerated, making this system economically viable [23].

1.4. Methods of preparation

The catalyst preparation technique has a great influence on the behavior of the catalyst. Catalysts can be modified and fine-tuned, by altering the catalyst preparation procedure. Some of the factors, which are affected by the preparation technique, include particle size, selectivity, activity, stability, and mechanical strength. It is for this reason that the effect of catalyst preparation has been studied in depth to fully understand the contribution of the preparation techniques and methods [8, 30, 32, 33]. The preparation technique can be altered in a number of ways e.g. a change in the metal precursor salt, pH, and stirring time and calcination temperature etc.

It is of commercial importance to produce a catalyst, which has high surface area, uniform pore size, and high mechanical strength. It is for this reason that there has been continuous development in improving catalyst preparation procedures [11, 33]. Some of the most common catalyst preparation procedures include wet impregnation, co-precipitation, deposition-precipitation, and the sol-gel method.

Wet impregnation involves the addition of the dissolved metal salt added to the support. This mixture is then stirred for a period of time, followed by drying and calcination [30]. Co-precipitation requires a more controlled environment in terms of pH. One or more metals are precipitated together with the support, which undergoes three main stages: Supersaturation, nucleation and growth. Supersaturation occurs by evaporation of the solvent or an increase in pH, which allows the metal to deposit onto the support. Growth of the particle size depends on concentration of metal, pH and time [30]. Deposition precipitation uses the support to provide for the nucleation sites for the metal precursor. The addition of the base is important as it is a determining factor to allow for a gentle change in pH [30]. The sol-gel technique involves the metal precursor dissolving in a solvent, thereafter the addition of acid or base for hydrolysis to allow for gel formation. This is allowed to age followed by drying to remove excess moisture [30].

1.5. Types of reactors

Apart from the chemistry taking part on the catalytic surface, an important part of the catalytic process is the type of reactor used for the system. A large amount of research and engineering goes into designing and optimizing reactors. Common types are the fixed bed, fluidized bed and slurry bed reactor. However, there are also modified reactors which include bubble tower, spray tower, and falling liquid film [34].

Reactors are designed to improve and optimize a variety of different catalytic chemical processes. Many factors must be considered when choosing the type of reactor such as the catalyst choice, ease of operation, solvent effect, heat control, deactivation studies, economics and start-up costs. There are three main types of reactors

1.5.1. Batch flow reactor

In this set up the reactants are added together and allowed to react for a certain period of time without interruption. Once the reaction is complete, the products are removed. This allows excellent contact between the catalyst and reactants. Advantages of this type of reactor are good temperature control, and they are suitable for long reaction times and small scale production. These are generally used in the polymer and food industry [34, 35]. Major disadvantages involve the difficulty of cleaning the reactor, and deactivation of the catalyst, which could occur when the solvents are emptied out from the reactor [36]. An example of a batch reactor design is shown in Figure 1.3.

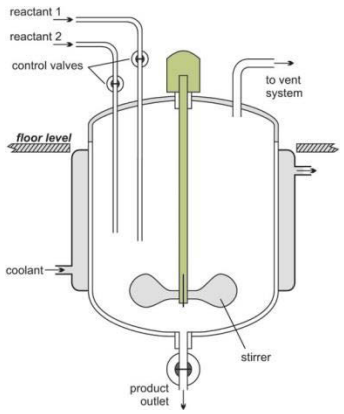

Figure 1.3. Diagram of a batch flow reactor [37].

1.5.2. Continuous flow reactor

This type of reactor can be used for gas and liquid phase reactions. They are typically used for simple reactions. It is economically viable as production costs are lower and products can be removed during the reaction, as compared to a batch reactor. This set up can be used on a laboratory scale or an industrial scale. Within this type of reactor, further modification allows for a fluidized bed reactor or a fixed bed reactor.

In a fixed bed reactor, the reactant (gas/liquid) is fed downstream and is in close contact with the catalyst bed shown in Figure 1.4. A fluidized bed reactor is known for its heat and mass transfer control. The reactants and catalysts are usually dispersed with flow entering from the bottom of the reactor creating a dispersed fluid set up which can be seen in Figure 1.4b. A few important factors to take into consideration are temperature control, especially with exothermic reactants and pressure control. Since the catalyst is in a fixed position, there must be sufficient void space to allow the reactant to pass through without clogging which could cause back pressure or a pressure drop. The catalyst must be mechanically stable to withstand disintegration. Continuous reactors have an increased operating efficiency compared to batch reactors as there are fewer start-up and shut-downs required [34-36, 38-40].

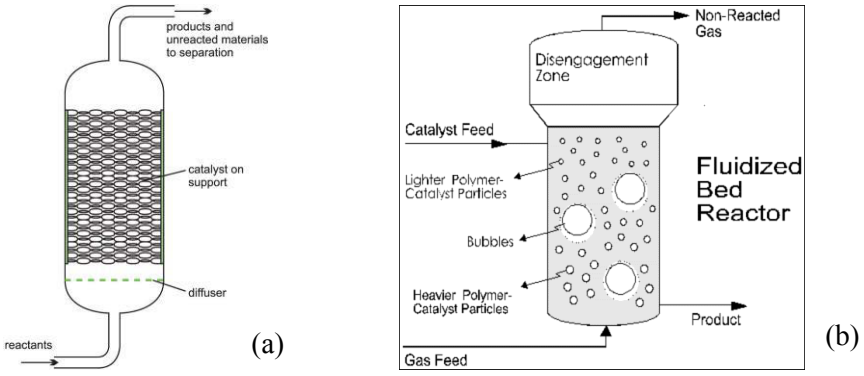

Figure 1.4. Schematic diagram of (a) fixed bed reactor [37] and (b) fluidized bed reactor [41].

1.5.3. Plug flow reactor

One or more fluids can be pumped through the reactor pipes. This set up is commonly used under high temperature and pressure conditions [34, 35]. In this work, a continuous plug flow fixed bed reactor was used and will be explained in detail in chapter 2

1.6. Hydrogenation

1.6.1. History of hydrogenation

Hydrogenation describes the addition of hydrogen atoms to an unsaturated molecule and is a valuable reaction to organic chemistry [42]. James F. Boyce is known for his work in vegetable oils and fat for the manufacture of soaps and detergents in the late 19^{th} to early 20^{th} century. His work involving the hydrogenation of cottonseed oil was considered to be a scientific breakthrough which allowed for further work and applications [43].

French chemist Paul Sabatier is considered to be the father of hydrogenation, for his contribution in the late 1890's to work on the hydrogenation of gaseous organic compounds using a trace amount of nickel as a catalyst [8, 44-46]. The reaction involving the formation of methane and water from carbon dioxide and hydrogen using a nickel catalyst, called the Sabatier process, was based on the work done by James. F. Boyce [47]. Wilhelm Norman extended the application of catalyzed hydrogenation of liquid organic compounds like oleic acid, over a nickel catalyst in the presence of gaseous hydrogen [47]. Since then, major hydrogenation processes and applications have been developed as shown in Table 1.2 [46-48].

Table 1.2. A few notable catalytic advances in the hydrogenation field.

Process	Year	Description
Chilling	1902	Hydrogenation of liquid vegetable oils
Haber process	1905	Hydrogenation of nitrogen
Fischer-Tropsch	1922	Coal to liquid fuel
Murray Raney	1924	Amines to nitriles
BASF	2009	Selective hydrogenation of alkynes

1.7. Catalytic hydrogenation

Hydrogenation is used in many fields industrially such as the petrochemical industry, polymers, fine chemicals and pharmaceuticals. Catalytic hydrogenation is one of the most widely used steps in organic synthesis and is invaluable in both the fine chemicals and pharmaceuticals industry [32]. The preferred option in industry is using supported metal as the catalysts due to its ability to diffuse hydrogen on the surface and to allow the reactants to be hydrogenated. The hydrogen atom can be made to react readily with many functional groups and can be selective in the right conditions. It is also the most economical method of reducing of unsaturated functional groups for both laboratory and industrial scale production, and can be used in gas phase or liquid phase reactions [36].

Some critical parameters of catalytic hydrogenation include the choice of catalyst used e.g. Pd/C, Ni/Al_2O_3, operating conditions, and catalyst preparation. The performance of the catalyst depends on the nature of the active metal as well as the support. As stated by Sabatier, the adsorption of reactants should neither be too strong or weak for high catalytic activity [49]. A good balance must be attained between the strength of adsorption between the reactant and catalyst, as this is a desirable catalytic property, and will be able to desorb the product without deactivating the catalyst. A weak interaction will not adsorb the reactant sufficiently making an unfavorable catalyst. The tendency of metals to dissociate the hydrogen bond is summarized in Figure 1.5. The active catalyst must have sufficient surface area, be able to adsorb and dissociate hydrogen, and allow for easy desorption of the product.

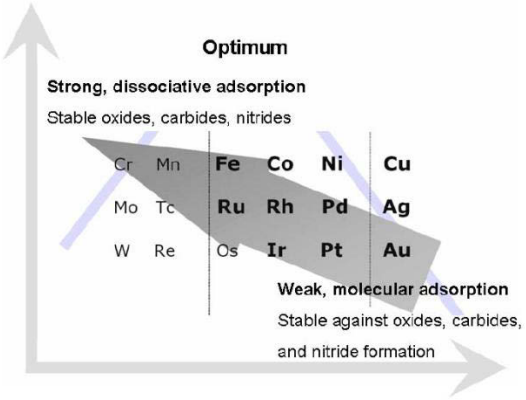

Figure 1.5. The tendency of transition metals to dissociate a hydrogen bond [50].

Some of the factors, which influence the hydrogenation ability of the catalyst, are: [8, 32]

The choice of the metal, as this plays a major role towards the catalytic activity. The two main categories of metal catalysts are precious metals, which include Pt, Pd, Ru, Rh, Os, Ir, Ag and Au, and base metals, such as Cu, Ni, Co, Fe, which are relatively cheaper than the precious metals. The type of support plays a significant role in the effectiveness of the catalyst properties and behaviour. Types of support used can be acidic, basic or amphoteric. Common types of supports used in hydrogenation are alumina, silica, ceria, titanium dioxide, magnesium oxide nd zeolites. γ-alumina is a common support due to its high surface area and thermal stability. It has been reported by Bachiller-Baeza *et al.* [42], that Rh showed to be effective in the selective hydrogenation of α,β-unsaturated aldehydes when supported on Mg and Ce. This study was done in both the gas and liquid phase [42]. Hydrotalcite have also been investigated as a hydrogenation catalyst for acetone, acetophenone, and phenol compounds [51, 52]. It was also found effective in selective hydrogenation of α,β-unsaturated aldehydes which includes crotonaldehyde, cinnamaldehyde, citral, and acrolein [53].

The support plays a role in the metal particle size, the metal-support interaction, as well as the deactivation rate, thus affecting the overall activity of the catalyst [5, 30, 54]. To further elaborate, in a paper reported by Mori *et al.* [55] poisoned Pd/C showed to be effective in chemoselective hydrogenation for alkenes in the presence of aliphatic and aromatic ketones, however the catalyst deactivated over time, with recyclability of the catalyst proving difficult. However, Hong *et al.* [56] showed that when palladium was supported on titania (Pd/TiO_2), the catalyst proved more stable over time for the selective hydrogenation of acetylene. Apart from the metal-support interaction, the structure and pore size of the support plays an important role in activity and selectivity. As a compromise between the most efficient and most economical catalyst, the loading, type of metal and support is constantly studied to reach an effective balance.

Hydrogenation can be separated into two distinct groups, which are bulk hydrogenation, which entails the hydrogenation of in most cases a mono-functional group, and selective hydrogenation which entails the hydrogenation of one particular functional group in the presence of another functional group e.g. alkyne in the presence of an alkene.

1.8. Hydrogenation of alkenes (C=C)

Carbon-carbon double bonds can readily be hydrogenated to the alkane under mild conditions [57]. Palladium is the most well-known and common metal for the hydrogenation of alkenes, however Pt, Ru, and Ni has also been used in the past [36, 58-62]. Steric factors and substitutions of the alkene determine the hydrogenation of the compound.

A great deal of work has been conducted over the past 40 years to determine the mechanism of the catalytic hydrogenation of alkenes. The Horiuti-Polanyi mechanism is most well accepted over a range of different heterogeneous catalyst due to the mechanism being supported by results obtained regarding stereochemistry, double bond isomerization and deuterium labeling of the alkene hydrogenation reaction [63]. The mechanism, shown in Figure 1.6, is rather simple with the diatomic hydrogen dissociated onto the active catalyst surface (1). The reactant is adsorbed onto the surface via the double bond (2), the hydrogen is allowed to interact with the weakly adsorbed alkene bond (3), the alkane desorbs from the catalyst while reacting with the second hydrogen to form the product (4).

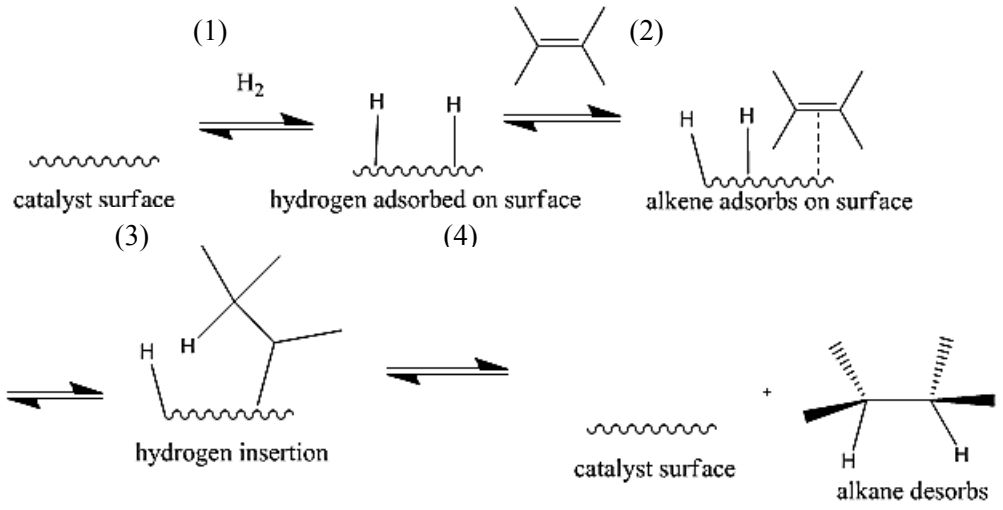

Figure 1.6. Mechanism of the catalytic hydrogenation of an alkene [64].

1.9. Possible mechanisms for alkene hydrogenation

1.9.1. Langmuir-Hinshelwood mechanism

This mechanism involves the dissociative chemisorption of the reactive gas (hydrogen) on the surface. The hydrogen then migrates across the surface until interaction occurs with the reactant molecule, which is adsorbed to the catalyst surface. Once the reactive gas and reactant interact, the product is desorbed from the surface allowing a new reactant molecule and gas to adsorb [65, 66]. Augustine and co-workers [63] have also stated that the rate of reaction depends on the amount of the chemisorbed species on the surface, which in this study is hydrogen. Considering that this may be the mechanism, which occurs, in this catalytic system, there are a few possible products, which could form as explained in this chapter. Figure 1.7 shows a simple illustration of the Langmuir-Hinshelwood mechanism for a hydrogenation reaction.

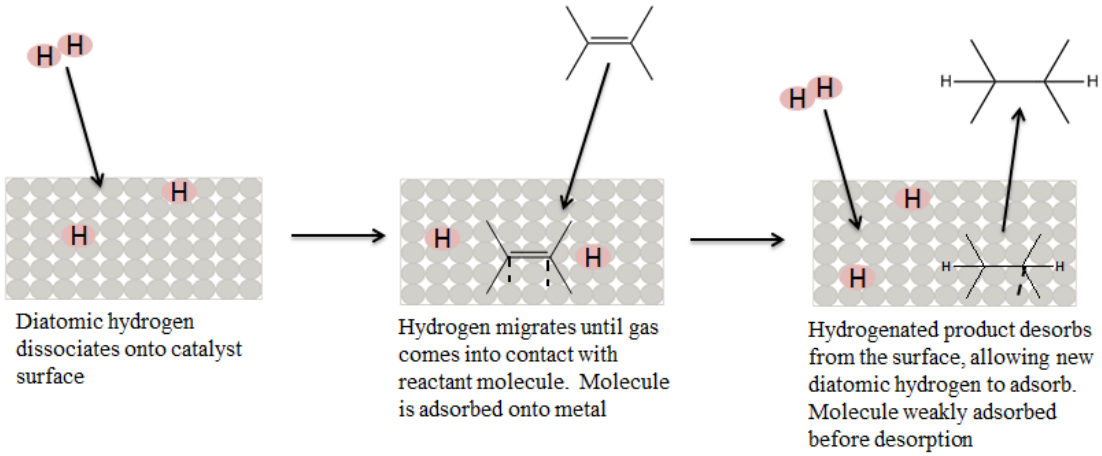

Figure 1.7. Illustration depicting the Langmuir-Hinshelwood mechanism.

1.9.2. Horiuti-Polanyi mechanism

The Horiuti-Polanyi mechanism involves the dissociation of a hydrogen molecule, followed by the addition of the atomic hydrogen to the substrate in a stepwise reaction shown in Figure 1.8. There are two possible pathways, with the first case being the addition of the dissociated molecule to the carbonyl oxygen forming a hydroxyalkyl species. The second pathway occurs via the addition of the dissociated hydrogen to the carbonyl carbon, leading to the alkoxy

species. The hydrogen dissociation was said to have a low energy barrier on palladium when the study was first conducted by Horiuti and Polanski in the 1930's [67]. In addition to the energy barrier required to dissociate hydrogen on the palladium surface, studies were also conducted for nickel, copper, silver and gold catalysts [64, 68].

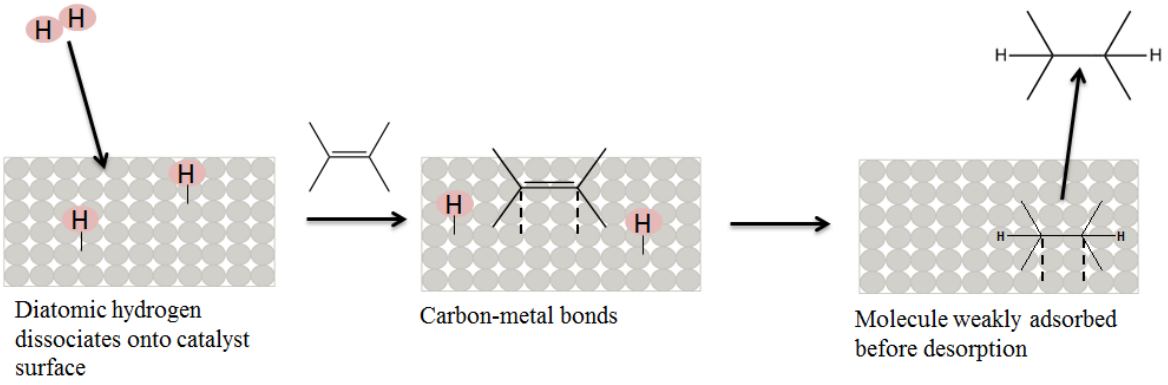

Figure 1.8. Illustration of the Horiuti-Polanyi mechanism.

1.10. Hydrogenation of aldehydes

The aldehyde functional group undergoes a dihydro-addition to form a primary alcohol [57]. Low valent metal hydrides can be used in this reduction such as $LiAlH_4$ and $NaBH_4$. Another method is catalytic hydrogenation with the use of a supported metal catalyst that is able to dissociate diatomic hydrogen and allow the carbonyl group to react with the hydrogen atom. The hydrogenation of aldehydes is an important reaction in the fine chemicals and pharmaceuticals industry [69, 70].

Govender [71] investigated the use of copper in an aldehyde feed containing water over three types of supports, which were alumina, chromite and silica. This study showed copper to be effective in the hydrogenation of octanal to octanol at temperatures ranging from 120 – 180 °C and pressures up to 60 bar. The presence of water did not affect the activity of the catalyst, and was stated to improve the selectivity towards octanol formation. This trend was seen with alumina and chromite supports. The silica supported catalyst showed conversion to decrease over time indicating deactivation [71].

There are two possible mechanistic pathways which have been stated by Sitthisa *et al.* [72] for the hydrogenation of acetone and propanal. Figure 1.9 shows the two possible mechanisms, whereby Mechanism (1) shows that the addition of hydrogen to the carbonyl group takes place at the C atom of the carbonyl group, leading to an alkoxide intermediate. The second hydrogen is then added to the alkoxide intermediate resulting in the alcohol. Another possible reaction pathway, Mechanism (2), is when the hydrogenation occurs at the O atom forming a hydroxylalkyl intermediate, followed by the addition of the second hydrogen producing the alcohol [72].

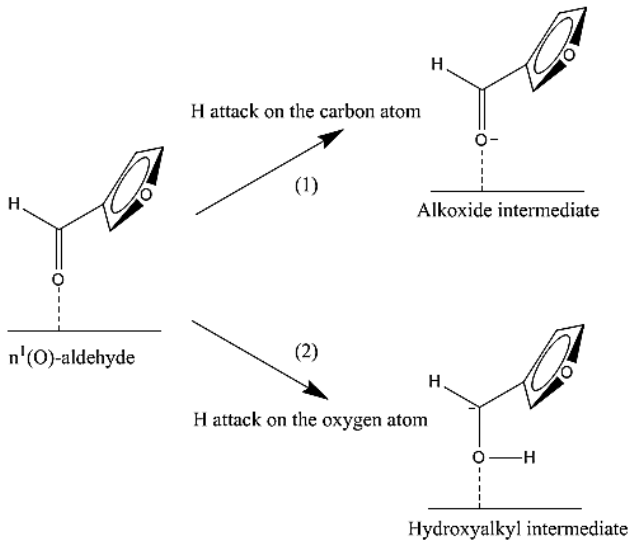

Figure 1.9. Possible intermediates for the hydrogenation of an aldehyde [72] (Redrawn with permission from Elsevier © 2014).

1.11. Catalytic selective hydrogenation

Selective hydrogenation involves the hydrogenation of a specific functional group while preventing or avoiding the hydrogenation of other possible functional groups present. This becomes difficult in cases where the wanted reaction is not favoured due to kinetic or thermodynamic reasons. It has been well documented that there is a heirachy as to the hydrogenation of certain functional group for example, C=C < C≡C, the alkyne is thermally less stable and hydrogenates to the alkene at a faster rate than the alkene to the alkane [73]. This can

also be extended to other functional groups such as C≡C > C=C > C=O (aldehyde) > C=O (ketone), mainly due to higher reactivity of the aldehyde than the ketone which is vulnerable to steric hindrance as well as electronic effects. With selective hydrogenation being the focus of this study, an insight into the hydrogenation of a few of these functional groups was warranted.

Early advances in hydrogenation were mainly done for olefin hydrogenation to the paraffin product, which was further extended to chemo- and regio-selective hydrogenation, namely the preferential hydrogenation of conjugated olefins over non-conjugated olefins. This was also extended to carbonyl and nitrile hydrogenation [74].

1.11.1. Partial hydrogenation of alkynes to cis-olefins

Partial hydrogenation of alkynes to *cis*-alkenes is an important class of reactions, which is used in the natural products and petrochemicals industry. A widely used catalyst for this reaction is the Lindlar's catalyst, however, the use of lead acetate and quinoline makes this method environmentally unfriendly [75, 76]. Metals such as Ni, Rh, Cu and Cr have been used to accomplish the partial hydrogenation of alkynes, however, a Pd based catalyst investigated by Sajiki *et al.* [77] showed promising results with a 97 % selectivity toward the desired product Figure 1.10 shows the partial hydrogenation of butyne to form *cis*-butene or *trans*-butene.

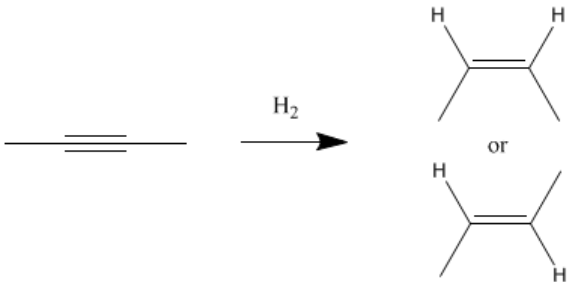

Figure 1.10. Hydrogenation of butyne to possible butene products.

The hydrogenation of 2-butyne-1,4-diol to 2-butene-1,4-diol is a well-studied reaction due to its application in the production of vitamins A and B_6, as well as in the polymer industry [78, 79]. Rode *et al.* [79] reported on the ability to manipulate the catalytic system to obtain the desired

composition of products by varying the reaction conditions using a $Pt/CaCO_3$ catalyst. The selectivity was largely dependent on the hydrogen pressure; at lower pressure, the selectivity to butane-diol was almost 80 %. It was also noted that as the pressure increased, so did the conversion of the butyne-diol to butane-diol, and the selectivity towards the butene-diol increased to approximately 50 % [79]. It was reported by Winterbottom *et al.* [59] that the use of Pd/TiO_2 achieved a >95 % selectivity of butene-diol and Pd/charcoal promoted with lead additives gave selectivities between 92 – 98 % towards butene-diol. The possible hydrogenation products are shown in Figure 1.11, where 2-butene-1,4-diol forms via selective hydrogenation and 2-butane-1,4-diol forms via total hydrogenation.

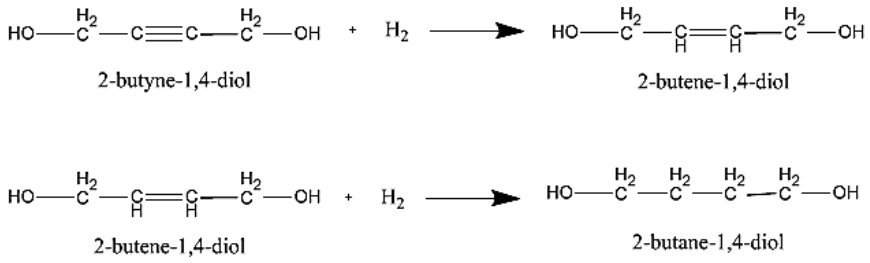

Figure 1.11. Reaction scheme for the hydrogenation of 2-butyne-1,4-diol [79] (Redrawn with permission from American Chemical Society © 2014).

1.11.2. Hydrogenation of furfural to produce furfuryl alcohol

Furfuryl alcohol is widely used in the chemicals industry in synthetic fibres, farm chemicals, thermostatic resin, plasticizers, and in the production of vitamin C and lysine. It is for this reason that the hydrogenation of furfural has been extensively studied using Cu, Ni, Co, Ru, Pt and Pd based catalysts to achieve the most efficient hydrogenation system [80, 81]. Pd based catalysts were also found to have a significantly high selectivity toward the formation of byproducts and promote the decarbonylation reaction to produce furan. Copper is reported to be preferred for this type of reaction due to its high activity and selectivity to the desired product, and there is a minimal formation of byproducts like 2-methyl furan [53, 81, 82]. Figure 1.12 shows the possible products, which can be obtained from the hydrogenation of furfural.

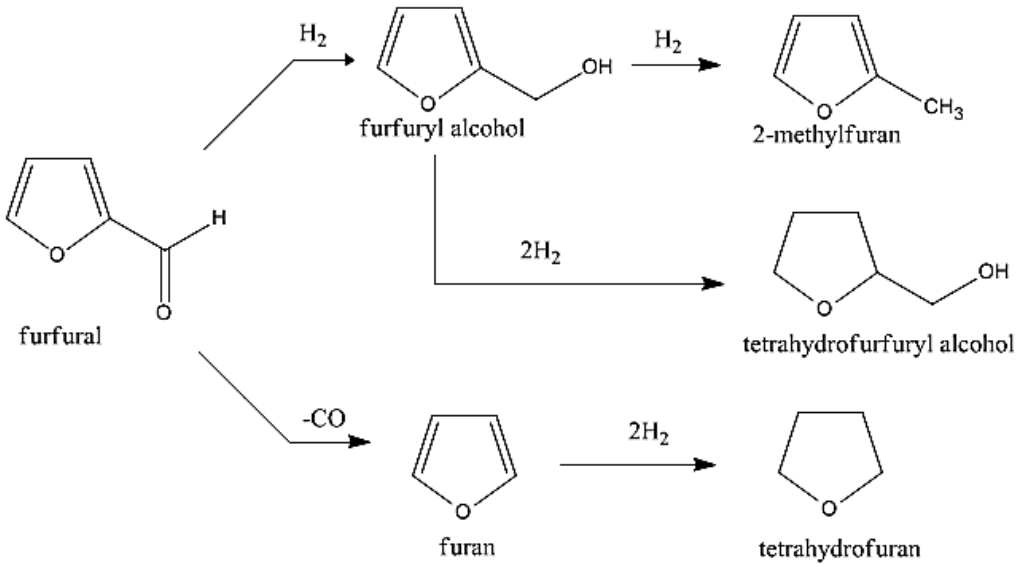

Figure 1.12. Hydrogenation reaction pathway of furfural [80] (Redrawn with permission from Elsevier © 2014).

1.11.3. Hydrogenation of acetylene and diene impurities in alkene feedstocks

Alkenes have a wide range of applications especially in polymer production and processes like hydroformylation [83]. Some of the streams may contain undesired components like alkynes and dienes [13, 83-85]. These components tend to poison the process catalysts downstream [85]. Ethylene and propylene streams, derived from cracking, contain components like acetylene, propadiene and propyne which are removed by selective hydrogenation whilst minimizing alkene loss [83].

In butyl and pentyl systems, undesired components such as vinyl acetylene and dienes must also be removed from the system to avoid the conversion to lower valued components. Selective hydrogenation was reported to be carried out on various catalytic systems which include palladium, platinum, nickel, copper, copper/nickel, copper/chromium, copper/nickel/chromium, zinc/chromium, or nickel/molybdate catalysts [84, 86].

1.11.4. Selective hydrogenation in the hydroformylation process

Hydroformylation (also called 'the oxo process') of a wide range of olefins (C_2- C_{24}) is an industrially practiced application to obtain aldehydes and alcohols, which act as intermediates for surfactants, detergents, plasticizers, and the perfume industry. This reaction involves the addition of a carbon monoxide and hydrogen molecule to an alkene, forming aldehydes. Commercially a rhodium-phosphine modified complex is often used under mild conditions for the hydroformylation of small chain alkenes, however this is not used for longer carbon chains as the rhodium complex decomposes during separation of the reaction mixture [87]. Cobalt was reported to be better suited for the hydroformylation of higher alkenes under homogeneous conditions as it is stable against higher temperature, pressure and longer reaction time. There is a continuous effort into improving these processes by studying the effect of the ligands, synthesis method, process conditions and heterogeneous catalysis [53, 87, 88]. Tadd *et al.* [88] showed the possible products from the hydroformylation process using 1-hexene, shown in Figure 1.13

Hydroformylation has been investigated using a range of different types of catalyst namely homogenous [89, 90], heterogeneous [91, 92], supported aqueous phase catalysis [93, 94] and supported ionic liquid phase catalysts (SILP) [95]. SILP studies by Riisager *et al.* [95], on the hydroformylation of propene and 1-octene reported on a conversion of 1 % and 100 % selectivity to the aldehyde using a rhodium-phosphine based catalyst. The conversion to the final product (alcohol) ranged from 47 – 67 % [95]. The unreacted alkenes can be separated by distillation before entering the hydrogenation reaction, or the alkenes are selectively hydrogenated in the presence of aldehydes [86].

In a study done by Rivas *et al.* [89], ligand effects in a rhodium catalytic system were shown to be a major factor on the conversion and selectivity to the desired product. Aldehydes were reported to have selectivity greater than 95%, with octane and octene forming less than 5 % selectivity.

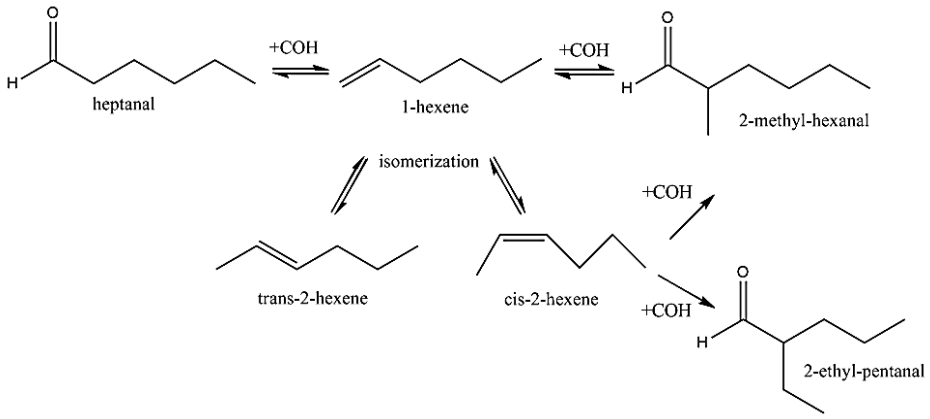

Figure 1.13. The possible products from hydroformylation of 1-hexene [88] (Redrawn with permission from Elsevier © 2014).

The desired product in hydroformylation is the aldehyde, which can then be hydrogenated to a primary alcohol. Sasol has commercialized a process in 2001 using a rhodium catalyst to produce primary alcohols from 1-heptene, which is a product from the Fischer-Tropsch process. The hydroformylation product, octanal, is hydrogenated to give 1-octanol [24, 96].

Selective hydrogenation reactions between octene and octanal in a combined feed have only been recently studied. Interest has increased due to their importance from an industrial point of view. It can be noted that in the hydrogenation of aldehydes from the hydroformylation reaction, there may be some unreacted olefins present [84, 86]. These olefins are regarded as valuable commodities, which can be recycled to the hydroformylation reactor. If these olefins are passed to the hydrogenation step, they will form paraffins, which are undesired. Either the unreacted olefins can be separated via energy intensive distillation processes or the aldehyde can be selectively hydrogenated in the presence of the olefin. In this system there is a competitive reaction where either the octene or octanal could interact with the active site. Previous studies have shown copper to be effective in this competitive reaction between octene and octanal with minimal hydrogenation of the octene [97]. Selective hydrogenation of these components in process streams have not been investigated extensively, therefore the behavior and interaction of the alkene and aldehyde functional group must been investigated. The system that closely resembles this type of reaction is the selective hydrogenation of α,β-unsaturated aldehydes, where the aldehyde is selectively hydrogenated to produce the unsaturated alcohol.

1.12. Possible reactions from the hydrogenation of octanal in the presence of octene

1.12.1. Main reactions

Figure 1.14 shows the reaction scheme of the desired reaction, which is the formation of octanol from octanal. Selectivity is based on the attraction of the carbonyl group to the active site on the catalyst surface. Gallezot *et al.* [98] stated that the selectivity of carbonyl hydrogenation can be improved by increasing the interaction between the carbonyl molecule and the Lewis acid sites present on the catalyst surface. The Lewis acid sites lower the electron acceptor nature of the π_{co} bond which increases the back bonding interaction of the π_{co} bond, favoring the carbonyl hydrogenation [98].

Considering that both reactants allow for a competitive reaction environment, the aim is to preferentially hydrogenate one component while avoiding the hydrogenation of the other component present as shown in Figure 1.14 and 1.15 In this case, the octene hydrogenation is an undesired reaction, shown in Figure 1.16. From the reactants used in this study, Figures 1.14 and 1.15 are considered to show the main reaction processes in this work.

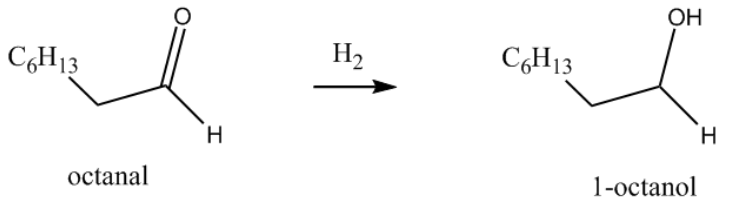

Figure 1.14. Reaction scheme depicting the hydrogenation of octanal to octanol.

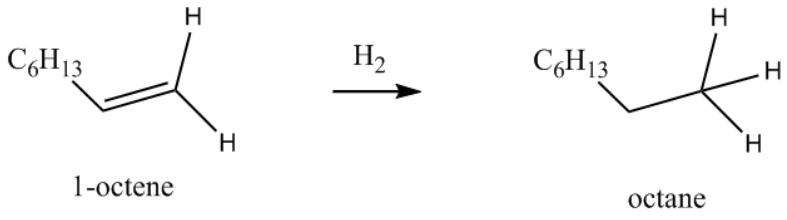

Figure 1.15. Reaction scheme depicting the hydrogenation of octene to octane.

1.12.2. Byproducts

In some cases, side reactions could occur depending on the active site or support. Some of the possible side reactions, which can form in the hydrogenation of octanal, are octyl octanoate, octanoic acid, 2-hexyl decanol, C16 diol, C14 acetal, and C16 saturated alkanes which are shown from Figures 1.18 – 1.20.

C16 diol and 2-hexyl decanol as by products

Many organic textbooks explain the aldol condensation between two aldehyde molecules involving the formation of an enolate resulting from the deprotonation of one aldehyde molecule. This enolate then reacts with the electrophillic carbon atom next to the carbonyl group in the second aldehyde molecule, resulting in the C16 aldol intermediate [99-101]. This intermediate product is further hydrogenated to form the C16 diol (shown in Figure 1.16). This reaction takes place on basic sites on the support and has been reported previously in literature [60, 71]. The basic environment can further dehydrate followed by hydrogenation of the C16 diol to form 2-hexyl decanol (shown in Figure 1.17) [102, 103].

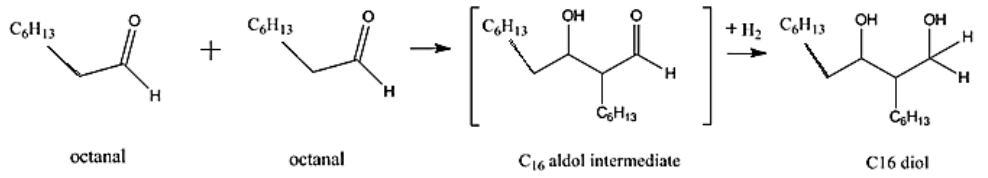

Figure 1.16. Reaction scheme depicting the aldol reaction between two octanal molecules.

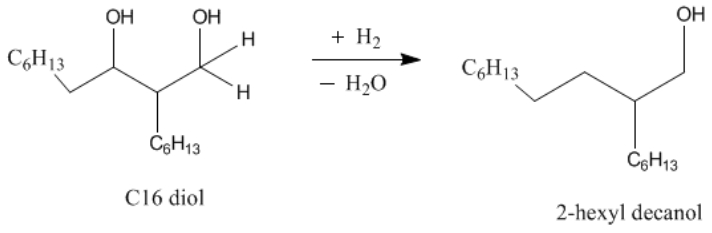

Figure 1.17. Reaction scheme depicting the formation of 2-hexyl decanol.

Octyl octanoate as a byproduct

The industrial feed used contained many by-products including octanoic acid, therefore formation of the ester could occur by the addition reaction between the acid and alcohol followed by dehydration in an acidic environment. Additionally, the ester could form by the dehydrogenation of octanal, followed by hydration producing an acid, thereafter the ester forms as mentioned previously [104, 105]. This reaction scheme can be seen in Figure 1.19.

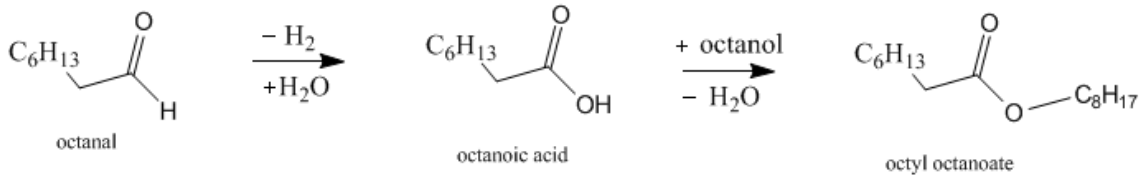

Figure 1.18. Reaction scheme depicting the formation of octyl octanoate.

Octyl ether as a byproduct

A study by Bethmont *et al.* [106] showed that ether formation depends of the catalyst acidity. The aldehyde reacts with an alcohol molecule, thereafter undergoing dehydration to form the ether. The ether can also form by first forming a ketal, which then undergoes hydrogenolysis to form the ether and alcohol as a by-product. This reaction scheme is shown in Figure 1.19:

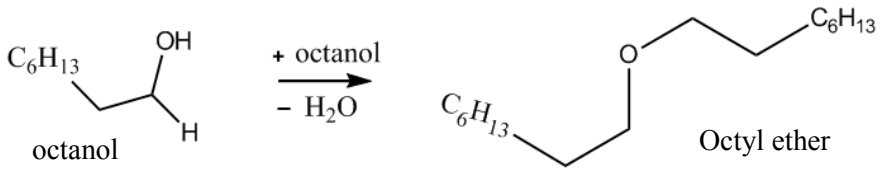

Figure 1.19. Reaction scheme depicting the formation of octyl ether.

C24 acetal as a byproduct

The formation of acetals has been well documented to occur on acidic sites [85, 107], with an exception reported by Millman *et al.* [108] where acetal formation on basic sites was observed. Figure 1.20 shows that the acetal is formed when the carbonyl group on the aldehyde becomes protonated, which then reacts with the incoming alcohol group, which is in excess as it is the

solvent and desired product. This addition reaction forms a hemi-acetal, which is able to further react by undergoing a substitution reaction with a second alcohol molecule. This reaction occurs due to the increase in electrophilic nature of the carbon attached to the hydroxyl group in the presence of an acid site, thus forming the acetal product.

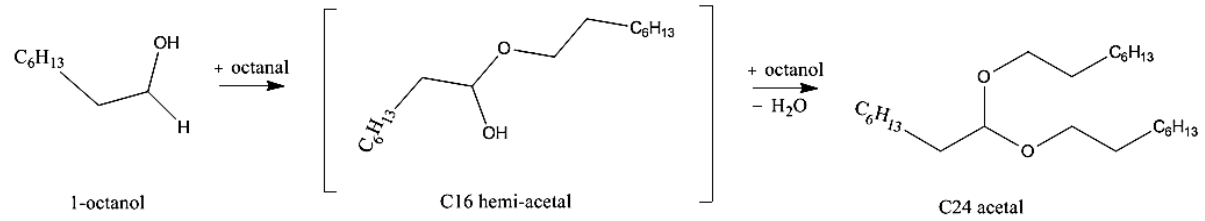

Figure 1.20. Reaction scheme depicting the formation of C24 acetal.

1.12.3. Hydrogenation of α,β-unsaturated aldehydes

The α,β-unsaturated aldehydes can be involved in intra-molecular selective hydrogenation. In intra-molecular selective hydrogenation, there are steric and electronic effects that govern selectivity towards the selective hydrogenation of the carbonyl group. Compounds with bulky groups around the double bond disfavours adsorption of the C=C bond due to steric hindrance, or electron donating groups in the conjugating system increase the electron density at the carbonyl bond which promotes adsorption to the active site [109, 110].

The compounds chosen, in this study, are similar concerning carbon chain length and are a linear molecule with only the functional group of interest in the primary position of both molecules. This makes it more difficult to ensure the selective hydrogenation of the aldehyde as opposed to the alkene molecule.

The selective hydrogenation of α,β-unsaturated aldehydes has been extensively studied industrially and academically due to its importance in the fine chemicals and pharmaceuticals industry. The hydrogenation of this type of molecule is particularly difficult due to the presence of an alkene and aldehydes functional group on the same compound [58, 70, 111].

The hydrogenation of the C=O bond in the presence of a C=C bond, as in the case of α,β-unsaturated aldehydes, is considered to be a difficult reaction. This difficulty is a result of the

formation of saturated aldehydes is favoured over the unsaturated alcohol due to the C=C alkene (Δ H = -120 kJ. mol^{-1}) bond being more reactive then the C=O bond (Δ H = -50 kJ. mol^{-1}). Steric hindrance around the C=C bond contributes to the selective formation of the unsaturated alcohol [58, 62, 69, 98, 109, 110, 112, 113].

The are many proposed mechanism for the hydrogenation of α,β-unsaturated aldehydes which illustrates the difficulty of selective hydrogenation of unsaturated aldehydes. One such reaction process is illustrated in Figure 1.21:

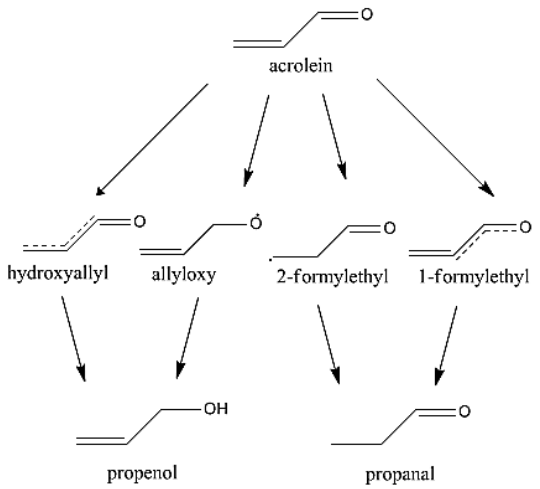

Figure 1.21. Elementary steps for the hydrogenation of acrolein [113] (Redrawn with permission from American Chemical Society © 2014).

Acrolein has been studied extensively to determine the mechanism in catalytic hydrogenation as it is the simplest α,β-unsaturated aldehyde. This study was done in the gas phase; therefore the intermediates form radicals which bond strongly to the catalyst surface. The hydroxyallyl and the 1-formylethyl radials are considered more stable due to the attack on the terminal center sites, causing a delocalization of the π electrons. This leads to the hydroxyallyl radical being the most favourable pathway to the unsaturated alcohol, propenol [113].

There are many factors which influence the ability of a catalyst to allow for selective hydrogenation which includes; the type of support, steric effects, particle size, promoters and type of metal or metals [70].

1.13. Selective hydrogenation catalysts

1.13.1. Platinum group metals

Noble metals have been investigated for the hydrogenation of propanal and acetone in a competitive reaction environment. As reported by van Druten and Ponec [61], the platinum group metals hydrogenate both the propanal and acetone with the aldehyde hydrogenating faster than the ketones in a homogenous catalysis system, and the ketones being hydrogenated faster than aldehyde hydrogenation using a heterogeneous catalyst [61].

da Silva *et al.* [54] reported on the use of noble metals for the selective hydrogenation of cinnamaldehyde, the results showed Pd to be non-selective and iridium being the most selective to the unsaturated alcohol. The rest of the metals followed the trend Pd < Rh < Ru < Pt < Ir. They also investigated the effect of promoters such as tin and iron, which gave improved the activity in the conversion of the aldehyde to the alcohol. This work showed that the Pt-Fe/C catalyst was approximately 7 times more active than the monometallic Pt/C catalyst and the Pt-Sn/C catalysts. This was attributed to the metal-metal interaction between the platinum and iron, as well as the combined metal-support interaction, which was not observed in the Pt-Sn/C catalyst.

Delbecq and Sautet [109] looked at a theoretical approach, investigating the adsorption of C=O and C=C functional groups on Pd and Pt surfaces. It was found that the carbonyl group adsorbs onto the metal surface via back donation of the metal orbital into the π_{CO} orbital. This adsorption can be further increased by the presence of Lewis acids, which in turn decreases the adsorption of the C=C bond with the surface [109].

Pd/C is able to convert the C=C bond in α,β unsaturated aldehydes to saturated aldehydes with high conversion and selectivity under mild conditions. It was reported by Du *et al.* [110] that the C=C bond binds to the palladium center, and the C=O bond adsorption is suppressed due to the high electron density of the Pd/C catalyst. Noble metals (Pt, Pd, Rh) was found to favour the hydrogenation of the C=C bond over the C=O bond in the absence of a promoter.

1.13.2. Group 11 metals (Cu, Ag, Au)

Gold and silver, for many years, was considered inert due to its common applications such as in jewellery and coins. It was only in the mid-20th century that the significance of silver as a catalyst was recognized for the oxidation of carbon monoxide (CO), the decomposition of formic acid and the epoxidation of ethylene. Copper-based catalysts have been used for a number of processes such as nitrogen oxide removal, amination, oxidation of organic compounds, as well as selective hydrogenation in the fine chemicals industry. Chetty [97] has investigated the use of Au/Al_2O_3 for the selective hydrogenation of octanal in the presence of octene. It was found that the method of preparation played a vital role in the selectivity to the desired product, e.g. large gold particles promoted the formation of byproducts, whereas small particles favoured the selectivity to the desired product, which was octanol.

1.13.2.1. Copper

Non-noble metals (Cu, Ni, Zn) were investigated and it was shown that these metals are able to preferentially hydrogenate the C=O bond over the C=C bond in α,β-unsaturated aldehydes. There have also been studies to support the ability of copper to be effective for the selective hydrogenation of aldehydes and ketones [114, 115].

Copper chromite catalysts used for the hydrogenation of non-conjugated unsaturated aldehydes, however, were not suitable for the conjugated α, β-unsaturated aldehydes as the C=C bond reactivity was increased and led to isomerization [116, 117]. It was later discovered by Hubaut *et al.* [117, 118] that the steric effects of the substrate played a major role in the selectivity for the desired product.

A good example is the use of Cu/SiO_2 for the selective hydrogenation of cinnamaldehyde to cinnamyl alcohol. The catalyst activity and selectivity depends on a number of factors, which has been discussed, however, in this case the high dispersion of the copper was responsible for the high selectivity, together with the metal-support interaction. It was found that an increase in dispersion increases conversion with no effect on the selectivity [111]. Chambers *et al.* [119] investigated the use of modified copper on silica catalysts for selective hydrogenation of cinnamaldehyde. This work showed that the active sites were the predominant sites, with less

free copper, which were found with larger particles or strong metal support interactions (SMSI) [98].

Marchi *et al.* [120] reported on the use of copper-based catalysts for the hydrogenation of cinnamaldehyde in the liquid phase. This study found that γ-alumina allows for a better dispersion of copper, as compared to silica. Copper dispersion was shown to increase the conversion but did not have a significant effect on the selectivity towards the desired product.

1.13.2.2. Silver

Silver has been used in many applications, for example the oxidation of volatile organic compounds (VOC's), epoxidation of ethylene and reduction of NO_x [121-123]. Silver is not commonly considered to be a heterogeneous hydrogenation catalyst due to its electron configuration of $4d^{10}5s^1$ which results in an inability to dissociate a strong bond such as diatomic hydrogen, nevertheless there have been many reports disproving this by showing the effectiveness of silver in the selective hydrogenation of α,β-unsaturated aldehydes [50, 121, 124, 125]. This propelled a need for greater understanding and insight to the catalytically active silver species. There are a few types of species that have been reported: isolated Ag^+ ions aggregated silver particles, silver-aluminate like species, and Ag_2O clusters [121, 124, 125]. Silver was found to have a low heat of adsorption value towards hydrogen, meaning the hydrogen does not strongly adsorb onto the silver surface. This allows the C=O bond to hydrogenate preferentially, as opposed to the C=C bond which has been documented to require strongly adsorbed hydrogen to hydrogenate [50, 126].

Nagase *et al.* [127], first reported silver as a hydrogenation catalyst in 1983 for the selective hydrogenation of α, β- unsaturated aldehydes [123, 128]. A great deal of research has been done by Claus *et al.* [129], which reported on the chemoselective properties of silver in the study of α,β-unsaturated aldehydes to their corresponding alcohols. Chen *et al.* [128] reported on the hydrogenation of chloronitrobenzenes and the chemoselective properties of supported silver catalysts. Similarly, chemoselective hydrogenation of synthetic substrates in the presence of the supported silver catalyst reduces halonitrobenzenes to their respective aniline form as shown by Crook *et al.* [123].

Acrolein is the simplest α,β-unsaturated aldehyde with a low boiling point and no bulky groups, increasing its difficulty in undergo selective hydrogenation. Grunert *et al.* [130] used Ag/TiO_2 for gas phase hydrogenation of acrolein. This catalyst was prepared by wet impregnation, which allowed for strong metal-support interaction, showed high selectivity towards the allyl alcohol (42%) [130]. Since then, there have been many reports of silver supported catalysts with supports such as aluminium foil, single crystals, wet impregnation and deposition precipitation over a wide range of inorganic supports such as titania, zeolites, silica and alumina [124, 130, 131]. A supported silver silica catalyst was found to be effective in selective hydrogenation of which was attributed to the edges and kinks which favour the formation of the allyl alcohol [125, 132]. Bron *et al.* [131] tested a range of silver based materials, this study concluded that surface coverage (or pressure) plays an important role in adsorption of both acrolein and hydrogen, thus affecting selectivity. The higher pressure promotes the adsorption of acrolein whereby the C=C bond tilts away from the metal, increasing the activation of the C=O bond, thus favouring allyl alcohol formation [129, 131, 133]. Bron *et al.* [131] tested a range of preparation techniques of Ag/SiO_2 which showed sputtered silver to favour the formation of propionaldehyde while nanocrystalline silver favoured the allyl alcohol formation .

Wei *et al.* [132] used Ag/SiO_2 to investigate the effect of the particle size of silver, on the acrolein hydrogenation to allyl alcohol, resulting in selectivities ranging from 20-35 %, with a maximum conversion of 88%. This shows that the higher selectivity was attributed to the larger particle size. Chen *et al.* [128] reported on Ag/SiO_2 which was also found effective for the hydrogenation of o-chloronitrobenzene to *o*-chloroaniline, with a complete conversion and 100 % selectivity.

Claus *et al.* [134] reported on use of silver supported on SiO_2 and TiO_2 for the selective hydrogenation of crotonaldehyde. The silica based catalyst showed an improved selectivity towards the formation of allyl alcohol compared to the titania based catalyst. Grunert *et al.* [130] showed the effect of reduction on Ag/TiO_2, with high temperature reduction (500 °C) having a lower selectivity to the allyl alcohol (27 %) compared to the low temperature reduction (200 °C) in which a selectivity of 42 % was obtained.

Volckmar *et al.* [135] showed the influence of support, whereby the highest acrolein conversion (~90 %) was obtained with the pure supports silica and alumina. Mixed supports comprising of

varying ratios of SiO_2 and Al_2O_3 showed conversion to be in the range of 20-60 % with selectivity reaching a maximum of 40 %.

1.13.2.3. Gold

Gold have been reported to be highly catalytically active, when in the nanoparticle range, but reduces its catalytic activity as the particle size increase [136]. Catalysts containing gold nanoparticles have been used for low temperature CO oxidation and hydrogenation [137, 138] with complete conversions obtained as low as 30 °C on Au/Al_2O_3 catalysts [139]. Bond and Sermon [140] were the first to report on the catalytic activity of gold, in the 1970's, for the hydrogenation of olefins. Since the 1970's, a great deal of research was undertaken to explain the catalytic activity of gold when in the nanoparticle range [141].

Perret *et al.* [142] reported on the selective hydrogenation of benzaldehyde to benzyl alcohol using Au/Al_2O_3, Pd/Al_2O_3, and Ni/Al_2O_3 catalysts. The gold catalyst showed a lower activity initially when compared to the nickel and palladium catalysts; however, the gold catalyst offered superior stability compared to the other catalysts. In addition, gold catalysts were used in the oxidation of benzyl alcohol to benzaldehyde as the main product (~80 %) with a maximum conversion of 20 % [143]. Hugon *et al.* [144] reported on the effectiveness of gold catalysts for the selective hydrogenation of 1,3-butadiene in the presence of alkenes, whereby gold offered a higher selectivity compared to palladium based catalysts.

1.14. Bimetallic catalyst

A surface containing two metals has unique surface properties as opposed to the monometallic system due to the interaction of the two metals with each other and with the support. This will modify the surface and alter the behavior of the catalyst. There are two distinctive categories when it comes to a bimetallic catalyst: [145]

(a) Alloy – is defined when one metal dissolved in another and they cannot be distinguished from each other. One of the metals would have a lower surface energy causing segregation between

the two species resulting in a higher surface concentration of the metal with the lower surface energy.

(b) Intermetallic compound has a definite stoichiometry and unit cell containing both metals. Wei *et al.* [146] stated in their work that in the case of unsaturated aldehydes, when metal A is combined with an electropositive metal B; metal B acts as an electron donor, increasing the electron density of the host metal A. An increase in electron density in the active metal causes a repulsion towards the C=C bond, therefore the binding energy of the C=C bond decreases resulting in an increase in C=O bond adsorption and activation which leads to an increase in selectivity. The presence of a second metal has the potential for improving selectivity and activity. A bimetallic system offers more possibilities of fine tuning the reaction. It can result in the change of electronic properties of the catalytic surface and active sites [146].

Bimetallic catalysts are significantly different from the monometallic counterparts due to the combined effect of both metals producing a synergistic effect, which may alter selectivity, stability, and activity, etc. [33]. There are four main types of bimetallic systems shown in Figure 1.22. Ferrando *et al.* [145] discuss these types of arrangements in detail. [33].

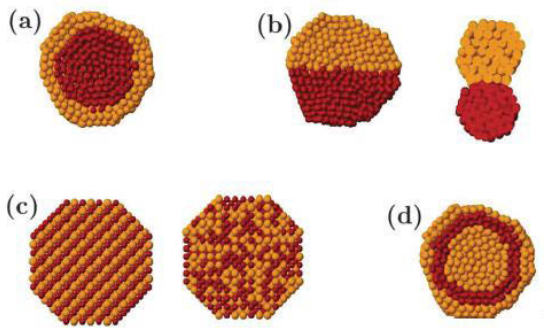

Figure 1.22. Possible mixing patterns of bimetallic catalysts. These alloys can be described as (a) core shell, (b) sub-cluster segregated, (c) ordered or random mixing and (d) multi-shell [145] (Redrawn with permission from American Chemical Society © 2014).

Cazayous *et al.* [147] correlated TEM and Raman data to determine the composition of Cu-Ag particles. These techniques were able to determine core shell particles and monometallic particles. A study on surface structures of Pt-Ni bimetallic catalysts, by Murillo *et al.* [148],

showed that within bimetallic systems the Pt-Ni-Pt(111) structure was more active for acrolein selective hydrogenation than the Ni-Pt-Pt(111) structure, indicating that characterization is vital in understanding the catalytic activity of bimetallic catalysts. Simionato *et al.* [149] showed, with the use of XRD, TPR, and Raman spectra, that the incorporation of silver on alumina supported cobalt catalysts aids in the reduction of cobalt, and assists in the formation of Co^0 sites which are considered to be the active sites. Sun *et al*. [150] reported on the use of $CuAg/Al_2O_3$ catalysts for hydrogenolysis of glycerol. As the silver content increased to 5 wt %, on the 55.5 wt % Cu/Al_2O_3 catalyst, the conversion increased to 100 %, as opposed to when no silver was present (94 %) and selectivity increased from 70 % to greater than 92 % with silver present [150]. Zheng *et al.* [151] showed the use of various characterization techniques for Au-Ag bimetallic catalysts. TEM and XRD were employed to differentiate Au-Ag alloys versus monometallic Au and Ag particles, with STEM-EDX and XPS indicating the formation of a homogeneous Au-Ag alloy as opposed to core-shell structures. The alloy was reported to have superior performance when compared to its monometallic counterparts.

Zhu *et al.* [152] showed the effect of the variation of silver ratio on a Pd/SiO_2 catalyst. The acetylene hydrogenation did not show much variation in terms of conversion; however, there were significant differences with regards to selectivity towards ethylene. It was shown that ratios 1:1 and 1:5 Pd:Ag showed selectivities of 58 % and 68 % respectively, while a ratio of 1:3 Pd:Ag showed the highest selectivity of 84 % at 150 °C, indicating that the composition of bimetallic catalysts play an important role in the catalyst activity. Deng *et al.* [153] showed in his work the effect of impregnation sequence of $CuCo/SiO_2$ catalysts for higher alcohol synthesis. The co-impregnated catalyst showed a stronger synergistic effect due to metal-metal interaction caused by the transfer of electrons from the copper to the cobalt species. The change in the method of preparation directly affected the conversion and selectivity obtained, with the co-impregnated showing moderate conversion, with a higher selectivity towards alcohols (51.5 %), while the catalyst with copper impregnated first showed higher conversion and a lower selectivity towards alcohols (39.9 %) [153]. Similarly, Jongpatiwut *et al.* [154] reported on the competitive hydrogenation for poly aromatic compounds showed that the effect of impregnation of Pd-F catalysts gave a significant difference, in conversion and selectivity towards the desired products, with respect to preparation methods. The order of impregnation showed that when Pd was impregnated first a lower CO uptake with a TOF value of 34 was obtained, and when

fluoride was impregnated first, the CO uptake was considerably higher and the TOF was reported to be 85 [154]. This indicates the position of the active metal plays a vital role in the catalytic activity.

Other notable work done using bimetallic catalysts found that zeolite Y-supported Pt-Ni catalysts showed better activity and stability as compared to their monometallic counterparts for acetophenone hydrogenation [155], while tungsten decreased platinum aggregation which was attributed to strong metal-metal interaction resulting in low toluene selectivity [156]. Bachiller-Baeza *et al.* [157] found that the higher selectivity towards the unsaturated alcohol observed in citral hydrogenation was attributed to the presence of iron, which increased the Lewis acidity in the ruthenium catalysts. Additionally, copper was shown to improve the silica supported-ruthenium catalysts metal dispersion, resulting in increased activity and selectivity to crotyl alcohol in work done by Reyes *et al.* [158]. There have also been cases whereby bimetallic catalysts showed an undesired effect, such as in work reported by Ashour *et al.* [159] for crotonaldehyde hydrogenation using Pd-Cu/SiO_2, where the copper was preferentially poisoned leaving palladium available to react with both functional groups. Lucas and Claus [160] reported on the use of silver to assists in the co-ordination of C=O bonds, and allowed for a 70 % yield of allyl alcohol, in the liquid phase selective hydrogenation of acrolein, when combined with indium.

In general, literature shows that bimetallic catalysts offer changes in structural, textural, and electronic properties of the catalyst, and it is this modification that affects the activity and selectivity [33]. Characterization of these catalysts becomes vital to fully understand the interaction between the metals and the metal-support interaction, and how this correlates with the results obtained from catalytic testing. There has been sufficient work done to show the benefits using bimetallic catalysts over their monometallic counterparts. It has been well documented that the incorporation of silver in monometallic catalysts systems has improved the catalytic activity. For this reason, silver was chosen to be incorporated into the γ-alumina supported copper catalyst, which was investigated in this study.

1.15. Aims and objectives

For this project, the effectiveness of γ-alumina supported copper-silver bimetallic catalysts in the selective hydrogenation of octanal in the presence of octene was investigated.

- A range of γ-alumina supported copper catalysts with a variation of the silver loading will was prepared, characterized, and tested in a continuous liquid phase fixed bed reactor.
- Catalytic reaction parameters such as temperature, pressure, hydrogen:octanal, and Liquid hourly space velocity (LHSV) will be investigated to determine its impact and contribution to the catalytic activity.
- The bimetallic CuAg/γ-Al_2O_3 catalysts will undergo further investigation to determine the impact of varying factors such as; the impregnation sequence and the intermetallic weight loadings of each metal, while maintaining a constant total metal loading.

Chapter 2
Instrumental Techniques and Reactor Design

The syntheses and characterization of the nine catalysts prepared are presented in this chapter. Wet impregnation was the technique chosen to prepare the monometallic and bimetallic catalysts. The catalytic reactor design and GC analysis method to identify and quantify the products are shown here.

2.1. Catalyst synthesis

Reagents for catalyst preparation

- Commercial γ-Al_2O_3, Alfa Aesar
- Copper nitrate, Sigma Aldrich
- Silver nitrate, Sigma Aldrich
- 1000 ppm copper ICP standard, DLD Suppliers
- 1000 ppm silver ICP standard, DLD Suppliers

2.2. Chemicals used for testing and analysis

The feed used for the selective hydrogenation of octanal in the presence of octene was made up of 2 % octene, 10 % octanal, 88 % octanol, which were supplied by Sasol. Octane, 1-octene, octanal and 1-octanol with purity >98 % were used for the calibration of the gas chromatograph instrument for product analysis and were purchased from Sigma Aldrich. Hydrogen, nitrogen and synthetic air with a purity greater than >98 % was obtained from Afrox. These gases were used for the analysis by gas chromatography and for catalytic testing.

2.3. Instrumentation and preparation

The catalysts prepared were characterized using Infrared Spectroscopy (IR), *in situ* and powder X-Ray Diffraction (XRD), Transmission Electron Microscopy (TEM), Scanning Electron Microscopy (SEM), Nitrogen Physisorption using BET, Inductively Coupled Plasma – Optical Emission Spectroscopy (ICP-OES), Temperature Programmed Reduction (TPR), Temperature Programmed Desorption using ammonia (NH_3-TPD) and Chemisorption using hydrogen and carbon monoxide.

2.3.1. Infrared spectroscopy – attenuated transmission reflectance

The infrared spectrometer used was a Perkin Elmer equipped with a Universal Sampling Accessory with a diamond crystal to reach an adequate force for analysis. The software used was Spectrum 100, which allowed the spectra obtained to be analyzed and edited. Samples required no prior preparation and were added to the sample holder, thereafter, the force was increased to 120 gauge to ensure sufficient contact between the surfaces. The samples were scanned within the range 350-3500 cm^{-1}.

2.3.2. Inductively coupled plasma – optical emission spectrometry

Quantitative and qualitative analysis of the catalyst were performed on a Perkin Elmer ICP-OES Optima 5300 DV. The catalysts powders were digested in 10 mL of nitric acid and made up to 100 mL using double distilled water. Multi element standards were prepared in 10 – 100 ppm concentration for copper and 2- 10 ppm concentration for silver. These standards were used to determine the accurate metal loading of the copper and silver on the catalyst prepared.

Table 2.1. The selected spectral lines for each of the elements analyzed by ICP-OES.

Element	Spectral Line /nm
Cu	224
Ag	243

2.3.3. X-ray diffractogram

X-ray diffraction (XRD) was carried out using a Bruker D8 Advance XRD diffractometer using a Cu Kα radiation (λ = 1.506 Å). Operating conditions were 40 kV and 40 mA with a scan rate of 0.5 ° min^{-1}, slit (2θ) and divergence slit and scatter slit of 1°. This XRD technique was used to determine two types of information, (1) crystallite size using the Scherrer equation in powder XRD, and (2) reduction and oxidation temperatures under *in situ* conditions. The Scherrer equation used 0.98 as the constant value (k). The operating conditions of *in situ* reduction used 5 % H_2/N_2 at a flow rate of 30 mL/min. The temperature was ramped at 10 °C/min till 600 °C, thereafter, the sample was cooled to 100 °C at the same rate. The re-oxidation was carried out by flowing N_2 for 2 hours at 100 °C to purge any hydrogen present. Air was used as the oxidant at a flow rate of 30 mL/min at a temperature ramp at 10 °C until 600 °C, thereafter the sample was cooled to 100 °C. The *in situ* XRD was conducted on selected samples.

2.3.4. Nitrogen physisorption

Samples were weighed and analyzed using the Micromeritics TriStar II 3020 surface area and porosity instrument and software. Sample preparation involved degassing at 90 °C for 1 hour to remove absorbed moisture, thereafter, the temperature was increased to 200 °C and the sample was kept under nitrogen flow overnight. The catalyst for which surface area was to be measured was placed inside a quartz tube and the adsorbate gas passed through while the tube is placed in a liquid nitrogen bath, where the temperature was maintained at 77.5 K. Nitrogen physisorption provides information about the surface area, pore size, and pore volume of the catalysts. All measurements were made in duplicate to ensure reproducibility.

2.3.5. Scanning electron microscopy- energy dispersive X-ray spectroscopy (SEM-EDX)

For sample preparation, a piece of two-way carbon tape was placed onto a metal stub. The catalyst powder was added to the tape and the excess powder was removed by gentle tapping. The powder was coated with carbon, using the polaron SC sputter coater, to provide an electron active surface. The samples were analyzed using the Joel JSM 6100 instrument. The energy dispersion X-ray spectroscopy (EDX) mapping was done using the Bruker EDX detector and was analyzed with the Espirit 1.8.5 software.

2.3.6. Transmission electron microscopy (TEM)

A small amount of the sample was added to an Eppendorf vial; thereafter a solvent such as acetone or ethanol was added. This mixture was sonicated for 5 minutes to allow the breakup of larger particles, which allows good dispersion onto the metal grid coated with holy-carbon. A copper or nickel grid was immersed into the Eppendorf tube to coat the grid with the mixture. The grid was placed into the Joel 1010 TEM instrument and analyzed using the Megaview III soft imaging system at an operating voltage of 100 kV.

2.3.7. High resolution- transmission electron microscopy - energy dispersive X-ray spectroscopy (HRTEM-EDX)

Samples were prepared in the same way as with TEM. The copper or nickel grid, coated with a holy-carbon film, containing the sample was placed into the sample holder and analyzed using the Joel JEM-2100 using the iTEM software for imaging at 200 kV. The microscope used a Lanthanum hexaboride (LaB_6) gun and a Gatan ultrascan camera for imaging. HRTEM was used for high magnification imaging as well as dark field imaging, mapping and line scan. HRTEM was conducted on selected catalysts.

2.3.8. Temperature programmed reduction/desorption (TPR/TPD)

The calcined catalyst (0.04-0.05 g) was added to a U-shaped quartz tube between two layers of quartz wool. This was fastened into the Micromeritics AutoChem II chemisorption analyzer. The catalyst was dried under helium to 400 °C at a rate of 10 °C/min. The sample was cooled to 70 °C, thereafter heated to 600 °C under 5 % H_2/Ar for the TPR analysis at a rate of 10 °C/min. After analysis, the sample was cooled to 40 °C under helium. In the case of TPD, 5 % NH_3/Ar was used instead of hydrogen to determine acid sites. All TPD analysis was conducted immediately after TPR analysis to ensure the analysis occurs on a fully reduced catalyst.

2.3.9. Chemisorption

The Micromeritics 2920 AutoChem II chemisorption analyzer was used to carry out pulse chemisorption using hydrogen and carbon monoxide. All calcined samples were degassed under nitrogen at 90 °C and under vacuum at 200 °C prior to the analysis using the Micromeritics Flow prep 060 sample degas system. The catalyst (0.03-0.04 g) was sandwiched between two layers of quartz wool in a U-shaped quartz tube, which was fitted onto the Micromeritics instrument. The analysis underwent an evacuation step using helium to ensure the sample has no moisture. The chemisorptive gas (H_2 or CO) was then passed through at a set temperature with increasing pressure; after analysis the sample was flushed with helium to terminate the analysis. All catalysts were analyzed in duplicate on separate samples to ensure reproducibility, and in duplicate on the same sample to ensure that the results correlate for both chemisorptive gas analyses.

2.3.10. Thermal gravimetric analysis – differential scanning calorimetry (TGA-DSC)

The TA SDTQ600 instrument was used for the thermal gravimetric analysis. Samples were weighed and placed in a sample holder. The analysis involves the sample being heated under air

with 50 mL/min flow rate from room temperature to 700 °C at a heating rate of 10 °C/min. This analysis was also conducted under nitrogen instead of air.

2.4. Gas chromatography

GC using a flame ionization detector (FID) was used for analysis and quantification of the products obtained from the hydrogenation of octanal in the presence of octene. A volume of 1 µL, using a SGE 1 µL syringe, was injected into the column with an initial temperature of 40 °C and a spilt ratio of 20. The injector temperature and pressure was 200 °C and 50 psi. The column temperature program for the Perkin Elmer TotalChrom software was ramped as follows: an initial temperature of 40 °C was held for 5 minutes, thereafter a set point of 240 °C with a heating rate of 3 °C/min. Afrox supplied both the carrier gases (He) and the flame gas (H_2). Gas chromatography-mass spectrometer was used to confirm all products using the Perkin Elmer Clarus 500 GC with a Perkin Elmer 560S mass spectrometer. The samples were analyzed using the same method as the GC FID. The mass spectrometer used a photo ionization detector with a positive electron ionization mode. The Turbomass 5.4.2. software was used to analyze the chromatographs and MS spectra.

2.5. Catalyst synthesis

2.5.1. The monometallic catalyst - 5Cu/γ-Al_2O_3

Commercial γ-Al_2O_3 pellets, obtained from Alfa Aesar, were ground into a fine powder using a mortar and pestle. Copper nitrate (0.250 g) was dissolved in 15 ml of deionized water and added slowly to a slurry of γ-Al_2O_3 (4.752 g). This mixture was stirred at room temperature for 6 hours; thereafter it was heated gently for 1 hour to remove the excess water until a thick paste remained. The paste was oven dried at 120 °C overnight, followed by calcination at 500 °C for 8 hours under a flow of air, with a temperature ramp of 1.6 °C/min.

2.5.2. The bimetallic catalyst - 4.5Cu-0.5Ag/γ-Al_2O_3

A 4.5 wt % Cu and 0.5 wt % Ag on γ-alumina catalyst was prepared using the wet incipient method. Copper nitrate (0.225 g) was dissolved in the minimum amount of deionized water together with silver nitrate (0.025 g) and added slowly to a slurry of γ-alumina (4.752 g). This mixture was stirred at room temperature for 6 hours; thereafter it was gently heated for 1 hour to remove the excess water until a thick paste remained. The paste was dried at 120 °C overnight, thereafter, calcined at 500 °C for 8 hours under a flow of air.

Sequential impregnation catalysts were prepared by firstly adding the metal (A) solution to the alumina slurry. This mixture was stirred for 6 hours and oven dried overnight at 120 °C. Once cooled to room temperature, a small amount of deionized water was added to form a paste. The second metal (B) solution was added and stirred for 6 hours. This mixture was then oven dried at 120 °C overnight. The final catalyst precursor was calcined at 500 °C for 8 hours under a flow of air. These catalysts are denoted by S-metal A wt % metal B wt %/γ-Al_2O_3. From here on the catalyst metal loading will be denoted by the number, as shown in Table 2.1.

Table 2.2: Mass of components used for the preparation of all catalysts.

Catalysts name:	Order of Sequence	Copper nitrate (g)	Silver nitrate (g)	γ-Alumina (g)
5Cu/γ-Al_2O_3	-	0.952	-	4.754
4.5Cu0.5Ag/γ-Al_2O_3	simultaneous	0.851	0.040	4.758
S-4.5Cu0.5Ag/γ-Al_2O_3	Cu, Ag	0.869	0.043	4.674
S-0.5Ag4.5Cu/γ-Al_2O_3	Ag, Cu	0.856	0.043	4.670
4Cu1Ag/γ-Al_2O_3	simultaneous	0.761	0.080	4.760
S-4Cu1Ag/γ-Al_2O_3	Cu, Ag	0.761	0.080	4.759
S-1Ag4Cu/γ-Al_2O_3	Ag, Cu	0.766	0.079	4.755
15Cu/γ-Al_2O_3	-	2.871	-	4.757
13.5Cu1.5Ag/γ-Al_2O_3	simultaneous	2.545	0.355	4.257

2.6. Reactor set up

The reactor set up was carried out using a fixed-bed continuous flow reactor and a gas chromatograph was used for analysis and quantification purposes. The feed used for the reactions described in chapter 4 contained 2 % octene 10 % octanal and 88 % octanol. All reactions were done in the liquid phase.

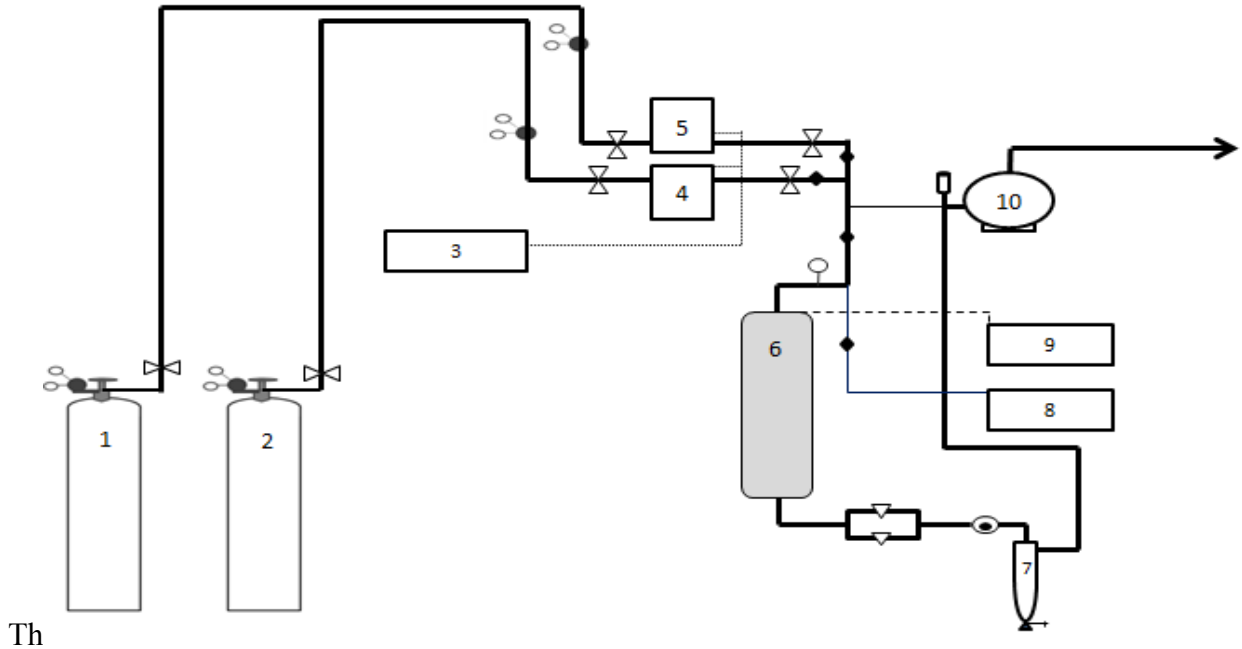

Th

1. H_2 gas cylinder
2. N_2 gas cylinder
3. Brooks gas flow control box
4. H_2 MFC (Mass flow controller)
5. N_2 MFC
6. Reactor
7. Catchpot
8. Feed pump
9. Thermocouple control box
10. Wet gas flow meter

pressure regulator
shut off valve
one way valve
reactor pressure gauge
Filter
regulator to set reactor pressure
back pressure relief valve
Vent line

Figure 2.1. Schematic of the reactor set up.

2.7. Catalytic testing

A 300 mm heating jacket was used to supply heat during the hydrogenation of aldehydes in a mixed feed. The reactor tube had a 7 mm inner diameter and 9 mm outer diameter. The catalyst bed was made up of approximately 2 mL of catalyst pellets (300-600 μm) diluted in a 1:1 ratio with 24 grit carborundum in a sandwich of glass wool. This catalyst bed was packed in the region considered to be the hotspot of a 350 mm 316 stainless steel reactor tube. 24 grit carborundum was used to pack either side of the catalyst bed, separated by glass wool, to allow mixing of the feed with gas and to pre-heat the gases before they reach the catalyst bed to allow for constant temperature. Glass wool was packed on either side of the reactor tube to prevent particulate matter from entering the product stream. The reactor was secured by bolts which were tightened by a torque wrench; thereafter a leak test was conducted by holding a high pressure (50 bar) of nitrogen over a period of time to ensure there were no leaks in the system. The reactor was covered with an insulating jacket to allow for an isothermal environment. The temperature was monitored by a thermocouple placed between the heating mantle and reactor tube to measure the outside temperature, which was controlled with a control panel. The actual temperature within the reactor tube was controlled by a thermocouple placed inside the reactor tube. A schematic diagram of the set-up is given in Figure 2.1.

Liquid phase hydrogenation was carried out using a continuous plug flow fixed bed reactor which operated in a down flow direction. The liquid feed was fed through the $1/8^{th}$ inch 316 stainless steel tubing feed lines, using a LabAlliance series II isocratic pump. $1/16^{th}$ 316 stainless steel product pipes contain a filter leading to the catchpot allowed the products to be collected in a 500 mL stainless steel catchpot. The hydrogen and nitrogen gas flow was controlled by Brooks mass flow controllers (MFC's) with the excess gas exiting through a Ritter Drum Type (TGI-model 5) wet gas flow meter. The pressure was maintained using a Tescom pressure regulator to set the reactor pressure, before the sampling catchpot.

The catalyst preparation prior to catalytic testing involved the catalyst drying at 200 °C overnight, followed by the blending of hydrogen at 160 °C. The catalyst was then reduced using 100 % hydrogen at a flowrate of 12 mL/min overnight at reduction temperatures ranging from 220 – 260 °C.

Chapter 3
Results and Discussion: Characterization

Apart from the material used in the preparation of the catalyst, the characterization of the catalyst provides insight and understanding in the behavior of the catalyst. Characterization essentially provides information of how the catalyst is likely to behave under reactor conditions and insight on the possible reaction pathways of the reactants.

All catalysts were characterized using the techniques discussed in Chapter 2 are reported and discussed here. This chapter shows all the characterization done on the catalysts before their use in reactions, called as "fresh" catalysts. The colour of the catalysts correlate with literature and is the first simple characterization technique used to indicate certain properties of the catalysts e.g. the $5Cu/\gamma\text{-}Al_2O_3$ and the bimetallic $4.5Cu0.5Ag/\gamma\text{-}Al_2O_3$ catalyst were blue-green in colour, due to the low loading and well dispersed copper species on the support. At higher weight loadings (>13 wt %), the colours of the copper catalysts changed to grey – dark grey, depending on the catalyst loading [161].

3.1. Infra Red-Attenuated total reflectance (ATR)

Figure 3.1 shows a broad range for the hydroxyl group from 3100 – 3600 cm^{-1}, adsorbed hydrogen from 1300 – 1670 cm^{-1}, the Al-O bands at approximately 500 cm^{-1} and 790 cm^{-1}. The main peaks observed from Figure 3.1 were due to the adsorbed water, due to the hydroscopic nature of alumina, and the peaks corresponding to Al-O bands.

The ATR spectra were obtained for all monometallic and bimetallic catalysts.

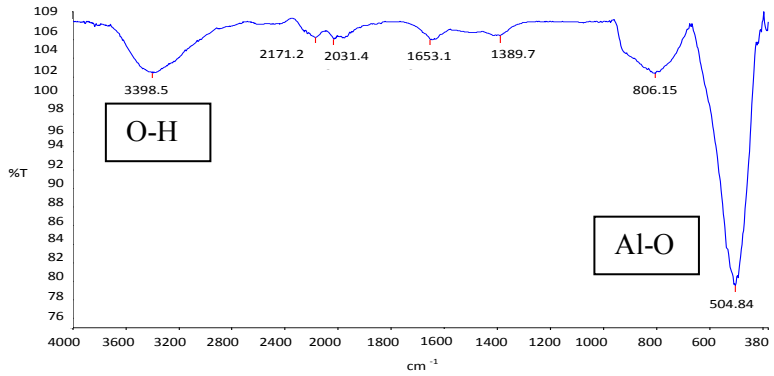

Figure 3.1. IR of 5Cu/γ-Al_2O_3.

Turek *et al.* [162] reported free hydroxyl alumina to be in the 3400 – 3800 cm^{-1} region. This is due to the O-H peaks within the lattice as alumina contains acidic and basic properties, as well as possible moisture absorbed by the hygroscopic support. In a study by Knözinger and Ratnasamy [163] surface hydroxyl peaks were investigated and assigned peaks in the region of 3690 cm^{-1}, which were attributed to octahedrally coordinated aluminium and are the most acidic hydroxyl sites. The most basic sites were found at 3785 cm^{-1} which are single coordinated hydroxyls [163]. Trueba and Trasatti [164] show the interaction between the Lewis acid and basic sites with water, allowing for hydration of the alumina support under atmospheric conditions. This occurs in two major steps, by the water initially adsorbing onto the alumina support, whereby the electrons from the lone pair on oxygen from H_2O are transferred to the aluminium atom on the alumina support. The second step is the dissociation of H_2O resulting in the hydroxyl group bonding to the aluminium and the hydrogen from the water molecule bonds to the oxygen atom. These steps are illustrated in Figure 3.2.

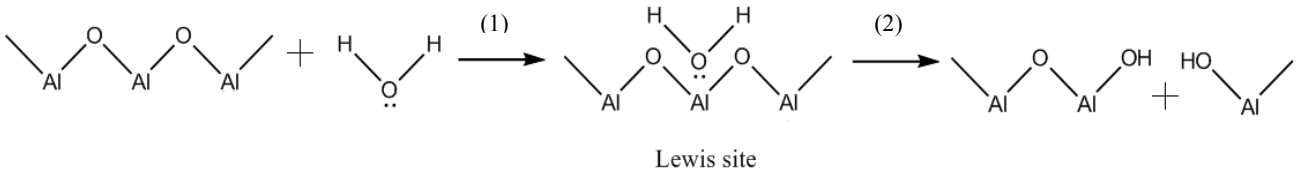

Figure 3.2. Schematic depicting the two major steps (1) adsorption of H_2O on alumina and (2) dissociative chemisorption of H_2O.

The IR results obtained are summarized in Table 3.1, showing the main peaks observed for all catalysts.

Table 3.1. Infrared Spectroscopy results for all catalysts.

Catalyst	O-H band (cm^{-1})	H_2O adsorbed (cm^{-1})	Al-O (cm^{-1})	
γ-Al_2O_3	3184	1645, 1335	508	789
5Cu/γ-Al_2O_3	3399	1653, 1390	505	806
4.5Cu-0.5Ag/γ-Al_2O_3	3445	1640	515	794
S-4.5Cu0.5Ag/γ-Al_2O_3	3484	1655	523	788
S-0.5Ag4.5Cu/γ-Al_2O_3	3428	1655	508	802
4Cu-1Ag/γ-Al_2O_3	3480	1641	513	804
S-4Cu1Ag/γ-Al_2O_3	3459	1635	511	846
S-1Ag4Cu/γ-Al_2O_3	3458	1687	508	840
15Cu/γ-Al_2O_3	3445	1645	532	864
13.5Cu-1.5Ag/γ-Al_2O_3	3441	1634	512	863

The peak due to adsorbed hydrogen as reported by Abadleh *et al.* [165], was observed at approximately 1594 cm^{-1}. Unlike the adsorbed hydroxyl species which were observed at peaks higher than 3100 cm^{-1}, peaks found between 1330 – 1670 cm^{-1} are due to the interaction between the alumina surface and the two hydrogen atoms in the water molecule [165]. Similarly to the results obtained from the infrared spectroscopy for all catalysts in this work, which showed alumina to have distinct peaks from 500 – 525 and 786 – 807 cm^{-1}, this is also in agreement with work published by Mo *et al.* [166] for bulk γ-Al_2O_3. Additionally, work done by Ramesh *et al.* [167] also attributed peaks observed at 580 and 840 cm^{-1} to the Al-O bond in γ-Al_2O_3, and Wang *et al.* [168] observed Al-O vibrational peaks at 584 and 778 cm^{-1}. Due to the low loading of metal on all catalysts, there are no significant differences in the data obtained from the IR

spectroscopy as seen from Table 3.1. The infrared spectra for all catalysts are shown in the Appendix.

3.2. Inductively coupled plasma-optical emission spectroscopy (ICP-OES)

The total metal loading for all catalysts were 5 wt % therefore in the case of the bimetallic catalysts the metals percentage were varied to achieve the maximum 5 wt % total metal content. A theoretical amount of metal salt was calculated and applied in the synthesis procedure. The catalysts were analyzed using ICP in duplicate and the average metal loading calculated is shown in Table 3.2.

Table 3.2. Weight loadings obtained from ICP-OES analysis for all catalysts.

Catalyst	Copper (wt %)	Silver (wt %)
5Cu/γ-Al_2O_3	5.82	-
4.5Cu-0.5Ag/γ-Al_2O_3	4.61	0.51
S-4.5Cu0.5Ag/γ-Al_2O_3	4.44	0.58
S-0.5Ag4.5Cu/γ-Al_2O_3	4.52	0.53
4Cu-1Ag/γ-Al_2O_3	4.23	1.08
S-4Cu1Ag/γ-Al_2O_3	3.82	1.13
S-1Ag4Cu/γ-Al_2O_3	4.09	1.23
15Cu/γ-Al_2O_3	15.7	-
13.5Cu-1.5Ag/γ-Al_2O_3	13.8	1.68

3.3. X-ray diffraction

3.3.1. Powder XRD

XRD provides information using the specific 2Θ and d-spacing values, which correspond with different phases of metal oxide and metal loaded catalysts. There are two functions an XRD instrument can perform, firstly, powder XRD which is a quick characterization technique showing the 2Θ and d-spacing values which assists in determining the metal oxide phase on the catalyst. The second function is the use of *in situ* XRD, which is a process of reduction and

oxidation allowing for the change in metal phase present, recorded over a number of scans during the analysis. This change is monitored by the disappearance or appearance of peaks in the diffractogram.

As shown in Figure 3.3, the power XRD for γ-Al_2O_3, 5Cu/γ-Al_2O_3, 15Cu/γ-Al_2O_3 and 13.5Cu1.5Ag/γ-Al_2O_3 catalysts. It can be seen at low weight loadings of 5 % Cu, there were no distinct peaks observed which has been well documented to suggest good dispersion of the metal [169]. Luo *et al.* [169] also stated that copper oxide peaks were not visible at weight loading less than 11%, this is consistent with work done by Kundakovic *et al.* [170] and Friedman *et al.* [171]. The results obtained correlated with what was observed in literature where CuO peaks were observed for the catalysts containing copper at 13 wt % loading and higher (Figure 3.3c-d). The CuO peaks were consistent with ICDD 80-1268, with the γ-alumina phase assigned to JCPDS 10-0425.

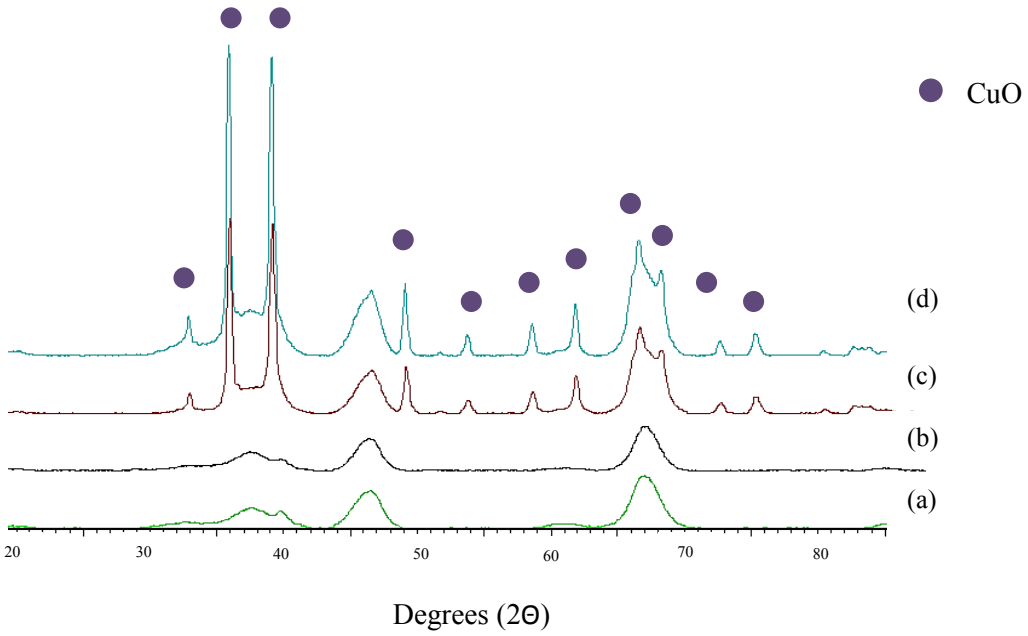

Figure 3.3. X-ray diffractogram for (a) bare γ-Al_2O_3 (green), and γ-Al_2O_3 supported with: (b) 5Cu (black), (c) 15Cu (red), (d) 13.5Cu-1.5Ag (blue) catalysts.

Figure 3.4 and 3.5 shows the XRD diffractograms of the 4.5Cu0.5Ag/γ-Al_2O_3 and 4Cu1Ag/γ-Al_2O_3 bimetallic catalysts prepared by simultaneous and sequential impregnation. This provides a comparison between the sequential and simultaneous impregnation effect as well as the effect of the silver loading.

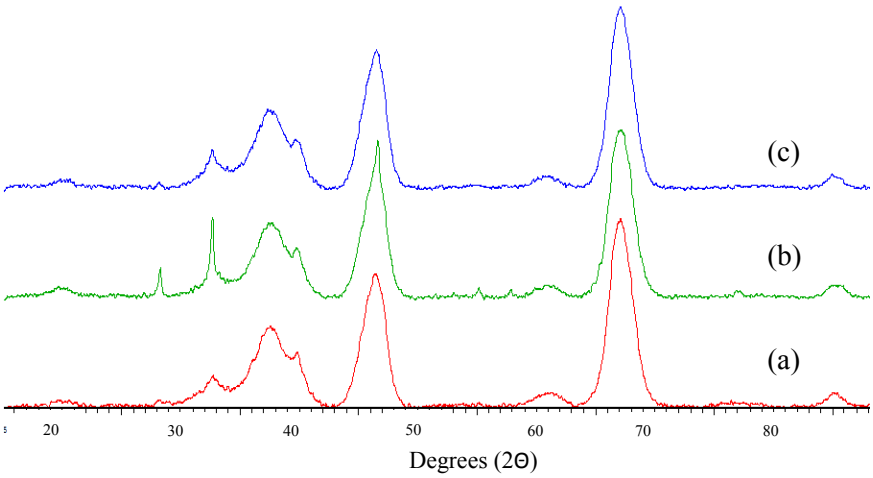

Figure 3.4. X-ray diffractograms for γ-Al_2O_3 supported with (a) 4.5Cu0.5Ag (red), (b) S-4.5Cu0.5Ag (green), (c) S-0.5Ag4.5Cu (blue) catalysts.

Figure 3.4a-c shows the catalysts containing 4.5 wt % Copper and 0.5 wt % silver/γ-Al_2O_3. The simultaneously prepared catalyst (Figure 3.4a) does not show distinct metal peaks, similar to the 5Cu catalyst. This is most likely due to the low metal loading present. Figure 3.4b shows that when copper was impregnated first followed by silver, the silver is able to form small crystallites on the surface of copper and the bare support allowing for distinct peaks observed in the diffractogram. A mixture of silver oxides was observed namely Ag_3O_4 corresponding to JCPDS 40-909, however, there is also a possibility of other phases present such as AgO (JCPDS 21-1272) and Ag_2O (JCPDS 12-0793) were present, which fall in the same region as the broad alumina peaks. A minor presence of Ag_3O_4 is also present for the 0.5Ag4.5Cu catalyst/γ-Al_2O_3 (Figure 3.4c).

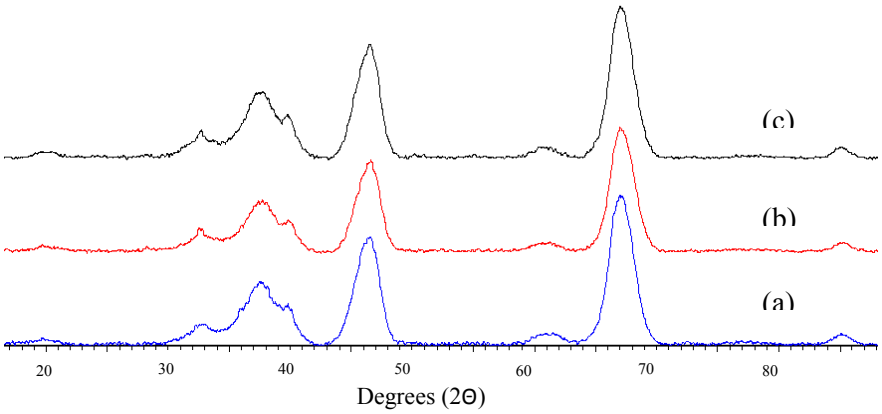

Figure 3.5. X-ray diffractograms for γ-Al_2O_3 supported with (a) 4Cu1Ag (blue), (b) S-4Cu1Ag (red), (c) S-1Ag4Cu (black) catalysts.

In the case of the 4Cu1Ag/γ-Al_2O_3 catalyst, there were no distinct peaks observed, unlike for what was observed for the 4.5Cu0.5Ag/γ-Al_2O_3 catalysts (Figure 3.4a-c). This is most likely due to the larger quantity of silver present, which allows a greater probability of silver oxides forming larger agglomerates, which may not be crystalline. Unlike the 4.5Cu0.5Ag/γ-Al_2O_3 catalyst, the 1 % silver does not form the Ag_3O_4 crystallite phase. There is a possibility of the AgO phase (JCPDS 21-1272) present, however, due to overlap of the copper and silver oxide phases, it cannot be confirmed [172]. AgO is reported to be unstable at room temperature and is able to decompose to metallic silver in the presence of light [173]. From the lack of metallic silver peaks in the diffractogram, it can be concluded that the silver is in the Ag_2O phase which is more stable, however, it is also possible for the catalyst to have a mixture of silver phases on the support, according to work reported by Page *et al.* [174].

3.3.2. *In situ* XRD

In general, the *in situ* XRD showed that all catalysts, using 5 % H_2/N_2 gas, have an initial reduction temperature of 200 °C. To determine the metal peaks, the catalyst had to undergo a reduction-oxidation process. The reduction occurred under a 5 % H_2/N_2 mixture while being heated to 600 °C at 50 °C intervals, with a ramp rate of 10 °C/min. The oxidation step followed with air as the oxidant while heated to 600 °C. The diffraction patterns in Figure 3.6 depicts the 5Cu/γ-Al_2O_3. catalysts undergoing reduction under 5 % H_2/N_2.

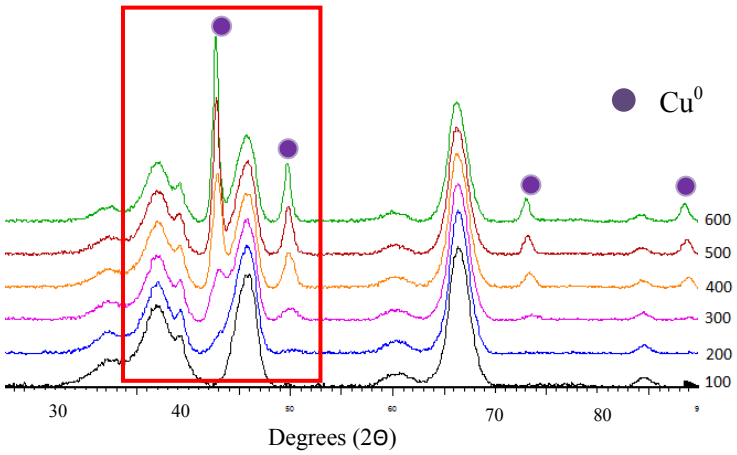

Figure 3.6. *In situ* X-ray diffractogram for 5Cu/γ-Al_2O_3.

The X-ray diffractogram of the 5Cu/γ-Al_2O_3 catalyst showed broad peaks for the γ-alumina support and sharp peaks for the copper metal, once reduced. The reduction profile for the bimetallic 4.5Cu0.5Ag/γ-Al_2O_3 and 4Cu1Ag/γ-Al_2O_3 catalysts are shown in the diffractogram in Figure 3.7. The oxidation *in situ* XRD show that all the copper which was reduced under hydrogen, is oxidized back to CuO (see Appendix).

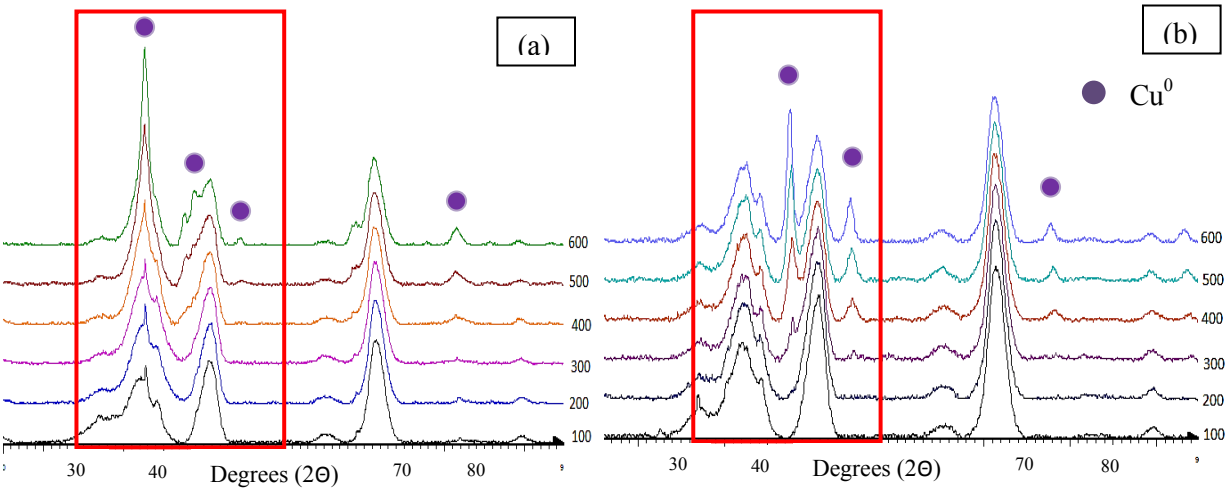

Figure 3.7. *In situ* X-ray diffractogram for (a) 4.5Cu0.5Ag/γ-Al_2O_3 and (b) 4Cu1Ag/γ-Al_2O_3 catalysts.

Figure 3.7a-b shows the reduction profiles of the 4.5Cu0.5Ag/γ-Al_2O_3 and 4Cu1Ag/γ-Al_2O_3 catalysts. On the reduction of the metal oxides, it is observed in Figure 3.7 that there is a shift of the metal peaks to a lower 2θ value; this could be due to a loss of crystallinity or an increase of

defect sites. There is also a minor presence of the Cu^0 peaks in its original position (Figure 3.6) suggesting some of the copper remained unchanged in terms of crystallinity, with the d-spacing values remaining consistent with Cu^0 JCPDS 04-0836. This result could be correlated to the low silver content allowing for a good dispersion of silver, thus allowing for intimate contact between the silver and copper atoms causing a synergistic effect.

The 4Cu1Ag/γ-Al_2O_3 catalyst showed a slight shift, and the d-spacing value to a lower value compared to the 5Cu catalyst; this is similar to what was observed with the 5Cu/γ-Al_2O_3 catalyst, however, the shift is not as significant. Due to the higher loading of silver present, the silver has a higher affinity to migrate or interact with other silver atoms present rather than the 4 % copper available. This catalyst also has a lower copper content, which allows for a higher dispersion and a greater area of bare support for silver to adsorb without coming into close contact with copper. This results in a similar *in situ* reduction profile to the 5Cu/γ-Al_2O_3 catalyst.

3.4. Brunauer-Emmet-Teller (BET) analysis

The total surface area of the catalyst was calculated from the amount of gas adsorbed by using the BET method. The use of BET analysis allows one to obtain useful information, namely the surface area and pore volume of the catalysts. The surface area measurements include external and internal surface area. The pore volume is indicative of the total internal volume per unit mass of the catalyst allowing for a greater understanding of the occupation of the metal within the support. Materials can be distinguished by their isotherms or pore size. Three main groups of pore sizes are (a) macropores (> 50 nm), (b) mesopores (2-50 nm), and (c) micropores (< 2 nm). Alumina is a typical mesoporous material therefore the expected pore size region is between 2 – 50 nm.

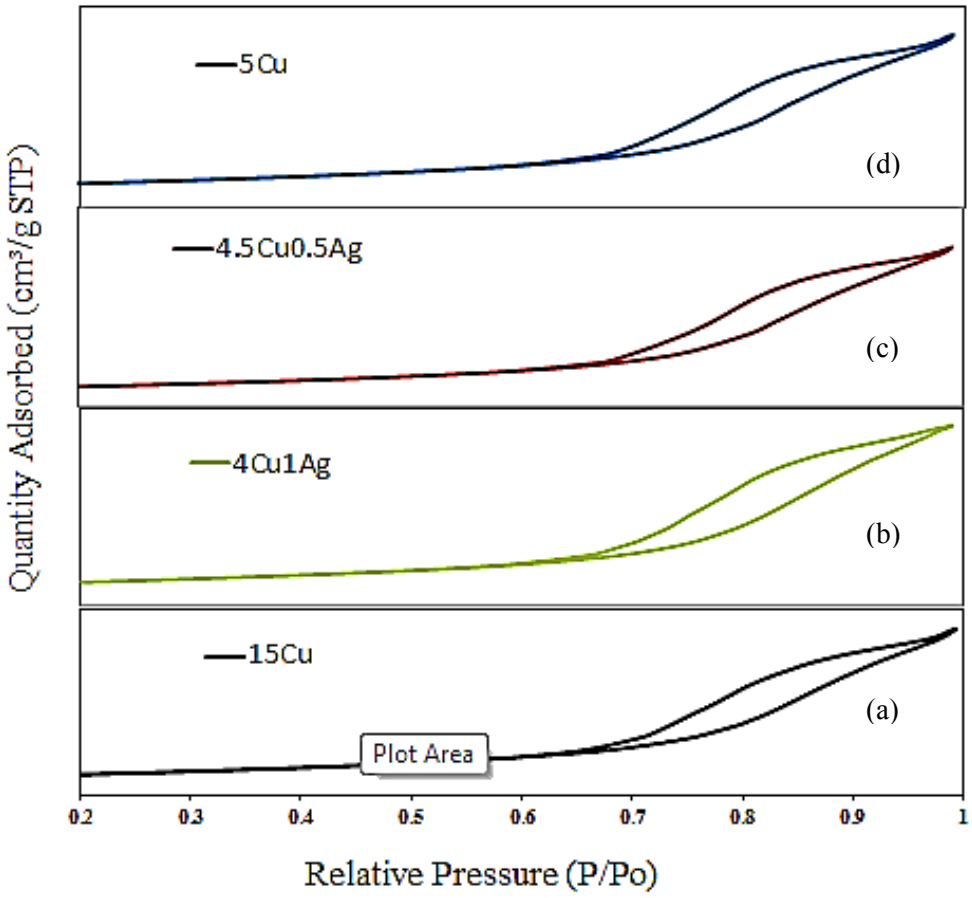

Figure 3.8. Hysteresis loops for γ-Al_2O_3 supported with: (a) 5Cu (Blue), (b) 4.5Cu0.5Ag (Red), (c) 4Cu1Ag (Green), and (d) 15Cu (Black) catalysts.

It can be seen in Table 3.3, that the 15Cu/γ-Al_2O_3 catalyst has a lower surface area compared to the 5Cu/γ-Al_2O_3 catalyst. This is attributed to the higher weight loading of copper, which forms CuO on the surface and within the pores, which decreased the pore size to a greater extent than the 5Cu/γ-Al_2O_3 catalyst. Figures 3.8 shows the adsorption/desorption isotherms obtained from the surface area analysis. All catalysts show a mesoporous nature consistent with γ- Al_2O_3. These isotherms were used to determine the surface area, pore size and pore volume of the catalysts. All catalysts showed a decrease in surface area because of the metal oxide deposition onto the alumina surface. The pore size and pore volume did not differ significantly due to the high surface area of the support; the deposition of the metal most likely occurs on the surface.

Table 3.3. Surface area measurements for all catalysts.

Catalyst	Surface Area (m^2/g)	Pore Volume (cm^3/g)	Pore size (nm)
γ-Al_2O_3	230	0.8	12.7
5Cu/γ-Al_2O_3	216	0.7	11.8
4.5Cu-0.5Ag/γ-Al_2O_3	224	0.7	12.8
S-4.5Cu0.5Ag/γ-Al_2O_3	210	0.7	14.3
S-0.5Ag4.5Cu/γ-Al_2O_3	195	0.6	12.6
4Cu-1Ag/γ-Al_2O_3	207	0.7	12.7
S-4Cu1Ag/γ-Al_2O_3	209	0.6	12.4
S-1Ag4Cu/γ-Al_2O_3	191	0.6	12.8
15Cu/γ-Al_2O_3	173	0.6	12.9
13.5Cu-1.5Ag/γ-Al_2O_3	151	0.5	13.1

Table 3.3 shows the 15 wt% catalysts have a lower surface area, which could be attributed to the higher concentration of metal available which covers more support and may enter the pores, thus decreasing the surface area and pore volume. This is consistent with what is reported in literature by Hammed *et al.* [175] and Alouse *et al.* [176], whereby a general trend of increased metal loading resulting in decreased surface area. There is no distinct trend concerning the total metal loaded 5 wt % bimetallic catalysts where 15-40 % decrease in the surface areas, when compared to the calcined γ-alumina, are observed. It was observed that there was an effect due to the metal loading where the 15 % total metal loaded catalysts has a lower surface area than the 5 wt % catalyst.

3.5. Chemisorption

Chemisorption is based on a technique that uses an adsorbate gas to chemically adsorb onto surface atoms, which possess electrons available for bonding. The adsorbate gas forms a monolayer on the metal active sites. This technique provides information regarding metal dispersion and active metal surface area. There are two main methods of chemisorption, which

are static and pulse chemisorption. The static method is when the reaction between the adsorbate gas and catalyst reaches equilibrium and therefore provides information of strongly adsorbed gas and weakly bound gas to the active sites. The static method uses a 'back sorption' method. The first adsorption of the reactive gas consists of both strongly and weakly adsorbed gas. Once the first analysis is complete, the sample is degassed. The weakly bound hydrogen is highly mobile, whereas the strongly bound hydrogen is said to adsorb onto the corner edges of the metal particle [177]. The sample undergoes a second analysis, in which case the sample the degassed removing the weakly bound species. The results from the second analysis will therefore show the adsorption of only the weakly bound species thus determining metal dispersion [178].

There are three types of conformations possible for CO bound to metals; linear, bridge and twin type. Figure 3.9 illustrates the three possible conformations:

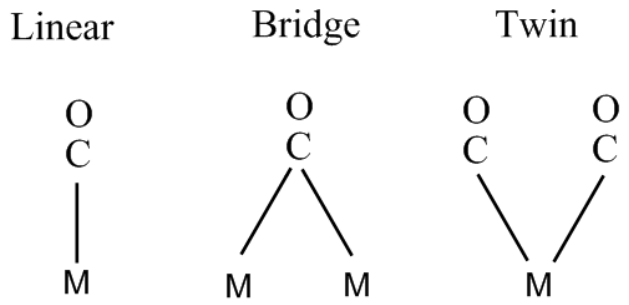

Figure 3.9. CO adsorption confirmation types [179].

Figure 3.9 shows the types of conformations a CO molecule can adsorb onto a metal. When a CO molecule is adsorbed onto two metal particles, it is called bridge type and lastly the twin type where one metal has two CO molecules adsorbed onto it. 'Coinage metals", namely Cu, Ag and Au, are largely dominated by linear type CO adsorption. High value metals such as Ru, Rh and Pd, can have linear and bridge type conformations, with Rh also having a twin type adsorption [179]. Nygren *et al.* [180], reported that CO gas molecules are able to adsorb onto copper clusters containing up to 20 atoms. In hydrogen chemisorption, the preferred cluster size contains up to 10 atoms of copper, according to studies done by Guvelioglu *et al.* [181] and Forrey [182].

Copper has been studied using various adsorption gases, however, there has always been a large drawback regarding accuracy of data of different adsorptive gases in relation to the copper dispersion. Literature shows N_2O is the most commonly used gas for the determination of metal dispersion in copper catalysts, following the decomposition reaction on the surface of copper as shown in the reaction below: [68, 119, 183-187]

$$\mathbf{N_2O_{(g)} + 2Cu_{(s)} \leftrightarrow Cu\text{-}O\text{-}Cu_{(s)} + N_{2(g)}} \qquad \text{(s) – surface species}$$

With this type of gas, the temperature plays an important role for differentiation between surface copper and bulk copper species. Extended exposure to this gas may also lead to the oxidation of the copper species, which will overestimate the metal dispersion [183]. By using hydrogen as the chemisorption gas, the following equation is expected:

$$\mathbf{H_2 + CuO \leftrightarrow Cu\text{-}H + {}^{-}OH}$$

Hydrogen has a weak adsorption on copper and has been considered one of the most common chemisorptive gases used where the dissociated hydrogen adsorbs onto the metal in a 1:1 ratio [181, 182, 188]. Table 3.4. shows the information used to calculate metal dispersion and metallic surface area of the catalysts.

Table 3.4. Atomic weight, cross sectional area, and density for copper and silver.

	Copper	Silver
Atomic weight (g/mole)	63.6	107.9
Cross sectional area (sq nm)	0.068	0.087
Density (g/mL)	8.9	10.5

The 5Cu catalysts were analyzed using reduction temperatures of 210, 250 and 290 °C to determine the effect of the temperature with regards to metal dispersion. Table 3.5 shows a summary of hydrogen chemisorption results.

Table 3.5. Summary of results obtained from hydrogen chemisorption for all catalysts.

Catalyst	Metal Dispersion: %	Metallic Surface Area: m^2/(g of sample)	Metallic Surface Area: m^2/(g of metal)	Crystallite Size (6.000 V / A): nm
5Cu/γ-Al_2O_3 (210)*	1.2	0.4	7.6	87
5Cu/γ-Al_2O_3 (250)*	3.3	1.05	21.3	33.1
5Cu/γ-Al_2O_3 (290)*	4.9	1.6	31.7	21.1
4.5Cu-0.5Ag/γ-Al_2O_3	8.6	3.0	60.6	19.2
S-4.5Cu0.5Ag/γ-Al_2O_3	8.8	2.7	53.6	12.1
S-0.5Ag4.5Cu/γ-Al_2O_3	4.9	1.5	30.7	21.6
4Cu-1Ag/γ-Al_2O_3	8.4	2.5	51.5	12.7
S-4Cu1Ag/γ-Al_2O_3	6.0	1.8	36.9	17.7
S-1Ag4Cu/γ-Al_2O_3	9.6	2.9	59.1	11.1
15Cu/γ-Al_2O_3	1.9	1.9	12.4	54.0
13.5Cu-1.5Ag/γ-Al_2O_3	1.9	1.8	12.0	55.3

*Reduction temperature during analysis

It was found that the higher the reduction temperature, the higher the metal dispersion which could be attributed to surface diffusion as a result of the high temperature [189]. The optimum reduction temperature was chosen as 250 °C, as it is slightly higher than the reported reduction temperature of copper, ensuring complete reduction [190, 191], and the analysis temperature was 120 °C. A high reduction temperature may cause an adverse result by showing an overestimation of metallic surface area and metal dispersion due to more kinetic energy introduced to the system [68, 119, 192].

The bimetallic catalysts prepared by simultaneous impregnation showed a higher metal dispersion than the copper catalysts. Silver does not adsorb hydrogen well [179], therefore the results obtained for hydrogen chemisorption assume that the bimetallic results are due to the dispersion of copper. The S-4.5Cu0.5Ag/γ-Al_2O_3 catalyst shows a similar metal dispersion to

the 4.5Cu0.5Ag/γ-Al_2O_3 which suggests that silver assisted in the chemisorption of hydrogen, this lowers the heat of adsorption required to the dissociated hydrogen to chemisorb to copper, as seen in the case of oxygen on transition metals [193].

When silver was impregnated first, the hydrogen chemisorption is significantly lower than for the 4.5Cu0.5Ag/γ-Al_2O_3 catalyst; this is due to the higher surface coverage of copper resulting in a similar metal dispersion to the 5Cu catalyst. The 4Cu1Ag/γ-Al_2O_3 catalyst showed an inverse result to the 4.5Cu0.5Ag/γ-Al_2O_3, this is due to the decreased synergistic effect between the copper and silver because the silver has a higher affinity to cluster to other silver atoms than to the copper present. The samples were also analyzed using carbon monoxide as the adsorptive gas. These results are shown in Table 3.6.

Table 3.6. Results obtained from carbon monoxide chemisorption for all catalysts.

Catalyst	**Metal Dispersion: %**	**Metallic Surface Area: m^2/(g of sample)**	**Metallic Surface Area: m^2/(g of metal)**	**Crystallite Size (6.000 V / A): nm**
5Cu/γ-Al_2O_3	5.6	1.8	36.4	22.3
4.5Cu-0.5Ag/γ-Al_2O_3	8.8	2.8	55.1	12
S-4.5Cu0.5Ag/γ-Al_2O_3	5.9	1.9	37	17.9
S-0.5Ag4.5Cu/γ-Al_2O_3	9.5	4.3	85.1	7.8
4Cu-1Ag/γ-Al_2O_3	6.7	2.0	40.8	16.6
S-4Cu1Ag/γ-Al_2O_3	5.3	1.6	32.5	20.2
S-1Ag4Cu/γ-Al_2O_3	6.8	2.1	41.6	15.7
15Cu/γ-Al_2O_3	2.6	2.5	16.5	40.6
13.5Cu-1.5Ag/γ-Al_2O_3	2.5	2.3	15.5	42.6

The sequential impregnation catalysts showed that when copper was impregnated first, there was a lower CO chemisorption value compared to when silver was impregnated first. This suggests that the silver is not as effective in adsorbing CO when compared to copper. The 5 wt % catalysts showed metallic surface areas between 1.6-4.3 m^2/g of sample, which is attributed to the metals being well dispersed. At higher metal loadings, the 15 wt %, copper formed larger crystallites, this decreases the metal dispersion. Similarly, when compared to hydrogen chemisorption (Table 3.5), the 15Cu/γ-Al_2O_3 and the 13.5Cu1.5Ag/γ-Al_2O_3 catalysts had a lower CO dispersion due to the large Cu agglomerates found at higher weight loading. All catalysts was between of 2.5 – 10 % metal dispersion, from CO chemisorption.

The CO molecule adsorbs more strongly to acid sites, indicating that the bimetallic simultaneous impregnation catalysts have more acid sites compared to the 5 wt % Cu catalyst. In most cases, CO chemisorption showed a higher metal dispersion than the hydrogen chemisorption. The calculated results are not used for the determination of crystallite size, but to provide information of the acidity of the catalyst surface. Carbon monoxide is a weak base and adsorbed selectively to Lewis acid sites via the sigma bond on alumina surfaces. There is also a possibility that the CO result could be due to both copper and the support surface as shown in work done by Mao *et al.* [194].

In a study of Cu-Co catalysts, strong CO adsorption was attributed to high alcohol selectivity for the FT synthesis. It was reported by Maity *et al.* [195] that CO chemisorption requires either an acidic or basic site, whereas for hydrogen chemisorption, both the acid-base pair must be present. In 2004, Rachel *et al*. [196] reported on the use of CO chemisorption to determine crystallite size, which showed as the copper metal loading increased, the crystallite size also increased.

In most cases, there is a higher quantity adsorbed in the case of CO chemisorption as compared to hydrogen chemisorption, which indicates that the carbonyl group is more readily adsorbed onto the catalyst surface than hydrogen. The higher the quantity adsorbed, the higher metal dispersion obtained. Metal dispersion is calculated using the information obtained from the quantity of gas adsorbed and this is directly correlated to the metal dispersion of the metal on the support.

3.6. Transmission electron microscopy (TEM)

The use of electron microscopy is by far the most common technique used in characterization of catalysts. Depending on the instrument, a wide range of information can be obtained such as particle shape, particle size, surface morphology, surface density, metal dispersion and spatial composition. When combined with EDS, elemental mapping of the catalysts can be achieved. Figure 3.10 shows the images obtained from TEM analyses for all catalysts.

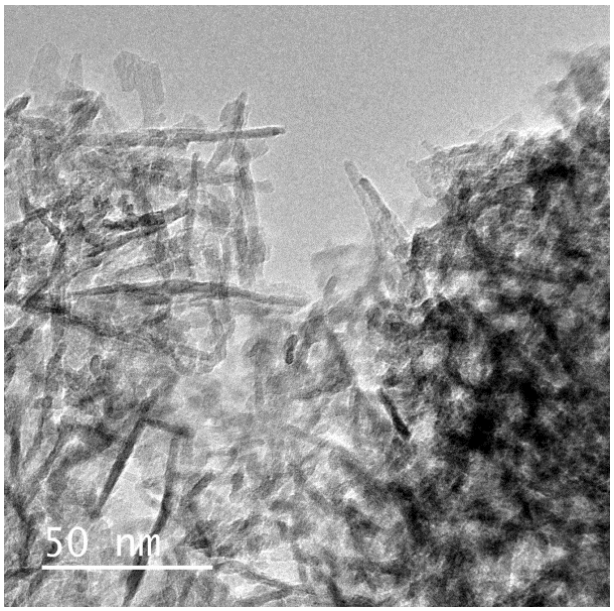

Figure 3.10. TEM image of bare γ-Al_2O_3

Transmission electron microscopy is a technique used to observe and measure particle size and shapes. All catalysts showed long rod-like structures consistent with that of γ-alumina. It has been reported that an increase in the copper loading would be deposited on the surface of the alumina support darkening the particle parameter, which was reported by Chetty [197] where the effect of copper loadings going up to 25 wt % copper supported on γ-alumina was investigated.

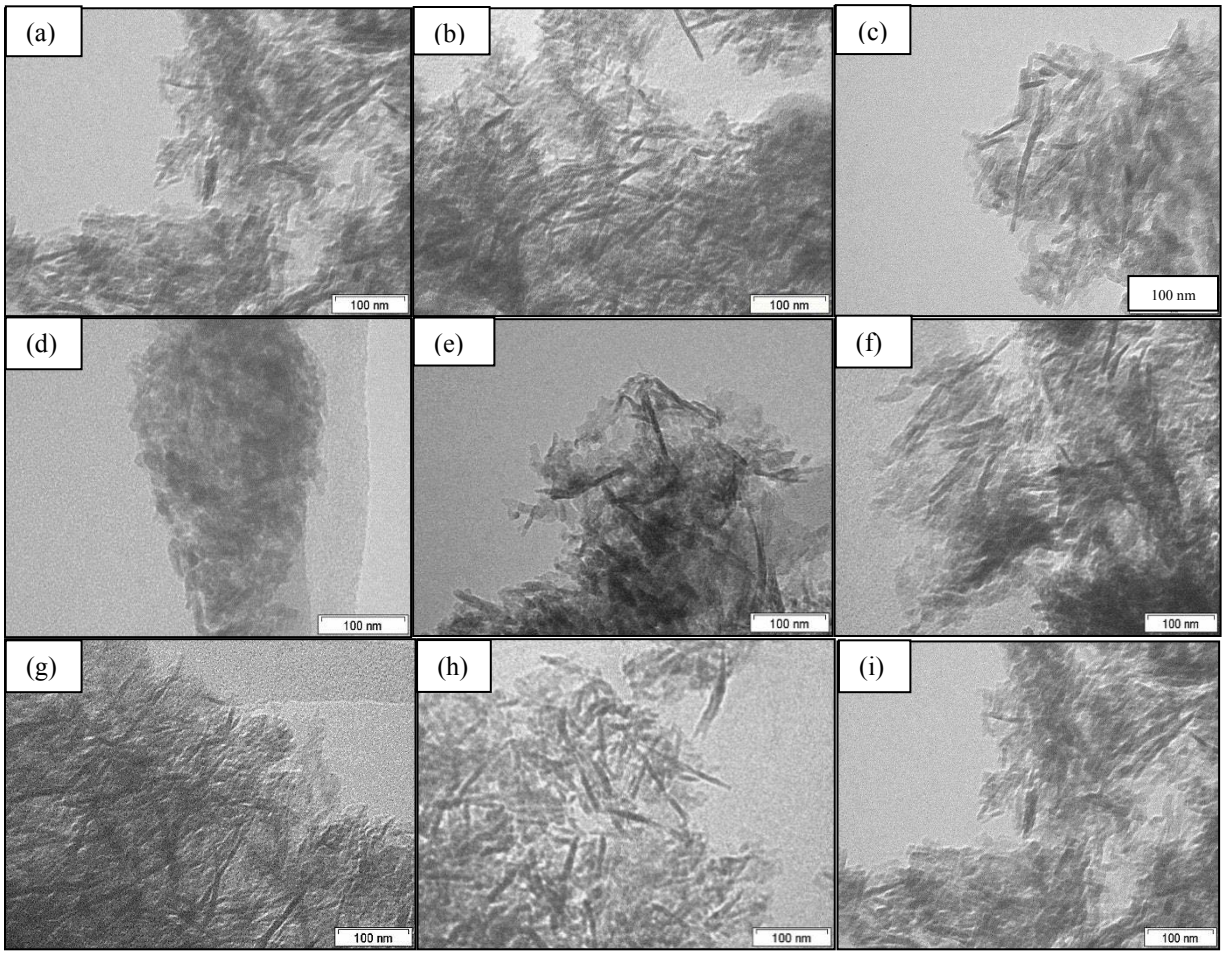

Figure 3.11. TEM images for γ-Al_2O_3 supported with (a) 5Cu, (b) 15Cu, (c)13.5Cu1.5Ag, (d) 4.5Cu0.5Ag, (e) S-4.5Cu0.5Ag, (f) S-0.5Ag4.5Cu, (g) 4Cu1Ag, (h) S-4Cu1Ag, (i) S-1Ag4Cu.

There were no metal oxide particles observed from Figure 3.10a-i, which is due to the low weight loading and the high surface area of the support. This is supported by the results obtained from XRD, where there were no distinct peaks observed due to the good dispersion of copper. γ-alumina is known for its high surface area and mesoporous structure, which favours high dispersion of the copper and silver species onto the support [111]. The bimetallic catalysts prepared in this work have low loading of silver, between the values of 0.5 % to 1.5 %, these weight loadings are most likely too low to show a difference between silver oxide particles and the alumina support. Other techniques were used to obtain a better understanding of the metals on the surface, such as SEM-EDX, XRD and TPR, which are shown in this Chapter.

3.7. Scanning transmission electron microscopy (STEM-EDX)

STEM is a technique used which shows the secondary electrons emitted from the HRTEM instrument. This technique shows the metal particle as brighter spots or regions which can easily be detected against the support at high magnification.

3.7.1. STEM-EDX mapping

STEM EDX was used for the bimetallic catalysts. A map of a bright area of sample on the grid indicates a high metal content region. STEM-EDX analyses were done on selected catalysts to obtain a general understanding of the metal distribution and metal-metal interaction of the 4.5Cu0.5Ag/γ-Al_2O_3, S-4.5Cu0.5Ag/γ-Al_2O_3 and 4Cu1Ag/γ-Al_2O_3 catalysts. This analysis was not conducted on the monometallic catalysts (5Cu/γ-Al_2O_3 and 15Cu/γ-Al_2O_3) as the map will not provide much information of the copper-alumina interaction.

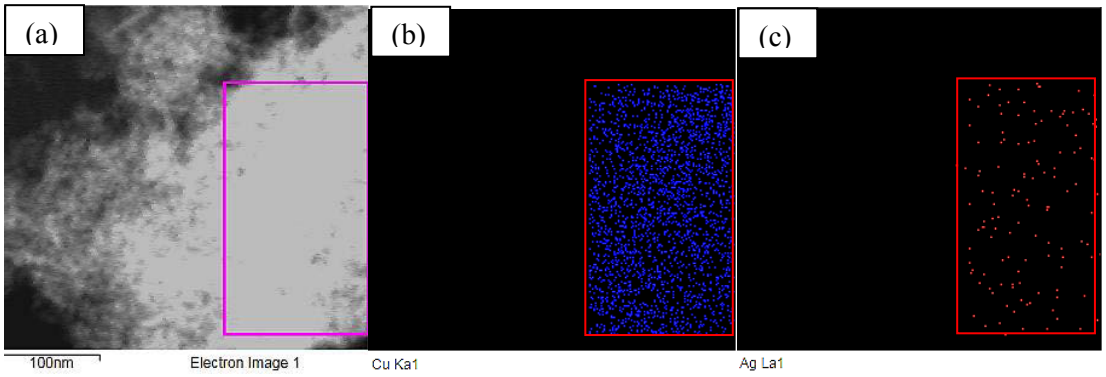

Figure 3.12. STEM-EDX images for 4.5Cu0.5Ag/γ-Al_2O_3 showing (a) dark field image, (b) copper map (blue), (c) silver map (red).

Figure 3.12a-c shows the STEM-EDX image and mapping for the simultaneous 4.5Cu0.5Ag/γ-Al_2O_3 catalyst. Figure 3.12b shows copper to be well dispersed across the support, similar to the silver map shown in Figure 3.12c. The mapping also served as a qualitative technique showing copper being present in a higher quantity compared to silver.

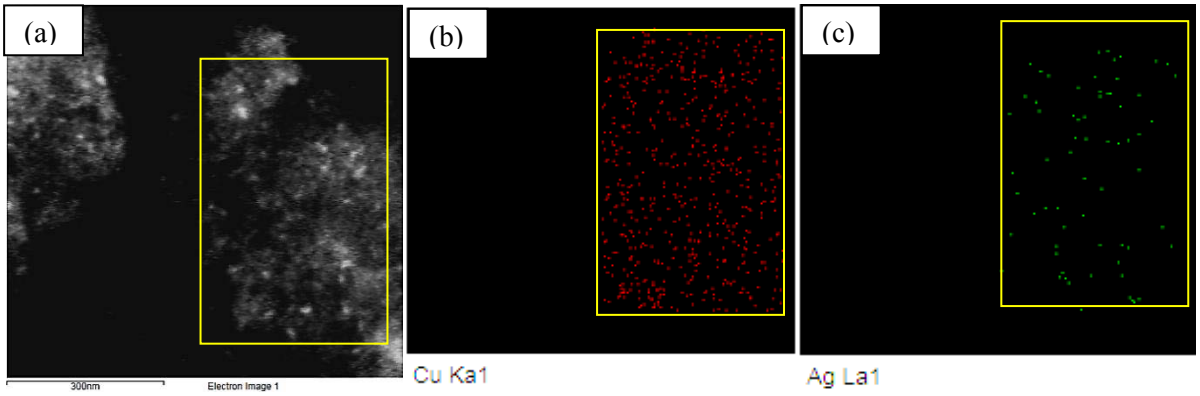

Figure 3.13. STEM-EDX images for S-4.5Cu0.5Ag/γ-Al_2O_3 showing (a) dark field image, (b) copper map (red), (c) silver map (green).

Figure 3.13a-c shows the STEM-EDX for the sequential catalyst where copper was impregnated first (S-4.5Cu0.5Ag/γ-Al_2O_3). Similar to the catalyst prepared in the simultaneous addition method, both copper and silver showed to be well dispersed across the support.

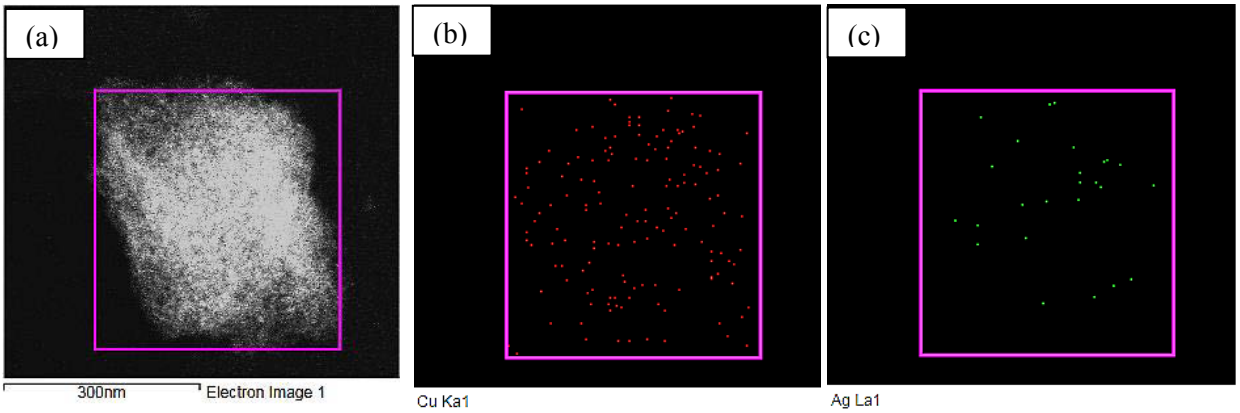

Figure 3.14. STEM-EDX images for 4Cu1Ag/γ-Al_2O_3 showing (a) dark field image, (b) copper map (red), (c) silver map (green).

Figure 3.14a-c shows the TEM-EDX dark field TEM and mapping for the 4Cu1Ag/γ-Al_2O_3 catalyst. Both metals showed good dispersion across the region analyzed. The amount of particles detected in the copper and silver scan is lower, when compared to Figure 3.12. This is due to the lower loading of copper (4 wt %), and the possibility of the formation of larger silver particles due to its higher loading of silver (1 %). This suggests TEM-EDX can be used as a qualitative technique to indicate an estimated metal quantity in a specific region.

3.7.2. STEM-EDX line scan

The mapping showed an even distribution of both metals present on the catalyst surface, however, the composition of the particles could not be determined using mapping. Further characterization using a line scan allows for further information on the particle composition. Figure 3.15 and 3.16 depict the line scans obtained for the 4.5Cu0.5Ag/γ-Al_2O_3 and the S-4.5Cu0.5Ag/γ-Al_2O_3 catalysts.

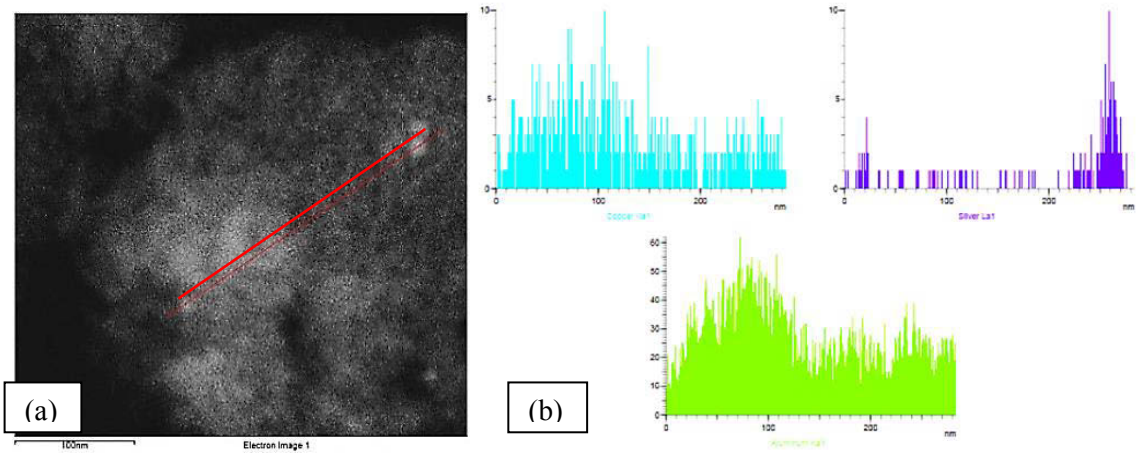

Figure 3.15. STEM-EDX images for 4.5Cu0.5Ag/γ-Al_2O_3 showing (a) line scan image, and (b) line scan spectra for copper (blue), silver (purple), and aluminium (green).

In Figure 3.15, a line scan across a specific region at a high magnification can provide information of the composition and metal-metal interaction between both metals. Aluminium was used as a base line for the support profile. The copper correlates well with the aluminium profile, indicating that the copper has a good dispersion across the support. The silver showed an increase in intensity in the regions of the bright spots which indicates that the particles are largely made up of an agglomeration of silver atoms on the catalyst surface.

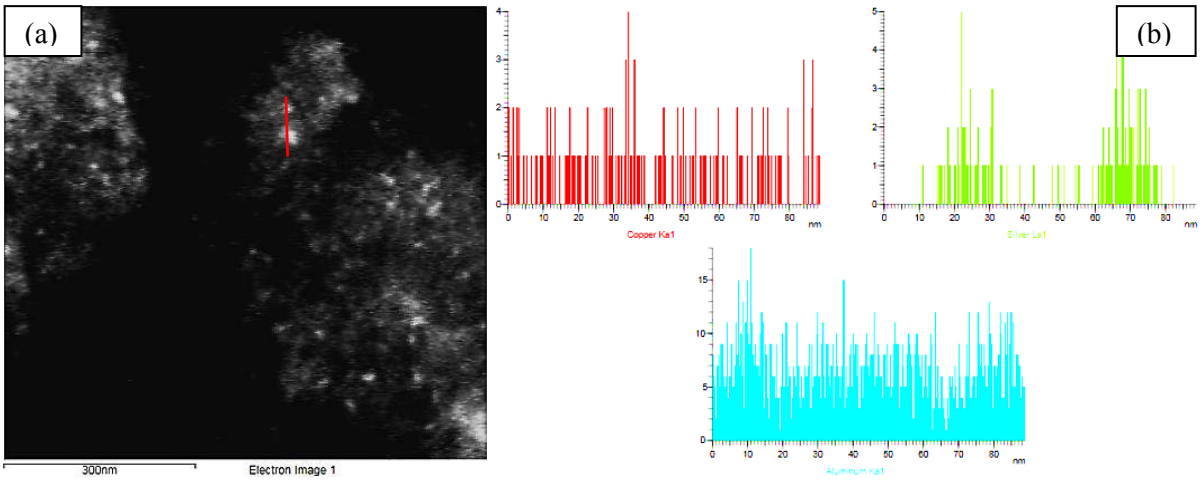

Figure 3.16. STEM-EDX images for S-4.5Cu0.5Ag/γ-Al_2O_3 showing (a) line scan image, and (b) line scan spectra for copper (red), silver (green), and aluminium (blue).

In Figure 3.16, the line scan results obtained for the S-4.5Cu0.5Ag/γ-Al_2O_3 shows a similar trend to the simultaneous 4.5Cu0.5Ag/γ-Al_2O_3 catalyst shown in Figure 3.15. The dark field image showed a higher amount of particles on the surface, this is most likely due to the copper being impregnated first, silver is on the upper layer, which could be detected more easily as seen with the powder XRD results (Figure 3.4). The result remains consistent in that the copper has a good dispersion across the support, with the particles consisting of silver agglomerates.

3.8. Scanning electron microscopy (SEM-EDX)

5Cu/γ-Al_2O_3

The image obtained from the scanning electron microscope shows the morphology of the monometallic copper supported on γ-Al_2O_3. The morphology shows smooth spherical particles of the metal on the support as shown in Figure 3.17. No large CuO peaks are observed at a magnification of 107 000 x confirming the well dispersed CuO species over the alumina support, which is in agreement with the XRD data. The EDS shows an even dispersion of copper on the support as shown in Figure 3.17c-d.

Backscattered images use the principle that the heavier metals will show brighter on the image compared to the support. The backscattered image, shown in Figure 3.17b, does not show any

bright regions due to the well-dispersed copper on the alumina support. Due to SEM and backscattered SEM not showing any particles, EDX mapping was done to illustrate the metal dispersion on the support. The EDX image showed an even dispersion of copper, however, two particles were observed from the results obtained by EDX mapping (in Figure 3.16d). The copper dispersion map confirms that these particles are an agglomeration of copper on the surface. This agglomeration could be due to the bulk CuO or $CuAl_2O_4$.

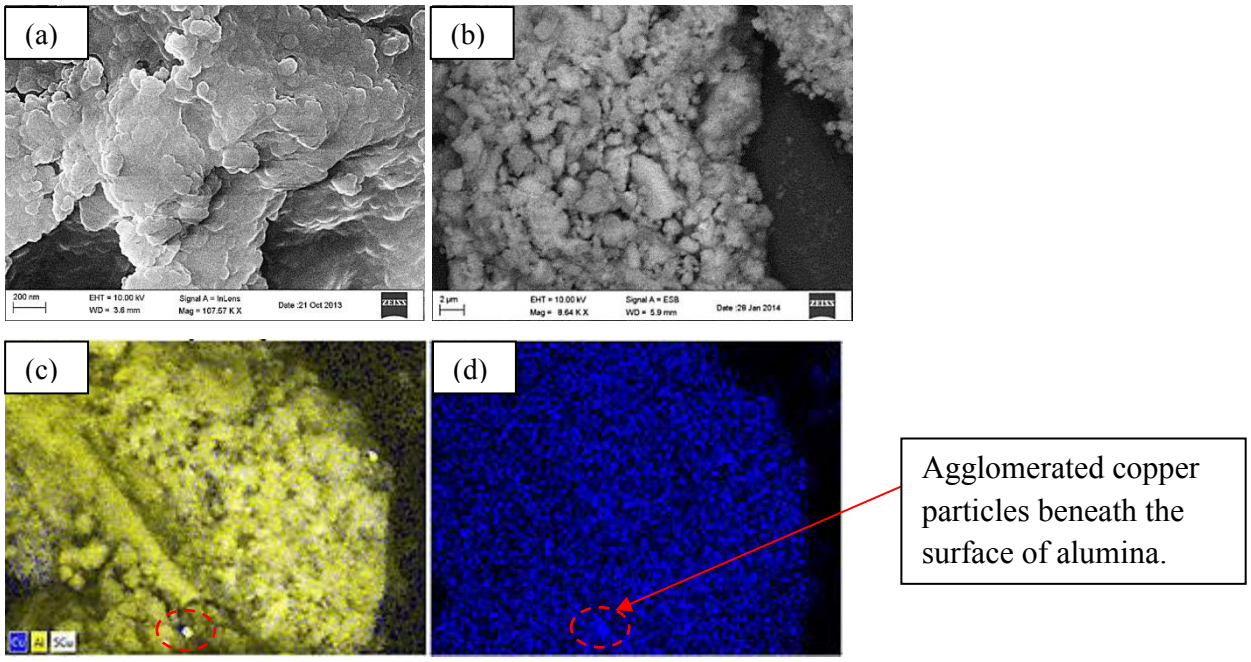

Figure 3.17. SEM image for 5Cu/γ-Al_2O_3 (a) SEM, (b) backscattered image, (c) SEM-EDX, (d) copper mapping (blue).

4.5Cu-0.5Ag/γ-Al_2O_3

Three catalysts containing 4.5 wt % copper and 0.5 wt % silver were prepared using simultaneous and sequential impregnation. Figure 3.18a-c shows backscattered SEM images for the 4.5Cu0.5Ag/γ-Al_2O_3 catalysts.

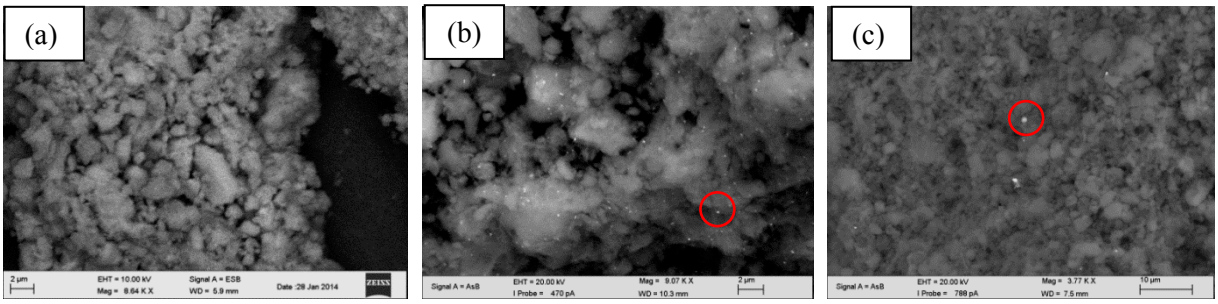

Figure 3.18. Backscattered SEM images of (a) 4.5Cu0.5Ag/γ-Al_2O_3 and (b) S-4.5Cu0.5Ag/γ-Al_2O_3 and (c) S-0.5Ag4.5Cu/γ-Al_2O_3 catalysts.

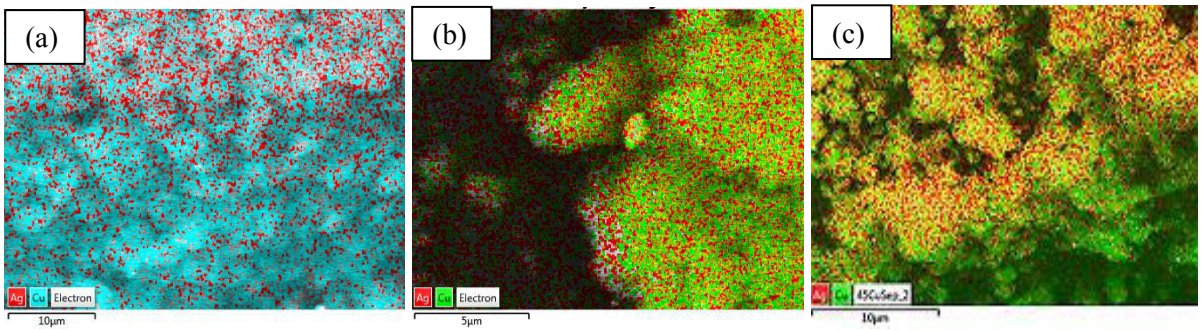

Figure 3.19. SEM-EDX mapping for (a) 4.5u0.5Ag/γ-Al_2O_3- Cu (blue), Ag (red), (b) S-4.5Cu0.5Ag/γ-Al_2O_3 - Cu (green), Ag (red), and (c) S-0.5Ag4.5Cu/γ-Al_2O_3 - Cu (green), Ag (red).

The simultaneously impregnated catalyst (4.5Cu-0.5Ag/γ-Al_2O_3) showed bright particles across the surface indicating that the metals are well dispersed. The S-4.5Cu0.5Ag/γ-Al_2O_3 showed many bright particles across the support, this could be linked to previous results where the bright particles from STEM-EDX (see Figure 3.16) showed bright particles to be made up of silver. The high quantity of bright particles observed in Figure 3.18b is due to the copper being impregnated first with the silver being on the upper layer of the catalyst surface, thus allowing for easy observation using backscattered SEM. The S-0.5Ag4.5Cu/γ-Al_2O_3 (Figure 3.18c) catalyst also shows a presence of metal agglomeration on the surface, this is also a result of sequential impregnation where the silver was impregnated first. The copper impregnated second will not adsorb onto the silver but rather the bare support, which allows silver to be observed clearly using backscattered SEM. The mapping was done on the simultaneous and sequential 4.5Cu0.5Ag catalysts shown in Figure 3.19a-c to obtain information on the metal dispersion at lower magnification compared to the STEM-EDX. The EDX was used to illustrate the metal

dispersion for selected catalysts shown in Figure 3.18a-c. All catalysts analyzed in Figure 3.19a-c showed a good dispersion for both copper and silver, therefore, does not provide enough information to differentiate between the surface characteristics of the catalysts prepared. Line scans were conducted on these catalysts to provide information on the composition of the particles. Figures 3.20-3.22 shows line scans for the 4.5Cu0.5Ag/γ-Al_2O_3 catalysts prepared using the simultaneous and sequential impregnation methods.

3.8.1. SEM line scan

4.5Cu0.5Ag/γ-Al_2O_3 catalyst

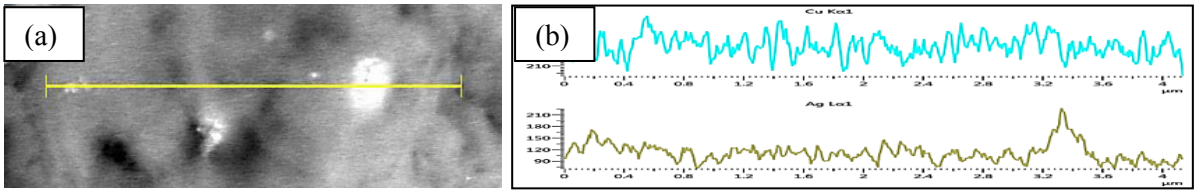

Figure 3.20. SEM image with (a) the line scan and the (b) spectra for 4.5Cu0.5Ag/γ-Al_2O_3 with copper (blue) and silver (dark green).

A region containing a bright spot was analyzed by conducting a line scan across the bright spot as shown in Figure 3.20a with the results of the line scan shown in Figure 3.20b. SEM-EDX and the line scan have a lower magnification compared to the STEM image (Figure 3.13) but the results show to correlation between these surface characterization techniques in that the silver is shown to increase across the bright region, while copper and aluminium showed a similar trend indicating the copper is well dispersed across the support. This is consistent with the results obtained from STEM line scan (Figure 3.15).

Sequential S-4.5Cu0.5Ag/γ-Al_2O_3 and S-0.5Ag4.5Cu/γ-Al_2O_3 catalysts

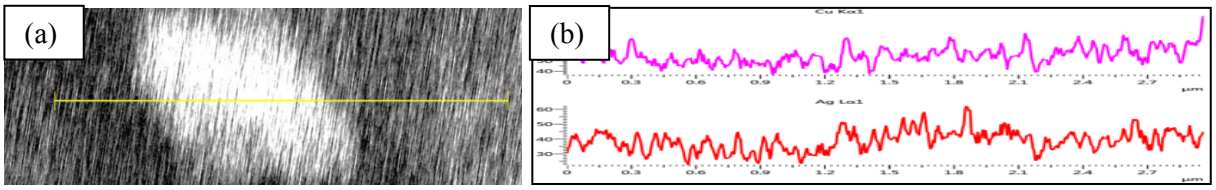

Figure 3.21. SEM image for (a) S-4.5Cu0.5Ag/γ-Al_2O_3 with (b) line scan spectra of copper (pink) and silver (red).

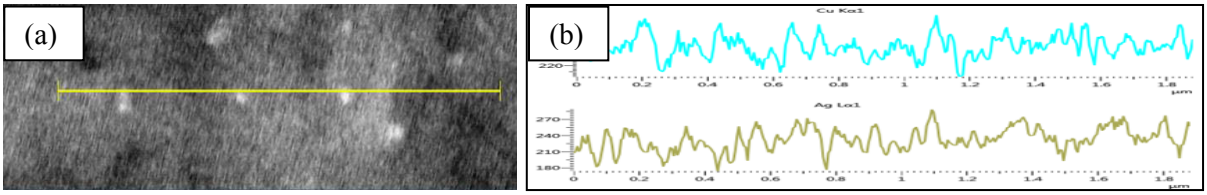

Figure 3.22. SEM image for (a) for S-0.5Ag4.5Cu/γ-Al_2O_3 line scan spectra of copper (blue) and silver (dark green).

In Figure 3.21, the S-4.5Cu0.5Ag/γ-Al_2O_3 line scan showed a more even distribution across a bright region indicating that the small crystalites of silver oxide (shown in XRD) are well dispersed across the support. In Figure 3.22, the S-0.5Ag4.5Cu/γ-Al_2O_3 showed a similar result where both metals are shown to be evenly distributed across the support. The results are evident that the method of impregnation has an impact on the metal distribution, where the simultaneous catalyst showed larger silver particles than the sequential catalysts.

Backscattered SEM proved to be an effective technique in focusing on metal rich areas compared to SEM. This technique provided information on the surface charecteristics of the bimetallic catalysts prepared. This showed that the silver particles are in close contact with copper, which may lead to synergistic effects which can alter catalytic activity. Deng *et al.* [153] showed that that the catalysts prepared by co-impregnated or simultaneous catalysts has a stronger synergistic effect than sequential impregnation catalysts. This strong interaction between copper and silver in the simultaneous impregnation, results in larger particles sizes seen from the line scan results.

15Cu/γ-Al_2O_3

Backscattered SEM showed a larger amount of agglomerated copper particles, which were confirmed from the EDX mapping showed in Figure 3.23a-c. The agglomerated copper is a result of the increased weight loading, which is consistent with the results from XRD (see Figure 3.3), which showed crystalline peaks characteristic of copper oxide. The agglomerated copper also decreases the active metal surface area and this is consistent with the result obtained from both hydrogen and carbon monoxide chemisorption (Tables 3.5 and 3.6). Backscattered SEM and EDX mapping was done for the 15Cu/γ-Al_2O_3 catalyst.

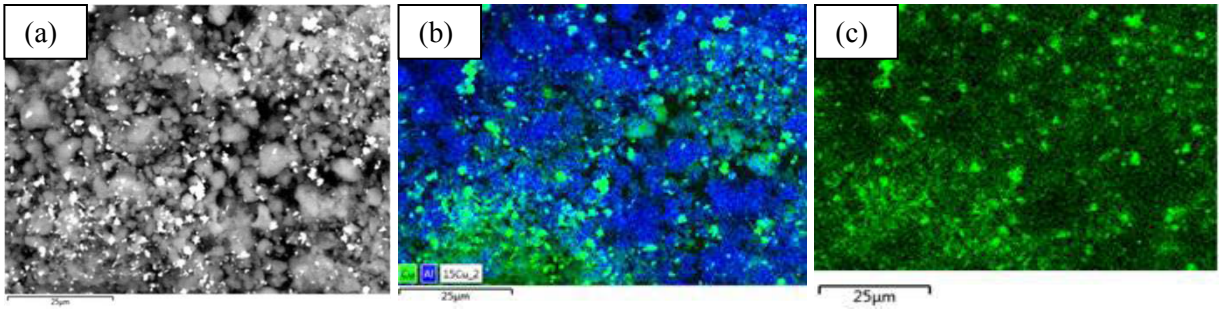

Figure 3.23. SEM images for 15Cu/γ-Al_2O_3 showing (a) backscattered image, (b) EDX mapping with aluminium (blue) and copper (green), (c) copper map (green).

13.5Cu – 1.5Ag/γ-Al_2O_3

SEM imaging showed an irregular morphology consistent with alumina supported catalysts. Figure 3.24a shows a SEM image of 13.5Cu1.5Ag/γ-Al_2O_3. The results obtained remains consistent with the 15Cu/γ-Al_2O_3.

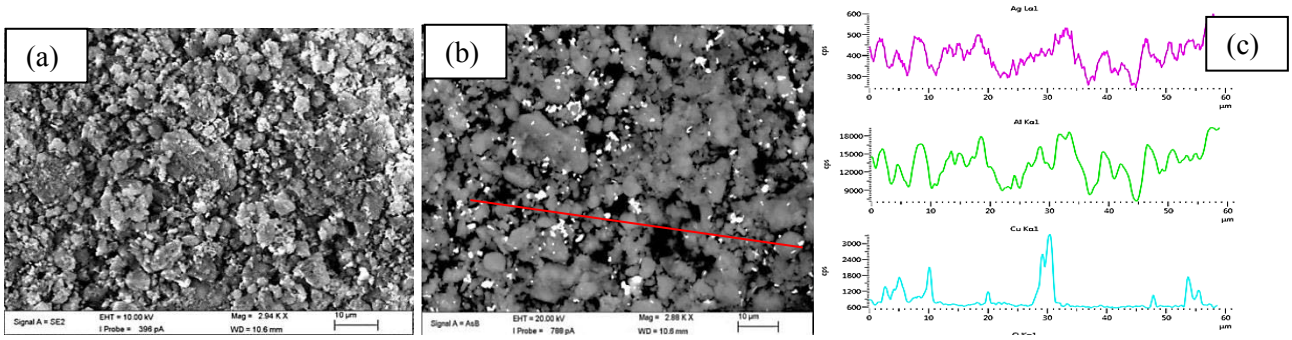

Figure 3.24. SEM images of 13.5Cu1.5Ag/γ-Al_2O_3 (a) SEM image, (b) backscattered image with line scan, (c) spectra obtained from line scan with copper (blue), silver (pink), and aluminium (green).

The backscattered SEM image (Figure 3.24b) for that the 13.5Cu1.5Ag/γ-Al_2O_3 catalyst correlated with the results obtained for the 15Cu/γ-Al_2O_3 catalyst (Figure 3.23), where the larger agglomerated particles are shown as brighter regions on the image. Figure 3.24b-c show the line scan over a region of the backscattered image, confirming that copper has regions of good dispersion, but due to the increased metal loading there are also larger agglomerates in some regions.

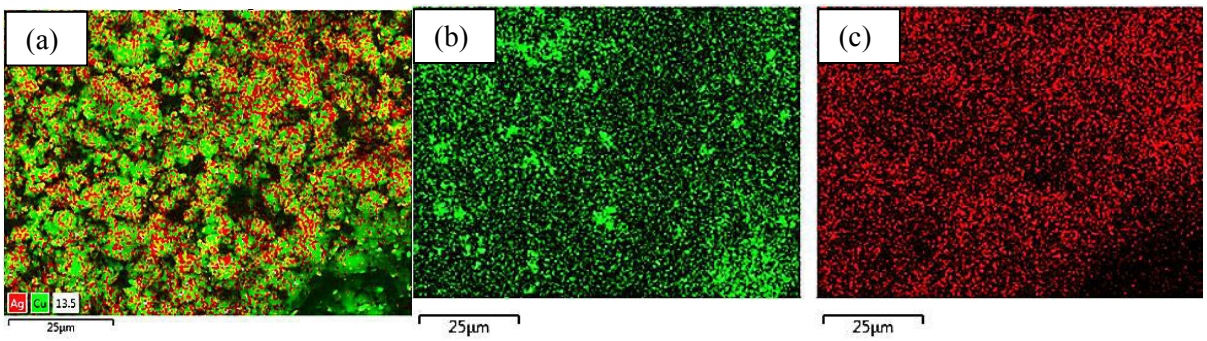

Figure 3.25. SEM images of 13.5Cu1.5Ag/γ-Al_2O_3 showing (a) EDX mapping, (b) copper (green), (c) silver (red).

Figure 3.25a shows the metal mapping of copper and silver. Silver shows to be well dispersed, while copper forms larger agglomerates. The line scan over a specific region allows for an understanding of the composition of the particles shown in the backscattered image. Figure 3.25b-c shows that the larger particles are made up of copper, while silver shows to be better dispersed than copper.

3.9. Temperature programmed reduction (TPR)

The TPR profiles were obtained for all catalysts were conducted to determine the reduction profiles shown in Figures 3.26-3.27. TPR shows the maximum temperature at which the metal reduces and the degree of reducibility of the catalyst.

5Cu/γ-Al_2O_3, 15Cu/γ-Al_2O_3, and 13.5Cu1.5Ag/γ-Al_2O_3

Figure 3.26a-c shows the reduction profile for the 5Cu/γ-Al_2O_3, 15Cu/γ-Al_2O_3 and 13.5Cu1.5Ag/γ-Al_2O_3 catalysts. The 5Cu/γ-Al_2O_3 catalyst shows a single intense reduction peak at 248 °C attributed to well dispersed copper and weakly adsorbed isolated copper ions (Figure 3.26a). Following the defined peak at 248 °C, there is a continuous peak up to 700 °C, attributed to a copper aluminate species ($CuAl_2O_4$).

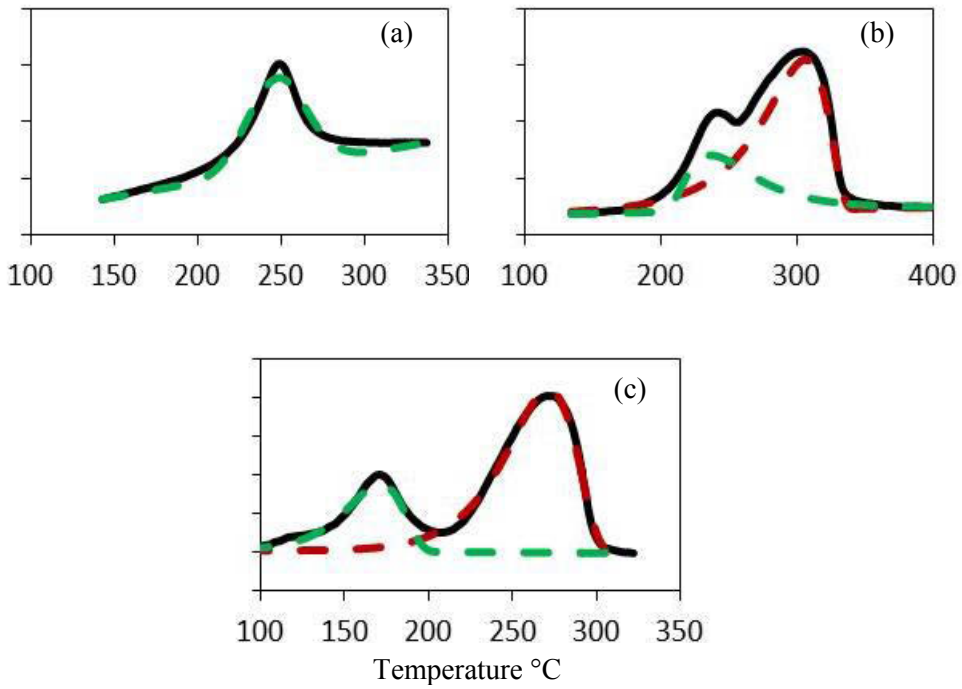

Figure 3.26. TPR profile for the γ-Al_2O_3 supported with (a) 5Cu, (b) 15Cu and (c) 13.5Cu-1.5Ag catalysts.

Kundakovac and Stephanopoulas [170] documented a broad reduction peak from 100 – 500 °C with 1 % Cu supported on γ-Al_2O_3, which was attributed to a copper aluminate phase, resulting from a strong interaction between the isolated copper ions and the support. Liang *et al.* [198] stated that the $CuAl_2O_4$ forms as a result of copper ions filling defect sites of the alumina surface, is reported to occur at calcination temperatures higher than 500 °C due to solid-solid interactions between the metal and support [169, 171, 175, 198, 199]. Within this copper aluminate phase, there is an octahedral surface aluminate, formed by well dispersed copper ions on the surface which is easy to reduce, as well as a tetrahedral spinel phase, which reduces at a much higher temperature.

It was also stated that at weight loadings of approximately 5 wt %, the copper is generally at the surface of the support and found as either copper ions or well dispersed copper [170, 171, 198]. Luo *et al.* [169] reported that Cu/γ-alumina calcined at temperatures of 400 – 600 °C form $CuAl_2O_4$, which occurs via interaction between the metal and support. The extent of copper diffusion is dependent on the calcination temperature, where an increase in calcination temperature increases the amount of copper diffused into the lattice. This is in agreement with

work done on the characterization of Cu/Al_2O_3 by Zhu *et al.* [200] and Friedman and Freeman [171].

Figure 3.25b shows the reduction profile of $15Cu/\gamma\text{-}Al_2O_3$ where two peaks was observed. The first peak was attributed to the well dispersed copper, similar to the 5Cu, while the second peak at a higher reduction temperature was attributed to the bulk CuO. A TPR study done by Dow *et al.* [161], reported on two reduction peaks observed for supported CuO catalysts. The low temperature peak was attributed to the highly dispersed copper and the high temperature peak due to the bulk CuO species [161], consistent with the results obtained in this study.

Garbowski *et al.* [201] explained that during the impregnation step, the Cu^{2+} ions interact with the hydroxyl groups via hydrogen bonding. When calcined, this interaction was increased between the metal and support during the removal of water. Considering that the Cu^{2+} species requires two –OH groups to adsorb to, this indicated that there is an exchange capacity. For high copper loadings (> 6 wt %), there are not enough hydroxyl groups to exchange ions with so it is said to have reached its exchange capacity. Once this exchange capacity has been reached, the bulk CuO species are formed [201]. The higher temperature needed for this bulk CuO reduction is needed because there is a smaller reactive surface due to large clusters of CuO.

Figure 3.25c shows that the peaks of the $13.5Cu1.5Ag/\gamma\text{-}Al_2O_3$ catalyst shifted to a lower reduction temperature for the well dispersed and bulk CuO. There is no silver reduction observed due to the low weight loading of silver, as well as the low reduction temperature of silver, reported to be less than 100 °C. Since silver is known to reduce at low temperatures, the reduced silver species adsorbed hydrogen, which is able to migrate across the silver species, thus reducing the copper faster. Bachiller-Baeza *et al.* [157] reported that the bimetallic Ru-Fe catalyst showed a shift to a lower reduction temperature compared to monometallic iron, this observation was attributed to the presence of ruthenium. A similar result was observed with $Pt\text{-}W/\gamma\text{-}Al_2O_3$ catalysts where the addition of platinum increased the reducibility of tungsten, in work done by Alexeev *et al.* [156].

4.5Cu0.5Ag/γ-Al_2O_3, S-4.5Cu0.5Ag/γ-Al_2O_3, and S-0.5Ag4.5Cu/γ-Al_2O_3

Figure 3.14a-c shows the temperature reduction profile of the simultaneous 4.5Cu0.5Ag/γ-Al_2O_3 and the sequential catalysts S-4.5Cu0.5Ag/γ-Al_2O_3 and S-0.5Ag4.5Cu/γ-Al_2O_3.

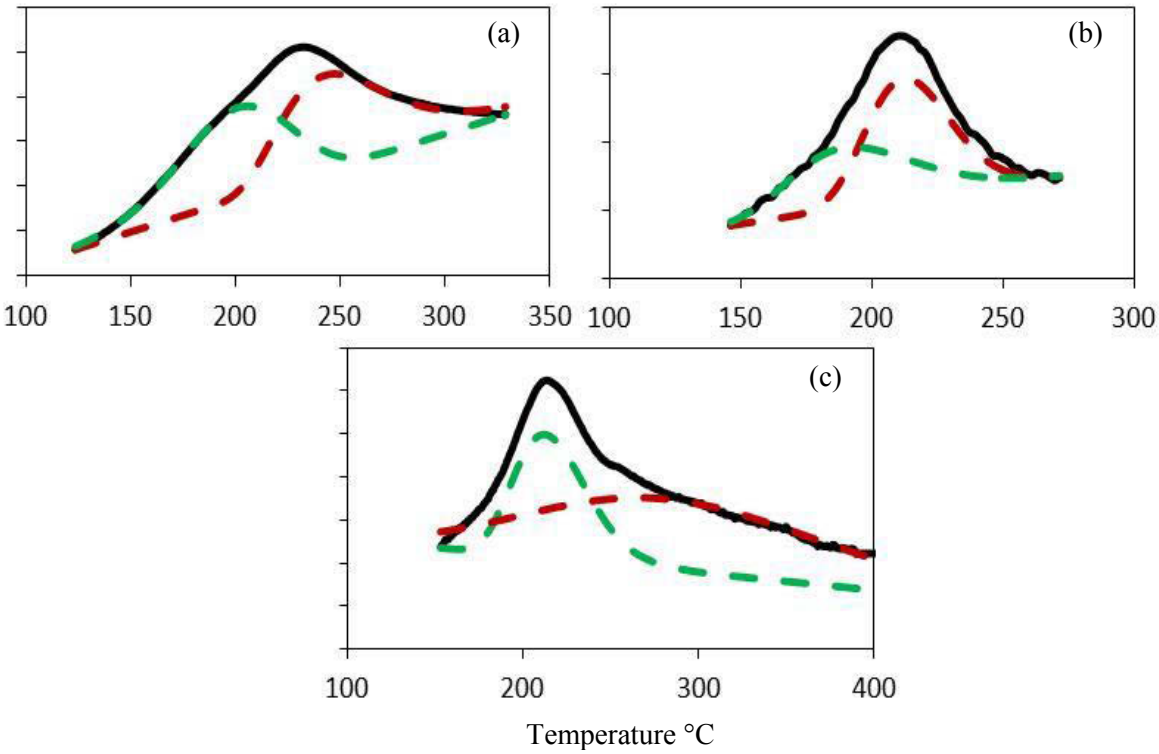

Figure 3.27. TPR profile for the (a) S-4.5Cu0.5Ag/γ-Al_2O_3, (b) S-0.5Ag4.5Cu/γ-Al_2O_3, and (c) 4.5Cu0.5Ag/γ-Al_2O_3 catalysts.

The bimetallic catalyst shows an overlap of peaks at the lower temperature as well as a small peak at the high temperature. Figure 3.27 shows one major peak due to the reduction of copper, however, upon deconvolution it shows a combination of two peaks. The early onset of reduction (shown in green) may be attributed to the copper in close contact with the silver as seen with the 13.5Cu1.5Ag/γ-Al_2O_3 (Figure 3.26c) and results from electron microscopy. The bimetallic catalyst has a low loading of silver; therefore, the silver reduction does not show a defined peak. The electron microscopy results showed the metals present are in close proximity to each other. This intimate contact can lead to a synergistic effect, which may alter the reduction temperature as seen from the results obtained from the reduction study.

The simultaneous impregnated catalyst (Figure 3.27c) showed that after the main reduction peak, there was moderate hydrogen consumption at temperatures greater than 300 °C. This was also

observed for the S-4.5Cu0.5Ag/γ-Al_2O_3 (Figure 3.27a), while the S-0.5Ag4.5Cu/γ-Al_2O_3 (Figure 3.27b), showed a more distinct reduction peak with minor hydrogen consumption after the main reduction peak. This hydrogen consumption is due to the strong interaction between the copper and support surface, which may form a copper aluminate phase. This interaction was also present in the 5Cu/γ-Al_2O_3 catalyst, which is consistent with work done by Luo *et al.* [169] and Zhu *et al.* [200]. The results obtained from TPR analysis is shown in Table 3.7.

Table 3.7. Summary of results obtained from TPR analysis on all catalysts.

Catalyst	Temperature at maximum (°C)	Degree of reducibility of Cu [a]	Average oxidation state of Cu based on H_2 consumed [b]
5Cu/γ-Al_2O_3	248	28	0.3
4.5Cu-0.5Ag/γ-Al_2O_3	215	20	0.2
S-4.5Cu0.5Ag/γ-Al_2O_3	233	20	0.2
S-0.5Ag4.5Cu/γ-Al_2O_3	135, 197	15	0.2
4Cu-1Ag/γ-Al_2O_3	184, 242	10	0.4
S-4Cu1Ag/γ-Al_2O_3	131, 193	12.1	0.3
S-1Ag4Cu/γ-Al_2O_3	158, 203	12	0.3
15Cu/γ-Al_2O_3	236, 299	40	0.3
13.5Cu-1.5Ag/γ-Al_2O_3	167, 271	45	0.4

a. Degree of reducibility = (moles of H_2/moles of reducible Cu)*100
b. Average oxidation state = oxidation state of Cu*(moles of H_2*2/moles of reducible Cu)

The S-4.5Cu0.5Ag/γ-Al_2O_3 catalyst shows higher hydrogen consumption, this is most likely due to the copper being impregnated first, increasing the interaction between the copper and support during the calcination step, whereas when silver is impregnated first, this may inhibit the

interaction between the copper and the alumina surface, thus decreasing the formation of copper aluminate.

Surface area measurements for the S-0.5Ag4.5Cu/γ-Al_2O_3 and 1Ag4Cu/γ-Al_2O_3 catalysts show a lower surface area due to a higher amount of copper on the surface instead of migrating into the lattice, as shown in Table 3.3. This is further supported from chemisorption studies where a higher metal dispersion was obtained for the S-0.5Ag4.5Cu/γ-Al_2O_3 and 1Ag4Cu/γ-Al_2O_3 catalysts silver inhibits the migration of copper into the alumina lattice (Table 3.5 and 3.6). The average oxidation state does not take into account silver, therefore, the value shown is an estimate as both metals gets reduced in the same region, and silver is known to reduce readily. The TPR profiles for the simultaneous and sequential 4Cu1Ag/γ-Al_2O_3 catalysts can be seen in the Appendix.

3.10. Temperature programmed desorption (NH_3-TPD)

The acidity and basicity studies are used to provide information on the surface chemistry and provide information of selectivity to the main product and byproducts. The most recent study, by Czaplinska *et al.* [192], using CuAg bimetallic catalysts, showed that the presence of silver increases the basicity, whereas copper promotes more Lewis acidity, which is in agreement with observations obtained in this study. The 5Cu/γ-Al_2O_3 showed a high concentration of Lewis acid sites (weak and moderate) and strong acid sites, whereas the 4.5Cu0.5Ag/γ-Al_2O_3 and 4Cu1Ag/γ-Al_2O_3 catalysts show a significant decrease in the concentration of acid sites, shown in Table 3.8. The 15Cu/γ-Al_2O_3 has a lower acidity compared to the 5Cu/γ-Al_2O_3, this is due to the higher metal coverage on the surface, which then blocks some of the lewis acid sites of the γ-Al_2O_3 support. Silver is known to increase basicity, this effect is more pronounced with the 13.5Cu1.5Ag/γ-Al_2O_3 catalyst, as this showed the lowest acidity overall, due to the highest loading of silver present.

Sequential impregnation catalysts showed that when copper was impregnated first, as in the case of S-4.5Cu0.5Ag/γ-Al_2O_3, a high acid concentration is obtained, most likely due to the close interaction between the copper and the alumina support. The S-4Cu1A/γ-Al_2O_3 g has a lower

copper to silver ratio of 4:1; the copper shows a lower acid concentration due to the increased presence of silver, which promotes basicity.

Table 3.8. Summary of results obtained from NH_3-TPD analysis on all catalysts.

Catalyst	Acid site concentration /mmol g^{-1}			Total acidity /mmol g^{-1}
	Weak sites (<250 °C)	Medium sites (250 – 450 °C)	Strong sites (>450 °C)	
5Cu/γ-Al_2O_3	0.66	8.95	1.76	11.37
4.5Cu-0.5Ag/γ-Al_2O_3	2.46	0.94	5.41	8.81
S-4.5Cu0.5Ag/γ-Al_2O_3	4.83	3.06	0.48	8.38
S-0.5Ag4.5Cu/γ-Al_2O_3	2.44	1.78	0.37	4.40
4Cu-1Ag/γ-Al_2O_3	2.45	1.56	0.47	4.48
S-4Cu1Ag/γ-Al_2O_3	0.932	0.36	0.50	1.79
S-1Ag4Cu/γ-Al_2O_3	2.17	0.48	2.78	5.43
15Cu/γ-Al_2O_3	3.26	0.62	1.90	5.42
13.5Cu-1.5Ag/γ-Al_2O_3	0.10	0.03	0.07	0.2

This correlates with work done by Czaplinska *et al.* [192] where the increase in basicity was due to the incorporation of silver in a copper-silver bimetallic catalyst system. Likewise, when silver was impregnated first as in the case of S-0.5Ag4.5Cu/γ-Al_2O_3 and S-1Ag4Cu/γ-Al_2O_3, the concentration was significantly lower due to the silver atoms inhibiting or limiting the copper and alumina interaction, which could be seen in the data obtained from chemisorption studies, surface area measurements and acidity studies (Tables 3.3, 3.5, 3.6,and 3.8)

From CO chemisorption results (Table 3.6), it was shown that the presence of silver affected the metal dispersion. The CO chemisorption results was used to provide information on the surface acidity of the catalyst as reported by Mao *et al.* [194]. This correlates with the results obtained

from the NH_3-TPD where the copper-silver bimetallic catalysts showed overall lower catalyst acidity compared to their monometallic counterparts.

3.11. Thermal gravimetric analysis –differential scanning calorimetry (TGA-DSC)

TGA-DSC is used initially to determine calcination temperature of a catalyst by observing the decrease in weight of the catalyst until it reaches a plateau. Figure 3.28 shows an example of an uncalcined catalyst. The initial weight loss (~8 %) from 0 – 150 °C can be attributed to the loss of adsorbed water from the catalyst. The intermediate weight loss (~5 %) from 150 – 250 °C is due to the decomposition of $CuNO_3$ to form CuO. The last weight loss (~6 %) from 250 – 420 °C is due to the interlayer moisture and adsorbed hydroxyl groups from the alumina support. The results of TGA-DSC show that the calcination temperature of 500 °C is sufficient for the formation of CuO and removing interlayer moisture from the alumina support.

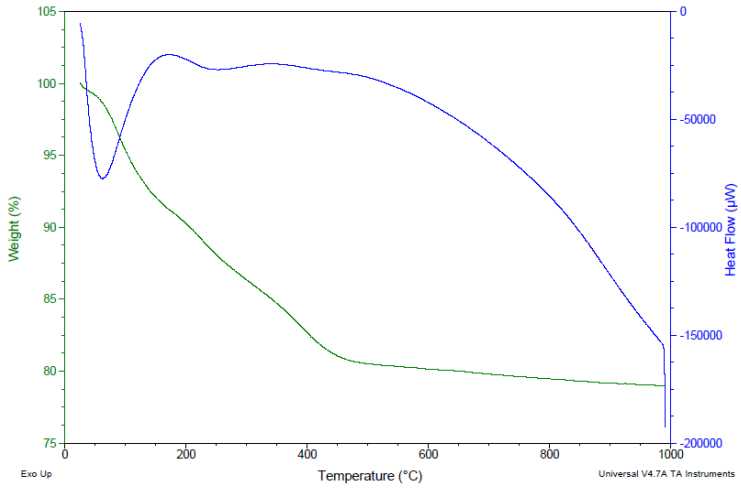

Figure 3.28. TGA-DSC results of 5Cu/γ-Al_2O_3 uncalcined catalyst.

Figure 3.28 shows the TGA-DSC of the uncalcined catalyst. This mainly shows the weight loss of approximately 12-15 wt % due to the adsorbed moisture on the catalysts, this is due to the hygroscopic nature of the alumina support which easily absorbs moisture at room temperature. TGA-DSC experiments were done on selected catalysts, as there is no significant variation between the results obtained.

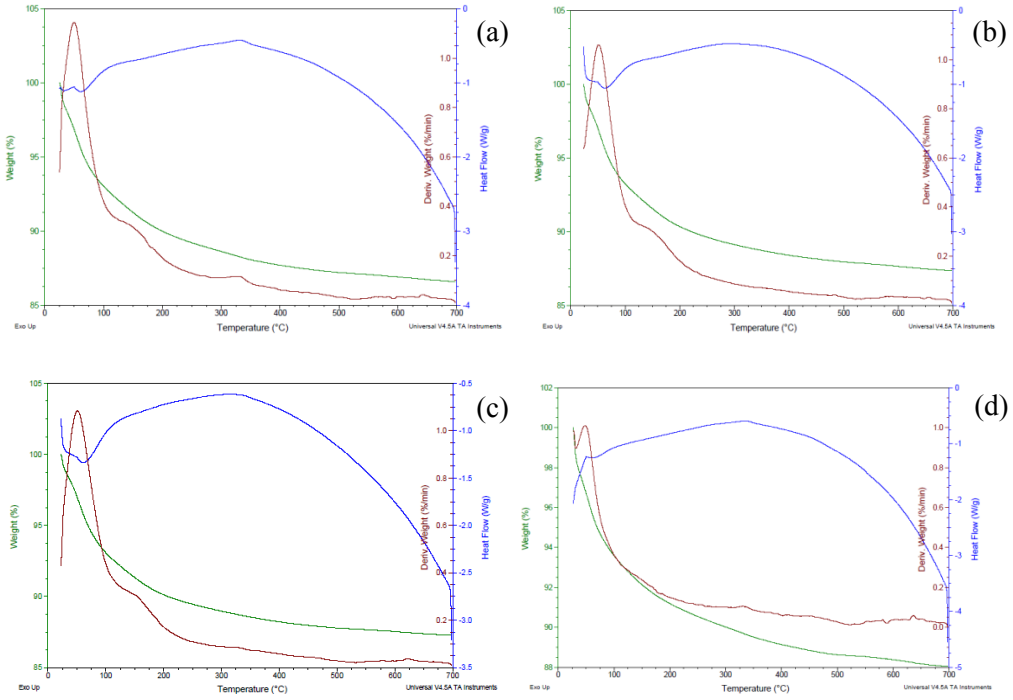

Figure 3.29. TGA-DSC results for uncalcined (a) 4.5Cu-0.5Ag/γ-Al_2O_3, (b) 4Cu-1Ag/γ-Al_2O_3, (c) 13.5Cu-1.5Ag/γ-Al_2O_3 and (d) 15Cu/γ-Al_2O_3 catalysts.

Figure 3.2a and b shows a total weight loss of approximately 20 %, which is due to the adsorbed water due to the hydroscopic nature of alumina, as well as the water within the interlayers of the support. The Figure 3.30c-d shows a weight loss of approximately 10 %, this is significantly lower than for the 5 wt % catalyst due to the higher metal loading covering a higher surface area compared to the 5 wt % catalysts. This increased metal loading decreases the amount of water able to adsorb onto the alumina support.

3.12. Summary

The characterization techniques used in this work provided useful information in an effort in understanding the surface composition and metal-metal interaction for the nine catalysts prepared. All weight loadings obtained using ICP-OES showed to be close to the theoretical values, allowing for an accurate comparison between the catalysts using the various characterization techniques.

Infrared spectroscopy does not give much insight into the metal-support interaction; however, it did confirm the hygroscopic nature of alumina due to the presence of the broad hydroxyl peak at ~ 3200 cm^{-1} and the adsorbed water at 1600 cm^{-1}. X-ray diffraction proved a useful tool to determine the presence of copper clusters at higher weight loading (>13 wt % Cu). For the 5 wt % catalysts, XRD has limited use in determining the crystallites for all catalysts, however, the S-4.5Cu0.5Ag/γ-Al_2O_3 showed crystalline silver oxide present due to the silver being on the upper layer resulting in well dispersed silver. A synergistic effect between the copper and silver were observed under *in situ* conditions, whereby the presence of silver showed to increase in the d-spacing values of the copper peaks, suggesting the presence of defect sites in the 4.5Cu0.5Ag/γ-Al_2O_3 catalyst. The 4Cu1Ag/γ-Al_2O_3 catalyst did not show this behavior due to the silver having a higher affinity to other silver atoms rather than copper atoms.

Surface area measurements showed a decrease in surface area with an increase in metal loading as well as a decrease in surface area when silver was impregnated first, as shown with the S-0.5Ag4.5Cu/γ-Al_2O_3 and S-1Ag4Cu/γ-Al_2O_3 catalysts. A few key differences were established depending on the effect of impregnation with the 5 wt % bimetallic catalysts due to the ionic radius of the metals, which showed to contribute significantly to the surface area measurements and metal dispersion from chemisorption studies. An example is the S-0.5Ag4.5Cu/γ-Al_2O_3 catalyst, which showed a higher metal dispersion compared to when copper was impregnated first. This trend remained consistent for the 4Cu1Ag/γ-Al_2O_3 catalysts.

Electron microscopy results showed that both the metals were well dispersed in all catalysts, with copper forming larger agglomerates at higher weight loadings. The line scan proved to be an effective method in determining distinct differences for particle composition of the sequential and simultaneous bimetallic catalysts. Simultaneous impregnation showed copper to be evenly dispersed across the support, with silver forming agglomerates in certain regions in addition to be fairly dispersed across the support. The S-4.5Cu0.5Ag/γ-Al_2O_3 and S-0.5Ag4.5Cu/γ-Al_2O_3 showed that copper was well dispersed with silver forming smaller agglomerates across the support, which was supported by XRD results.

The monometallic copper results were in correlation with literature, which showed well dispersed copper particles across the surface of the support. Dispersion also depends on weight loading with TPR differentiating between bulk CuO (~ 15 wt% Cu loading) and dispersed CuO

(~ 5 wt % loading). The TPD results showed acidity to vary with the impregnation sequence and metal loading. The overall observation was that the presence of silver increased the basicity of the catalyst as shown by the decreased acid sites concentration. TGA was used to determine the thermal stability of the catalysts. The TGA results for selected catalysts showed them to be thermally stable, with the weight loss being due to the removal of water.

Chapter 4
Catalytic Results and Discussion

The work carried out involved the hydrogenation of octanal in the presence of octene in a competitive reaction environment. The catalysts used were CuAg/γ-Al_2O_3 with varied Cu-Ag ratios. The catalysts were synthesized and characterized was discussed in Chapter 3.

The feed used consisted of 10 % octanal, 2 % octene and 88 % octanol to investigate the ability of the catalyst to selectively hydrogenate the octanal whilst minimizing or inhibiting the hydrogenation of the octene. Octanol is used as a diluent and is also the desired product from the octanal hydrogenation. Studies have shown octanol as a diluent, to have no effect on the overall result [197]. Due to the exothermic nature of octanal hydrogenation, the octanal quantity in the feed was kept at 1 0%, with octene at 2 %, as it is a byproduct and serves as a model of an unwanted component in an industrial feed. It has been reported that in the hydrogenation of aldehydes, minor byproducts like 2-hexyl decanol, octyl octanoate, C16 diol, and C24 acetal may form [60]. The undesired reaction forms octane from the hydrogenation of octene.

4.1. Optimization of reaction conditions using monometallic copper catalysts

Characterization showed that Cu/γ-Al_2O_3 has high surface area, with copper having a good dispersion as shown from TPR and SEM-EDX studies (sections 3.8 and 3.9). Based on previous work done on Cu/γ-Al_2O_3 catalysts, it was shown that this catalyst was stable for at least 28 hours [71], therefore, no time on stream reactions were conducted for the optimization study. Reactions for this study were conducted over a period of 8 hours, and tested at three temperatures (120, 140, and 160 °C). Pre-treatment of the catalyst involved drying under nitrogen at 200 °C, thereafter reduced using 100 % hydrogen. The liquid feed was fed through a continuous fixed bed reactor as explained in Chapter 2.

4.1.1. Effect of pressure using the 5Cu/γ-Al_2O_3,

Based on previous work done for this catalytic system, the optimum temperature was reported to be 140 °C [197]. This temperature of 140 °C was chosen as the initial reaction temperature with the variable pressures being investigated.

Figure 4.1a shows that the increase in pressure resulted in increased conversion of octanal and octene, with the maximum octene conversion reaching 12 % with complete selectivity towards octane. The increase in pressure increased the interaction between the incoming reactants with the catalyst; therefore, the increase in conversion was observed. Figure 4.1a showed the selectivity towards octanol. There is no significant difference in selectivity from 95 to 96 % with the increase in pressure from 10 bar to 50 bar.

Figure 4.1b shows the byproducts formation with C16 diol as a major byproduct as a result of aldol condensation, with other minor byproducts being 2-hexyl decanol, octyl octanoate, C24 acetal and others, which include octanoic acid, C16 saturated alkane and octyl ether. The increase in octanol selectivity leads to a decrease in the formation of the byproducts, however, an increase in C16 diols was observed, with an increase in pressure.

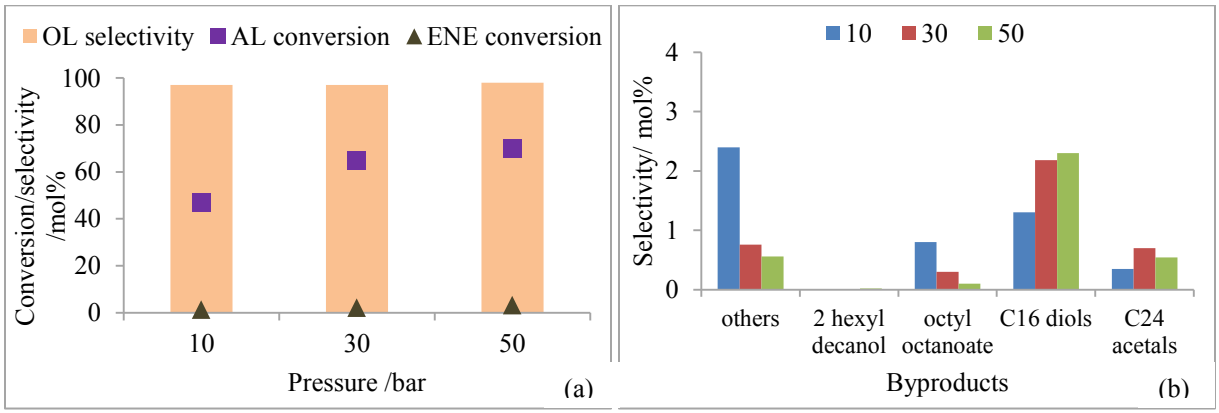

Figure 4.1. Graphs depicting the effect of pressure at 140 °C in terms of (a) octanal and octene conversion and selectivity to octanal, and (b) selectivity towards byproducts on the 5Cu/γ-Al_2O_3, using a 1:2 octanal:hydrogen ratio, and 18h^{-1} LHSV with 532 h^{-1} GHSV. The catalyst was reduced at 240 °C.

The hydrogenation of butanal in work done by Zakzeki *et al.* [26], showed an increase in conversion with the increase in pressure. Results showed a 60 % increase in conversion when the hydrogen pressure was increased from 0.75 MPa to 3.5 MPa indicating that relatively higher pressures favour hydrogenation, although the influence on selectively was not reported [26]. Additionally Sharma *et al.* [53] attributed the increase in conversion of the aldehyde with increase in pressure, in work done for the hydroformylation of 1-hexene, to the higher quantity of hydrogen present at higher pressures [53]. An increase in hydrogen pressure favoured ethane hydrogenation in work done by Kiss *et al.* using a rhodium based catalyst [202]. This correlates with the result obtained for octene conversion observed in this study, with the octene conversion increasing with higher pressures (Figure 4.1a). Bron *et al.* [131] observed an increase in conversion with an increase in pressure using a silver based catalyst. They attributed this trend to the higher surface coverage of hydrogen at higher pressures, thus resulting in higher conversion supporting the results obtained in Figure 4.1a.

4.1.2. Effect of reduction temperature on the 5Cu//γ-Al_2O_3

In three separate experiments, fresh catalysts were reduced at three different temperatures, which were at 220, 240 and 260 °C. With each of these catalysts, reactions were conducted at temperatures ranging from 120, 140, and 160 °C at 50 bar pressure. The results are shown in Figure 4.2a-c. There has not been extensive work done on the effect of reduction temperature and its effect on catalytic performance, allowing a few possible reasons to explain the significant effect on conversion for both substrates, with a change in reduction temperature.

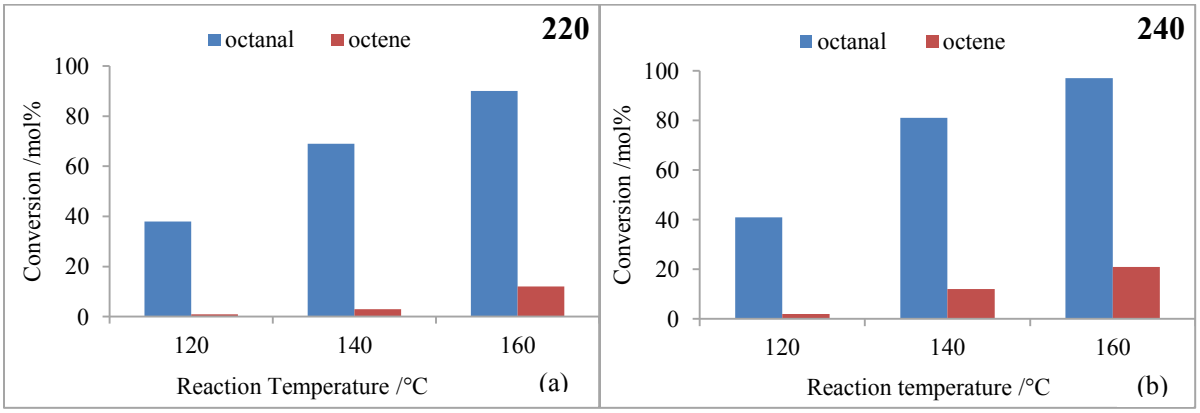

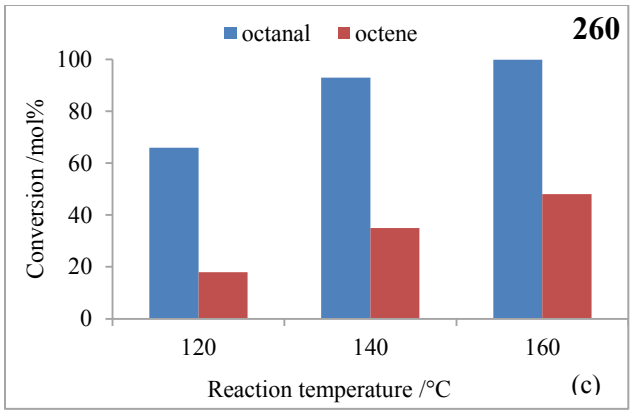

Figure 4.2. Conversion of octanal and octene at temperatures 120, 140, and 160 °C which were reduced at (a) 220, (b) 240, and (c) 260 °C. All reactions were performed at 50 bar, LHSV: 18 h^{-1}, and octanal:hydrogen ratio of 1:2 on the 5Cu/γ-Al_2O_3 catalyst.

Figure 4.2a-c shows that irrespective of reduction temperature, the increase in temperature resulted in the increase in conversion of octanal and octene. This is consistent with work done by Ma *et al.* [186] for their work on the characterization of copper particles on graphite nanofibers. From Figure 4.2a, the increase of temperature resulted in the increase of conversion reaching a maximum of 90 % conversion of octanal, and 12 % octene conversion at 160 °C.

Figures 4.2a-c shows that with an increase in reduction temperature, there is an increase in the conversion of octanal and octene. At a reduction temperature of 220 °C, the highest reaction temperature (160 °C) gave conversions of octanal and octene of 90 % and 12 % respectively. The highest reduction temperature of 260 °C showed conversions of octanal and octene reaching a maximum of 100 % and 48 % at a reaction temperature of 160 °C. Stolle *et al.* [62] showed the effect of reduction temperature on Pt/TiO_2 catalysts, which showed an increase in conversion of citral, with the increase in reduction temperature. The increase in reduction temperature can be concluded to have an overall negative influence, as a key objective is to prevent or inhibit octene conversion; therefore, the optimum reduction temperature was chosen to be 220 °C. Although the high reduction temperature produces an undesired effect, and is not suited for optimum results in this study, the contribution of the reduction temperature towards the catalyst performance was interesting.

Literature shows hydrogenation is favoured on certain types of sites, for example carbonyl groups hydrogenate on large particles and planes, whereas alkene molecules prefer to hydrogenate on edges and kinks [177]. This does not mean the hydrogenation of a specific substrate is site exclusive to edges or corners, but merely provides information of the surface interaction. Menon and Prasad [203] observed a similar result using a Cu-Al_2O_3-carbon catalyst applied in dehydrogenation. The exponential increase in metal dispersion with the increase in reduction temperature observed was attributed to the copper becoming more exposed on the support surface. A characterization study of copper containing catalyst, by Dandekar and Vannice [184], show that the increase of reduction temperature shows a lower CO chemisorption uptake and the crystallite size calculated using XRD showed a minor increase. There are many possible reasons, which could explain the increased activity, which would require a greater understanding of the surface characteristics. There has been significant work done to investigate the role of reduction temperature of copper catalysts, however it can be concluded from these efforts that in-depth characterization and understanding of the copper metal on the surface are important. The reasons are listed below:

(a) Sintering occurs when metal atoms become mobile and agglomerate on catalyst surface [4, 5]. Sintering is favoured at high temperatures for prolonged periods of time, as it provides sufficient energy for the metals to become mobile. At the highest reduction temperature (260 °C), the catalyst is reduced under 100 % hydrogen for 12 hours. This may provide a favorable environment for sintering to occur. Characterization studies showed copper to be well dispersed at low weight loadings, as well as the possibility of strong copper-alumina interaction and copper-aluminate phases present, which would affect the hydrogenation capability of the catalyst. To prove sintering of copper after reduction, the used catalyst characterization would assists in identifying key differences between the catalysts reduced at different temperatures.

(b) Migration of copper could occur from the alumina lattice to the surface of the support. It has been reported in literature that the increase in calcination temperature causes copper atoms to migrate into the alumina lattice decreasing the amount of copper atoms on the surface [171]. Calcination is a process where the catalyst is heated under flowing air to convert the metal salts into metal oxide on the catalyst. Using a similar logic, the

reduction of the catalyst involved the metal oxide being heated under a flow of hydrogen gas, converting the metal oxide to the reduced metal. This reducing environment can cause the migration of copper oxide from the lattice to the surface, which is then reduced on the surface exposing more active sites. Techniques such as Electron Spectroscopy for Chemical Analysis (ESCA) and Low energy ion scattering spectroscopy (LEISS) analyze the surface of the catalyst whereby the intensity ratio between Cu/Al can be obtained. These techniques are expensive, and due to the high reduction temperature not chosen as one of the optimum parameters, this will not be further investigated for a Masters study, however it will be investigated for a more detailed doctorate study. Hydrogen chemisorption can be used as a supporting technique, where the increase in reduction temperature resulted in a higher metal dispersion as shown in Chapter 3, Table 3.5.

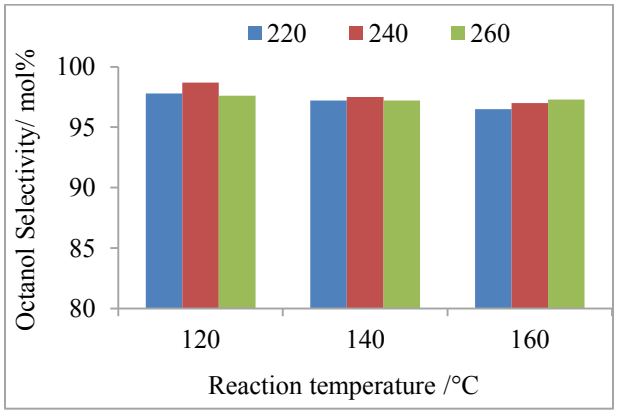

Figure 4.3. Selectivity towards octanol is shown at various reduction temperatures. All reactions were performed at 50 bar, LHSV: 18 h^{-1}, and octanal:hydrogen ratio of 1:2 using the 5Cu/γ-Al_2O_3 catalyst.

Figure 4.2a-c showed the reduction temperature had a significant influence on the conversion of octanal and octene, while Figure 4.3 shows that the reduction temperature did not have a strong influence on the selectivity towards octanol which ranged from 97 – 99 % across the different reaction temperatures and reduction temperatures. The 5Cu/γ-Al_2O_3 catalyst showed a low metal dispersion and metallic surface area from chemisorption studies (Table 3.5 and 3.6). This suggests that there is a large area of bare alumina, which can also interact with the incoming substrates. Figure 4.4 shows the major byproducts, which can form on the active metal sites as

well as the support, which contains both acidic and basic sites. As discussed by Wang *et al.* [60], the hydrogenation of octanal can undergo further reactions such as aldol condensation resulting in the formation of C16 diol, 2-hexyl decanol, octyl octanoate and C24 acetal. Minor by-products include octyl ether, octanoic acid, and C16 saturated alkanes make up the other products, which were confirmed by GC-MS (see Appendix). The reduction temperature of 220 °C offers a higher selectivity to C16 diols, while higher reduction temperatures (240 and 260 °C) show the formation of C24 acetals, indicating a change in the catalyst surface. The reduction temperatures at 240 and 260 °C show that with the increase in reaction temperature, there is an increase in the formation of C16 diol and C24 acetals. The higher reaction temperature across all reduction temperatures investigated shows an increase in aldol condensation products, which form on acidic and basic sites, on the 5Cu/γ-Al_2O_3 catalyst, as shown in Figure 4.4.

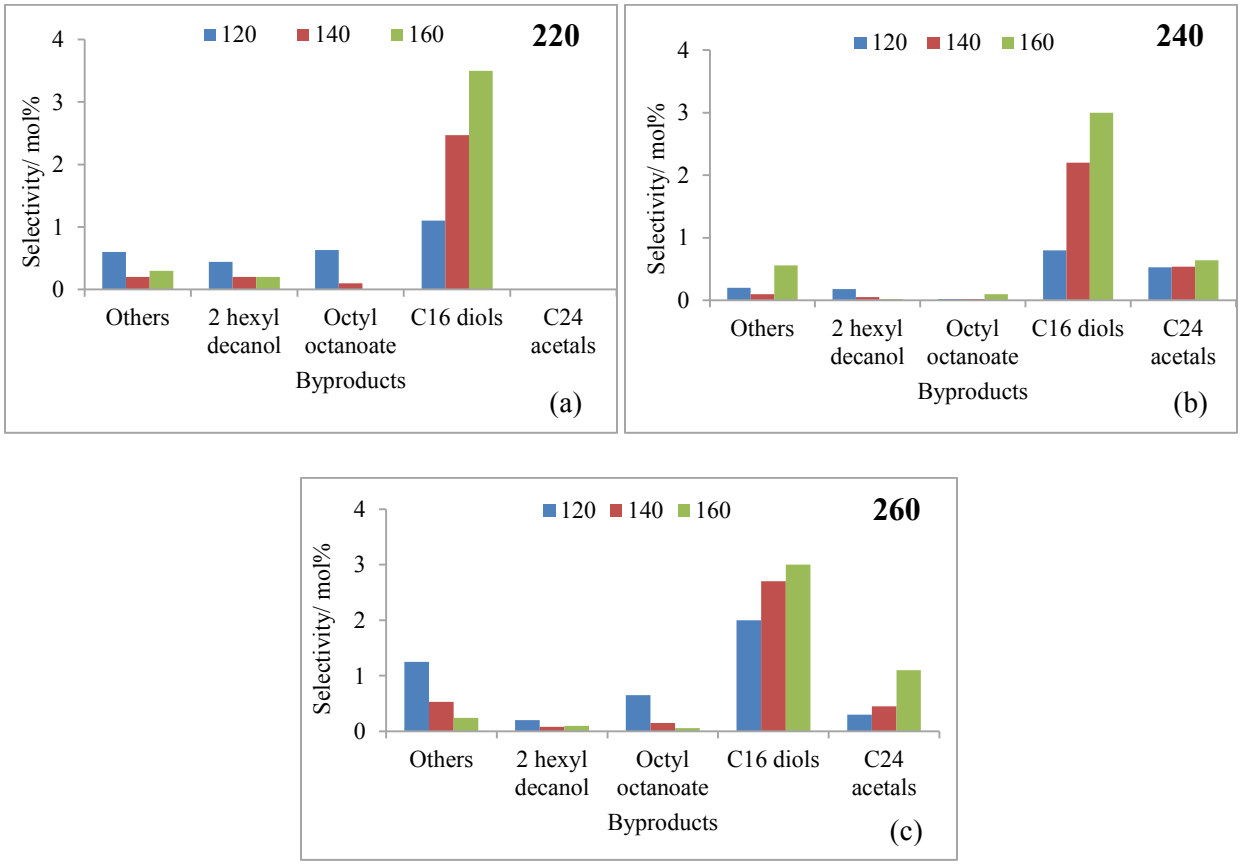

Figure 4.4. Selectivity towards byproducts is shown at various reduction temperatures and with reaction temperatures (a) 220 °C, (b) 240 °C, and (c) 260 °C. All reactions were performed at 50 bar, LHSV: 18 h^{-1}, and octanal:hydrogen ratio of 1:2 using the 5Cu/γ-Al_2O_3 catalyst.

4.1.3. Effect of temperature on a 15 wt% Cu/γ-Al_2O_3 catalyst

Generally, with more active metal present, the catalyst would be expected to show a higher activity as seen by Sun *et al.* [150] and Kusama *et al.* [204]. The metal loading was increased by a factor of 3 to determine the effect of metal loading for the selective hydrogenation of octanal in the presence of octene. The 15Cu/γ-Al_2O_3 catalyst was used to investigate factors such as the effect of LHSV and the effect of octanal:hydrogen ratio. Figure 4.5a-b shows the results obtained using the 15Cu/γ-Al_2O_3 catalyst at temperatures ranging from 120, 140, and 160 °C at an LHSV of 18 h^{-1} and a 1:2 octanal to hydrogen ratio. These conditions were chosen as the initial parameters based on results obtained from previous work done in the selective hydrogenation of octanal in the presence of octene.

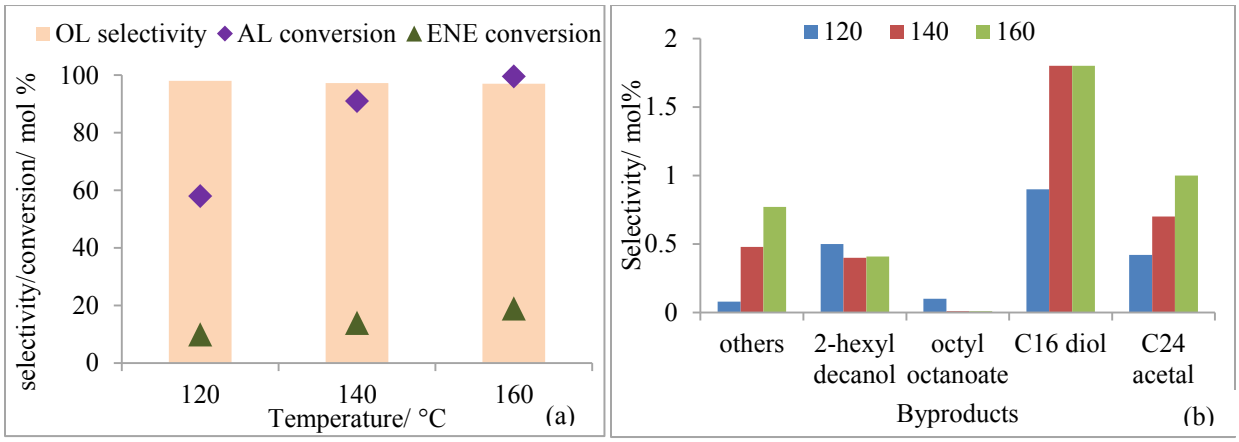

Figure 4.5. Graphs depicting the effect of temperature on a 15Cu/γ-Al_2O_3 catalyst in terms of (a) octanal and octene conversion and selectivity to octanol, and (b) selectivity towards byproducts on the 15Cu/γ-Al_2O_3 using a 1:2 octanal:hydrogen ratio and 18h^{-1} LHSV under a range of temperatures from 120 – 160 °C.

The increase in metal loading from 5 wt % to 15 wt % showed a positive influence on the overall activity of the catalyst. The study of the effect of metal loading was conducted over a range of temperatures to compare the results with the 5Cu/γ-Al_2O_3 catalyst. The results showed that in all cases the 15Cu/γ-Al_2O_3 catalyst gave an improved conversion of the octanal reaching a maximum of 100 % octanal conversion at 160 °C. The major drawback of increased metal loading was the increase in octene conversion, which ranged between 10 – 20 % over the temperature range 120, 140, and 160 °C shown in Figure 4.5a. This increased conversion is

attributed to the increased active sites available, which are able to adsorb and interact with a larger amount of incoming reactants. From TPR results, the 15Cu/γ-Al_2O_3 catalyst showed two peaks for the well-dispersed copper and bulk CuO (Figure 3.25). Under reaction conditions, the bulk Cu has been reported to favour the hydrogenation of carbonyl molecules [169]. It was also observed that with the increase in conversion of the octanal, there was a decrease in the selectivity towards octanol from 98 % at 120 °C to 95 % at 160 °C. This indicated that the increase in temperature provides more energy to allow for further reactions resulting in an increased selectivity towards byproducts. Figure 4.14b depicts selectivity towards byproducts, which show C16 diol and C24 acetal as the major byproducts. The selectivity towards C16 diol reached a maximum of 1.8 %, while the C24 acetal increased from 0.4 % to 1 % with the increase in temperature. This indicates that the increase in metal loading provided more active sites for adsorption of the incoming reactants, as well as the re-adsorption of the primary products for further reactions.

Table 4.1. Summary of the octanal and octene conversion, and selectivity over the 5Cu/γ-Al_2O_3 and 15Cu/γ-Al_2O_3 catalysts at reaction temperatures of 120, 140, and 160°C.

	5 Cu/γ-Al_2O_3			**15 Cu/γ-Al_2O_3**		
	Octene conversion (%)	Octanal conversion (%)	Octanol selectivity (%)	Octene conversion (%)	Octanal conversion (%)	Octanol selectivity (%)
120	1	38	98	10	58	98
140	3	69	97	14	91	96
160	12	90	97	23	100	95

*All values were rounded up to the nearest whole number

It can be seen from Table 4.1 that with the increase in metal loading, there is also an increase in conversion. The conversion of octanal increases from 90 % using the 5Cu/γ-Al_2O_3 catalyst to 100 % using the 15Cu/γ-Al_2O_3 catalyst at 160 °C, however, the selectivity to octanol decreases from 97 % to 95 %. The most significant difference between the two catalysts is the octene conversion whereby the maximum conversion obtained at 160 °C for the 5Cu/γ-Al_2O_3 and 15Cu/γ-Al_2O_3 catalysts were 12 % and 23 % respectively. Hydrogen chemisorption (Table 3.5)

showed a decreased metal dispersion from the 5Cu/γ-Al_2O_3 to the 15Cu/γ-Al_2O_3 catalyst, this indicates that larger copper particles available in the 15Cu/γ-Al_2O_3 (shown using SEM in Figure 3.23 and TPR Figure 3.26) favoured the hydrogenation of octanal and octene. The 15Cu/γ-Al_2O_3 catalyst showed a higher weak acid site concentration as shown in Table 3.8. These Lewis acid sites have been reported to favour the adsorption of carbonyl groups onto the active site [98].

This increase in conversion for both reactants can be attributed to the increase in active metal sites which allowed for a greater amount of reactant to be converted on the catalyst, as found by Yin *et al.* [187]. Similarly, Zhang *et al.* [205] reported on the effect of copper loading for hydrogenation of dimethyl oxalate, which showed that increase of metal loading promoted over hydrogenation due more active sites available. This result is similar to the results obtained in this study, in which the 15Cu showed a lower selectivity towards octanol compared to the 5Cu/γ-Al_2O_3. Additionally, the formation of C24 acetal is seen for the 15Cu/γ-Al_2O_3 catalyst, but not over the 5Cu/γ-Al_2O_3 catalyst.

4.1.4. Effect of liquid hourly space velocity (LHSV)

The effect of liquid hourly space velocity (LHSV) was investigated to determine the influence on the conversion and the selectivity towards octanol. Three LHSV's were investigated, which were 9 h^{-1}, 18 h^{-1}, and 27 h^{-1}. This was studied using the 15Cu/γ-Al_2O_3 catalyst at 160 ° C and 50 bar at a feed: hydrogen ratio of 1: 2. Figure 4.6a shows the effect of LHSV with respect to conversion.

At a high LHSV (e.g. 27 h^{-1}), the flow rate of feed passing through is higher compared to the other LHSV's. The high flow rate decreases the amount of time the reactant spends on the catalyst bed, limiting the amount of reactants, which can be converted.

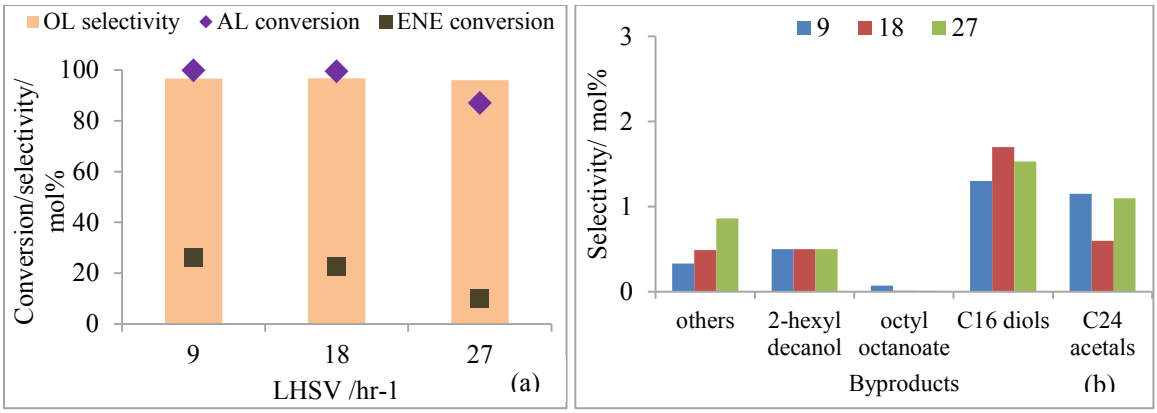

Figure 4.6. Graphs depicting the effect of LHSV at 160 °C at 50 bar in terms of (a) octanol selectivity, octanal and octene conversion, and (b) selectivity towards byproducts over the 15Cu/γ-Al_2O_3.

Figure 4.6a shows that the octanal conversion decreased from 100 % to 87 % with the increase of LHSV from 9 h^{-1} to 27 h^{-1} respectively. The octene conversion showed a similar trend to that of octanal, whereby as the LHSV increased, the octene conversion decreased as shown in Figure 4.6a. This observation is similar to that observed by Zhang *et al.* [206] who attributed the decrease in conversion with an increase in liquid hourly space velocity, to the decreased contact time between the reactants and the catalyst surface.

Figure 4.6a also shows that the selectivity remains constant between 96 – 97 % towards octanol, indicating there is no relationship between the LHSV and selectivity to octanol. There is no distinct trend that can be observed for the selectivity and by products, with C16 diol and C24 acetal being the major by products. There is also a minor formation of 2-hexyl decanol and octyl octanoate, indicated by the byproducts % formation or selectivities. Others include octyl ether, octanoic acid and C16 saturated alkanes.

From the results obtained in the investigation for LHSV, the optimum condition was chosen to be 18 h^{-1} as it provided high octanal conversion while a moderate octene conversion, consistent with results obtained from previous studies [71, 197]. At low LHSV conditions (9 h^{-1}) the octanal is converted almost completely, however the octene conversion was also increased which is undesired. This low liquid space velocity is also uneconomical due to the lower amount of product over after a period of time, as compared to the LHSV of 18 h^{-1}, which allows for similar conversion of octanal while the octene conversion is decreased from 26 % to 23 %. When the

LSHV was increased to 27 h^{-1}, although the octene conversion is decreased to 10 %, the octanal conversion also decreased by 12 %. Kinetic study by Bertero *et al.* [207] showed that one of the kinetic parameters was the competitive adsorption between the hydrogen and the substrate. Considering a similar case, with the increase in LHSV, there is a higher amount of reactant adsorbing onto the support, thus decreasing the amount of hydrogen adsorbed onto the surface which can lead to decreased conversion as there is insufficient hydrogen to react with the incoming substrates.

4.1.5. Effect of octanal: hydrogen ratio

Two ratios of octanal:hydrogen were considered, 1:1.5 and 1:2, to determine the effect of the amount of hydrogen present on the overall activity of the system, and the effect on the octene conversion, which is the unfavoured reaction. At a ratio of 1:2, there is 1 mole of octanal to 2 moles of hydrogen gas.

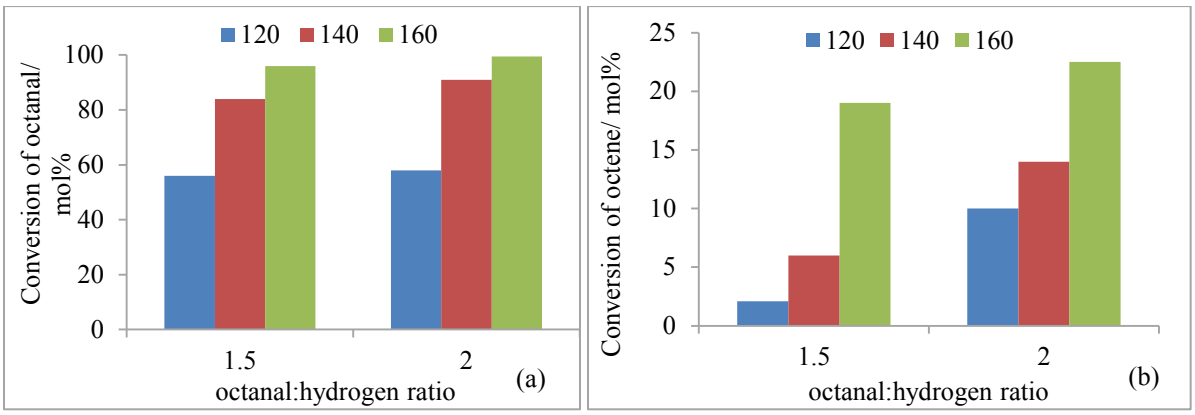

Figure 4.7. Graphs depicting the effect of octanal: hydrogen ratio at 50 bar showing (a) octanal conversion and (b) octene conversion, over the 15Cu/γ-Al_2O_3 catalyst.

The results of this study are shown in Figure 4.7a and 4.7b depicting the conversion of octanal and octene obtained using the 15Cu catalyst at temperatures 120, 140, and 160 °C. Figure 4.16a shows that the conversion of octanal increased with the increase of the octanal:hydrogen ratio. A similar trend was shown for octene conversion depicted in Figure 4.7b, which is the undesired reaction. At a higher ratio of 1:2, the conversion for both reactants is increased. It is also

observed that with the increase in temperature, the difference in conversion of octene between the two ratios decreases e.g. at 120 °C the difference in the two octanal:hydrogen ratios is 8%, whereas, the difference at 160 °C is 4 %.

It is common that the hydrogen is in excess to allow for higher activity, such as in work done in crotonaldehyde hydrogenation by Ashour *et al.* [159], who used a 1:14 ratio of subrate:hydrogen ratio, with Bron *et al.* [131] using a ratio of 1:20 for the substrate to hydrogen ratio in acrolein hydrogenation. Bridier *et al.* [68] showed in their work in the partial hydrogenation of propyne that with an increase in the hydrogen:substrate ratio, there was an increase in conversion. The selectivity towards propene showed an initial increase to the propene, thereafter a decrease with the increase in ratio along with temperature, resulting in a greater formation of the saturated, undesired product.

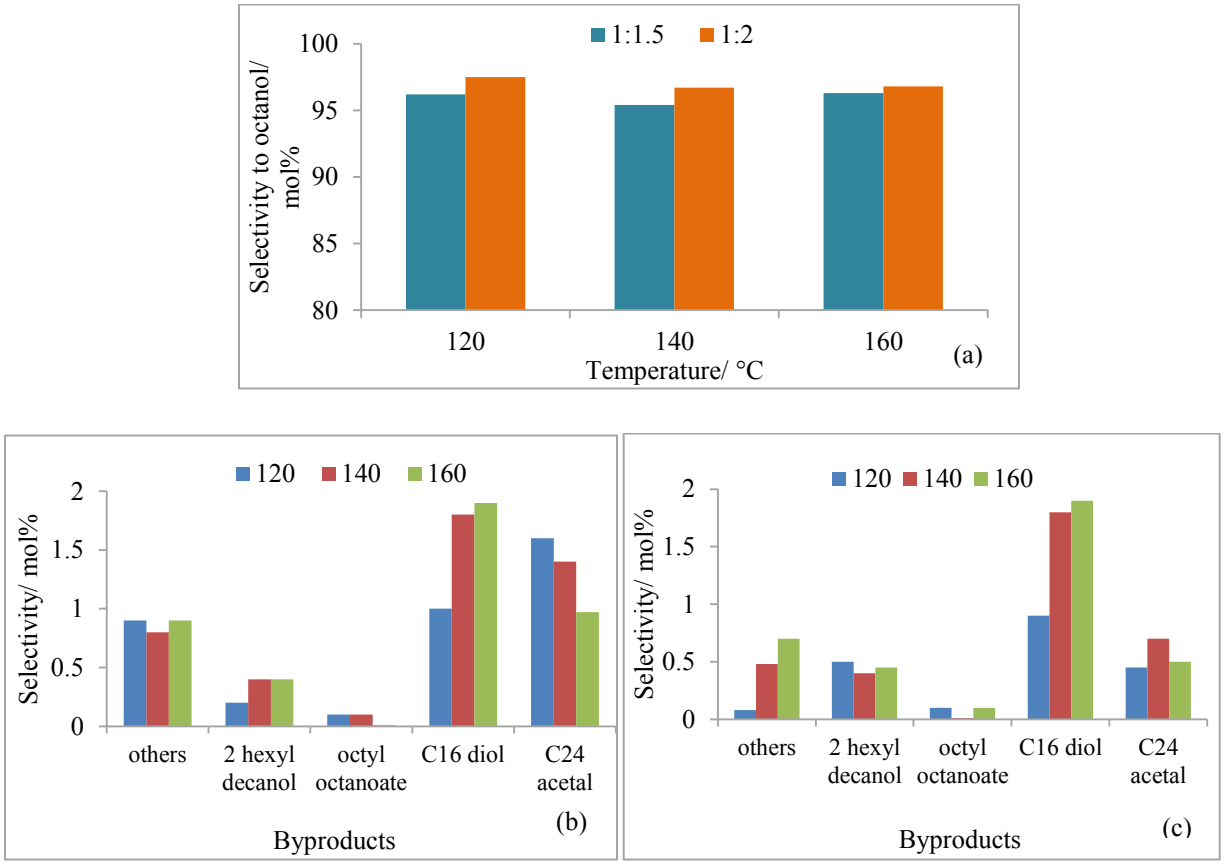

Figure 4.8. Graphs depicting the effect of octanal:hydrogen ratio at 50 bar for selectivity towards (a) octanol and (b) byproducts at 1:1.5 octanal:hydrogen ratio and (c) byproducts at 1:2 octanal:hydrogen ratio over the 15Cu/γ-Al_2O_3 catalyst.

Figure 4.8a shows the selectivity towards octanol at temperatures 120 – 160 °C. At 120 °C, the selectivities towards octanol are 96 and 98 %, at ratios 1:1.5 and 1:2 respectively, and with the increase in temperature to 160 °C, the selectivity towards octanol at both ratios is approximately 97 %. This indicates why 160 °C was chosen as the optimum temperature, as it allows for maximum octanal conversion, while selectivity remains unchanged compared to a lower octanal: hydrogen ratio.

Figure 4.8b-c showed the selectivity towards byproduct formation where C16 diol and C24 acetal were the major byproducts. The excess hydrogen present allowed for further reactions with the incoming octanal molecules and the adsorbed hydrogen present. At a ratio of 1:2, there is an overall lower formation of C24 acetal, which resulted from the increased adsorbed hydrogen on the surface reducing the re-adsorption of octanal and octanol molecules thus reducing the C24 acetal formation. Other minor by products included 2-hexyl decanol, octyl octanoate and others, which are made up of octyl ether, C16 saturated alkanes and octanoic acid.

4.2. Copper-silver bimetallic catalysts

As mentioned in chapter 1, silver was shown to be effective in the selective hydrogenation of α,β-unsaturated aldehydes [50, 123, 208]. For this reason, silver was chosen to be incorporated into the Cu/γ-Al_2O_3 system to improve the catalyst properties or behavior. The effect of silver was investigated by preparing and testing a range of seven γ-Al_2O_3 supported CuAg bimetallic catalysts. A few key factors were established; namely a suitable total weight loading, the weight loading of silver, and the impregnation technique. As mentioned in Chapter 2, the simultaneous impregnation involved adding both metals to the γ-Al_2O_3 at the same time, while sequential impregnation involved the addition if the first metal which is stirred and dried, followed by the addition of the second metal, with the final step being calcination.

These CuAg bimetallic catalysts were characterization and discussed in Chapter 3. Chemisorption studies indicated that the 5 wt % bimetallic catalysts prepared by simultaneous impregnation improved metal dispersion (Chapter 3, Table 3.5) and showed a decrease in the onset temperature for copper reduction (Figure 3.27) compared to the 5 wt % monometallic copper catalyst (Figure 3.26). A substantial amount of work done towards the characterization of

Cu based catalysts [171, 209-211] showed weight loadings of copper below approximately 13 % Cu were difficult to analyze using x-ray diffraction, and indeed, loadings at 5 wt % or below prepared in this work were difficult to analyze. The use of SEM-EDX and TEM-EDX provided information on the surface composition for the simultaneous and sequential impregnation catalysts as shown in Chapter 3. These bimetallic catalysts were applied for the selective hydrogenation of octanal in the presence of octene and the results are shown in this Chapter.

4.2.1. Bimetallic catalysts at 15 wt % loading

Based on the optimization study in this chapter, the 15Cu/γ-Al_2O_3 catalyst showed the most activity in terms of highest conversion obtained for octanal and octene. The 13.5Cu1.5Ag/γ-Al_2O_3 bimetallic catalysts were investigated, shown in Figure 4.9, to establish a comparison between the 15Cu/γ-Al_2O_3 and 13.5Cu1.5Ag/γ-Al_2O_3 catalysts.

The 15 % bimetallic catalyst consisting of 13.5Cu and 1.5Ag was investigated to determine the effect of silver in a copper system at high total weight loading. Under optimum conditions at 18 h^{-1} LHSV and a 1:2 octanal: hydrogen ratio, the 13.5Cu1.5Ag/γ-Al_2O_3 catalyst showed a maximum octanal conversion of 96 % at 160 °C.

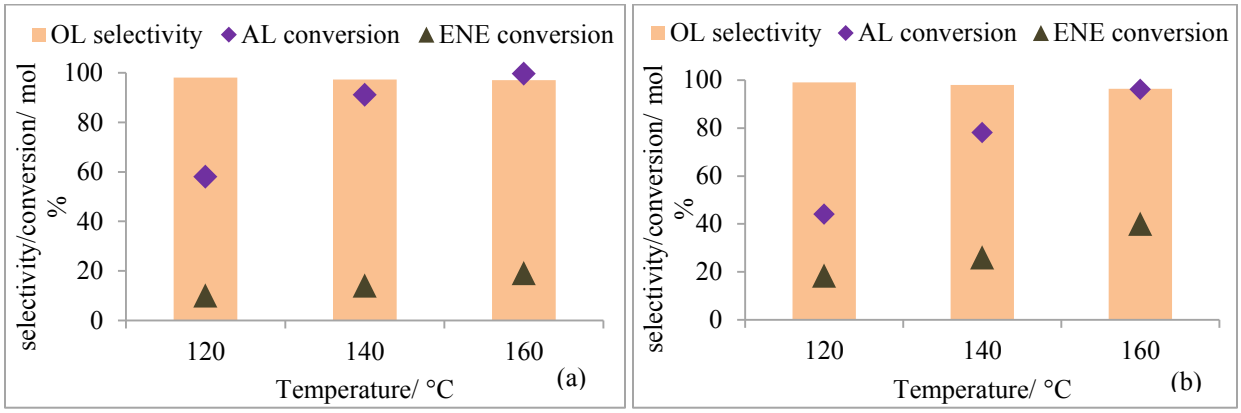

Figure 4.9. Graphs showing results obtained from 120 – 160 °C, conversion of octanal (AL) and octene (ENE) and the selectivity towards octanol (OL) over (a) 15Cu/γ-Al_2O_3 and (b) 13.5Cu1.5Ag/γ-Al_2O_3 catalysts.

Figure 4.9a-b showed the increase in conversion with temperature, for both the octanal and octene using the 15Cu/γ-Al_2O_3 and 13.5Cu1.5Ag/γ-Al_2O_3 catalysts. The octene conversion obtained for the 13.5Cu1.5Ag/γ-Al_2O_3 ranged from 18 % to 40 %, over the temperatures 120, 140, and 160 °C. This octene conversion for 13.5Cu1.5Ag/γ-Al_2O_3 was significantly higher compared to the conversion over the monometallic 15Cu/γ-Al_2O_3 catalyst, which showed a maximum of 22.5 % at 160 °C (Figure 4.9a), thus indicating that the presence of silver had a negative influence for the selective hydrogenation of octanal. A range of temperatures was investigated to observe the stability of the bimetallic catalysts, as it is known that silver reduces below 100 °C [121]. With higher temperatures, this may have caused agglomeration of silver which may reduce the synergistic effect of the bimetallic catalyst. It was also important to investigate the mobility of silver in the sequential catalysts, if the impregnation sequence contributed to the metal dispersion and mobility of the metals under reaction conditions.

The difference in the catalytic results could be explained from the results obtained from SEM-EDX. The SEM-EDX results (Figure 3.23) shown in chapter 3 showed the 15Cu/γ-Al_2O_3 catalyst formed small clusters in certain regions, with an overall good dispersion across the catalyst surface. The close contact between the silver and copper particles for the 13.5Cu1.5Ag/γ-Al_2O_3 catalyst showed a shift to a lower reduction temperature observed in TPR analysis, most likely due to the synergistic effect (Figure 3.25). This could result in a more favourable environment for the adsorption of octene, which has been reported to adsorb onto more basic sites [124], which could be seen from the decrease in acidity shown in the TPD results (Table 3.8).

The difference observed between the monometallic and bimetallic 15 wt % catalysts can be attributed to the synergistic effect between the copper and silver metals resulting in an increased selectivity towards octanol, where the octanol selectivity at 160 °C for the 15Cu/γ-Al_2O_3 and 13.5Cu1.5Ag/γ-Al_2O_3 catalysts are 95 % and 96 % respectively. This synergistic effect also promoted higher octene conversion, which is an undesired result. This increase in octene conversion for the 13.5Cu1.5Ag/γ-Al_2O_3 catalyst could be a result of octene or dissociated hydrogen on the surface becoming mobile on the silver particles, which increases the interaction between the reactants and hydrogen available, which resulted in higher octene conversion. The use of the 13.5Cu1.5Ag/γ-Al_2O_3 catalyst, although with the increase the octanol selectivity,

showed a lower octanal conversion and higher octene conversion. This makes this catalyst less suitable for selective hydrogenation of octanal in the presence of octene. Sun *et al.* [150] showed the effect of silver loading on copper-based catalysts for the hydrogenolysis of glycerol to 1,2-propanediol. Silver weight loading, catalyst weight and the reaction conditions are the key parameters for their selectivity towards the desired product, 1,2 propanediol. Under the same reaction conditions, an increase in the silver weight loading showed to maintain the conversion, while decreasing selectivity to 1,2 propanediol.

Selectivity towards octanol

Figure 4.9b shows that the 13.5Cu1.5Ag/γ-Al_2O_3 catalyst has a higher selectivity towards octanol at temperatures 120 and 140 °C compared to Figure 4.9a. It was also shown that with the increase in temperature, a general trend for both the 15Cu/γ-Al_2O_3 and 13.5Cu1.5Ag/γ-Al_2O_3 showed a decrease in octanol selectivity. This may be due to the higher amount of kinetic energy in the system which also allows for byproduct formation.

Selectivity towards byproducts

Figure 4.10a-b shows the selectivity towards byproducts for the 15Cu/γ-Al_2O_3 and 13.5Cu1.5Ag/γ-Al_2O_3 catalysts. The decrease in selectivity towards octanol resulted in a higher selectivity towards the byproducts, as shown in Figure 4.10b, with the major byproducts being the C16 diol and C24 acetal, similar to that observed with the 15Cu catalyst (Figure 4.10a). These byproducts formed on both acidic and basic sites with the C16 diol forming as a result of aldol condensation and C24 acetals forming on the Lewis acid sites [71]. These major byproducts showed to increase significantly with temperature together with a minor formation of 2-hexyl decanol, which is a result of aldol condensation, while a reduction in the formation of octyl octanoate was observed. "Others" include octanoic acid, and C16 saturated alkanes.

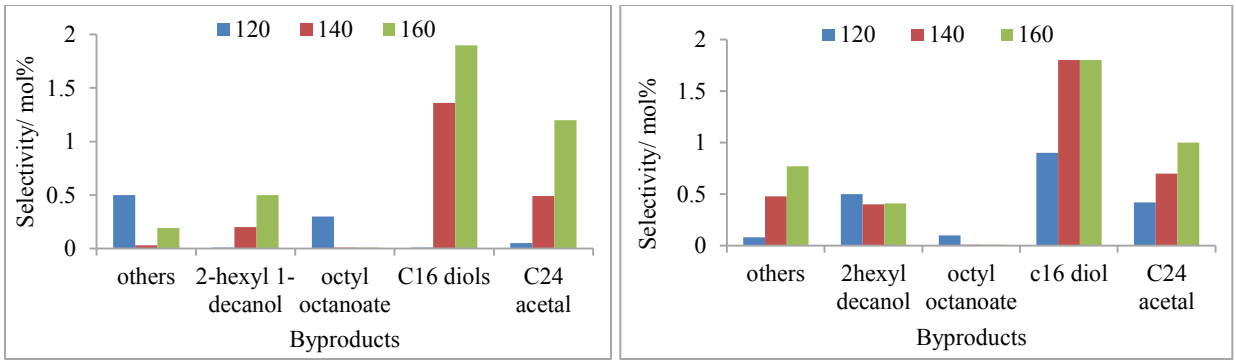

Figure 4.10. Selectivity towards byproducts over the (a) 15Cu and (b) 13.5Cu1.5Ag catalyst.

The 15Cu/γ-Al_2O_3 catalyst showed a high acidity compared to the 13.5Cu1.5Ag/γ-Al_2O_3 catalyst, which resulted in the formation of C24 acetal and C16 diol via aldol condensation. The formation of the C16 diol at 120 °C confirms that the aldol condensation can occur on acidic or basic sites on the catalysts investigated, where the C16 diol can form from the formation of the enol or enolate intermediate for octanal hydrogenation. As the temperature increased, the silver may become mobile exposing more acid sites, leading to an increase in C24 acetal. An increase in other byproducts were also observed, this includes C16 saturated alkanes and octanoic acid.

The investigation of the selective hydrogenation of octanal in the presence of octene using 15 wt % total metal loaded catalysts showed to have a negative influence of the desired result. The increase in active metal sites allowed for the hydrogenation of both the octanal and octene, and the presence of silver thus showed an unfavourable result.

4.2.2. Effect of bimetallic catalyst at 5 wt % loading

Three 5 wt % bimetallic catalysts were prepared, one catalyst was prepared by simultaneous addition of the metal precursors, and two catalysts were prepared sequentially in varying the addition of the metal precursor order. This was done to study the effect of silver, as well as to gain information about the nature of interaction between the copper and silver present on the support surface when prepared in different ways.

4.2.3. Effect of silver loading using 4.5Cu0.5Ag/γ-Al_2O_3 and 4Cu1Ag/γ-Al_2O_3

The ratio between copper and silver were varied to determine the effect of silver in a copper system, while maintaining the total metal loading. Two catalysts namely 4.5Cu-0.5Ag/γ-Al_2O_3 and 4Cu-1Ag/γ-Al_2O_3, were investigated. Figure 4.11a-b compares two 5 wt % bimetallic catalysts of varying Cu-Ag ratios, in which Figure 11a shows the use of 4.5Cu0.5Ag/γ-Al_2O_3 for selective hydrogenation of octanal in the presence of octene, while Figure 4.11b shows the catalytic results for the 4Cu1Ag/γ-Al_2O_3 catalyst.

Comparing the selectivity between the two 5 wt % simultaneously impregnated bimetallic catalysts, namely 4.5Cu0.5Ag/γ-Al_2O_3 and 4Cu1Ag/γ-Al_2O_3, showed the 4.5Cu-0.5Ag/γ-Al_2O_3 catalyst to have a higher selectivity to octanol as compared to the 4Cu-1Ag/γ-Al_2O_3 catalyst at lower temperatures, with the difference being negligible at 160 °C, as shown in Figure 4.11.

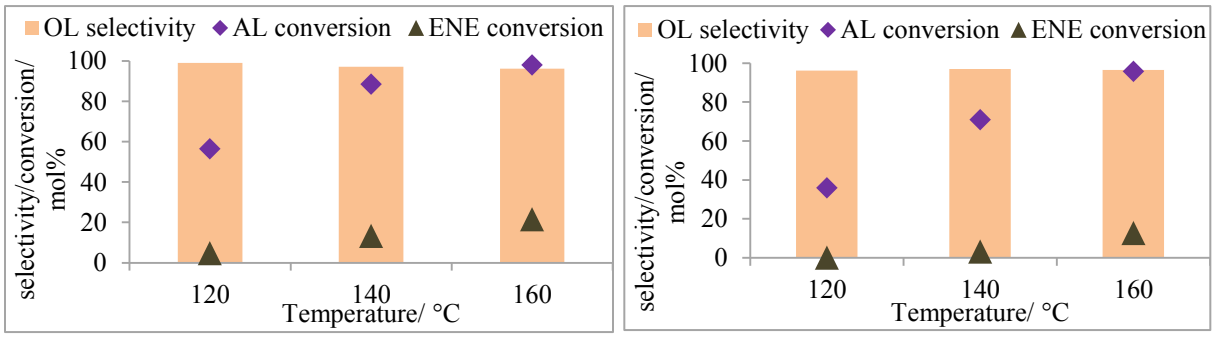

Figure 4.11. Octanol selectivity and the conversion of octanal and octene for catalysts (a) 4.5Cu0.5Ag/γ-Al_2O_3 and (b) 4Cu1Ag/γ-Al_2O_3.

Table 4.2. A comparison between the monometallic and bimetallic catalysts.

	5Cu/γ-Al_2O_3			**4.5Cu-0.5Ag/γ-Al_2O_3**			**4Cu1Ag/γ-Al_2O_3**		
	Octene conversion (%)	Octanal conversion (%)	Octanol selectivity (%)	Octene conversion (%)	Octanal conversion (%)	Octanol selectivity (%)	Octene conversion (%)	Octanal conversion (%)	Octanol selectivity (%)
120	0.9	38	99	5	57	99	0.1	36	96
140	3	69	97	13	89	97	3	71	97
160	12	90	97	22	98	96	13	96	97

The increase in silver loading showed a decrease in conversion at temperatures 120 and 140 °C, which is expected due to the slightly lower amount of active metal (copper) on the surface in the intermetallic ratio of the catalyst prepared in this study. At 160 °C the 4Cu1Ag/γ-Al_2O_3 catalyst had approximately 1 % lower conversion, which could be considered negligible, indicating that higher temperatures allow for a greater synergistic effect between the two metals, which results in a higher conversion for both bimetallic catalysts compared to the 5Cu/γ-Al_2O_3 catalyst (refer to Table 4.3). A major difference between the two 5 wt % bimetallic catalysts is the octene conversion, whereby the 4.5Cu0.5Ag/γ-Al_2O_3 shows a significantly higher octene conversion as compared to the 4Cu1Ag/γ-Al_2O_3 catalyst. This could be attributed to the low loading of silver creating more defect sites to allow to an increased possibility of octene adsorption and hydrogenation. *In situ* XRD supports this showing a change in the d-spacing values under reduction conditions (Figure 3.7). The 4Cu1Ag/γ-Al_2O_3 also showed a slight shift, which results in a similar octene conversion as the monometallic 5Cu/γ-Al_2O_3 catalysts (refer to Figure 3.7). The synergistic effect between the two metals allow for a lower loading of copper while maintaining the low octene conversion found with the 5Cu/γ-Al_2O_3 catalyst, as well as providing an increased conversion of octanal at high temperatures (160 °C).

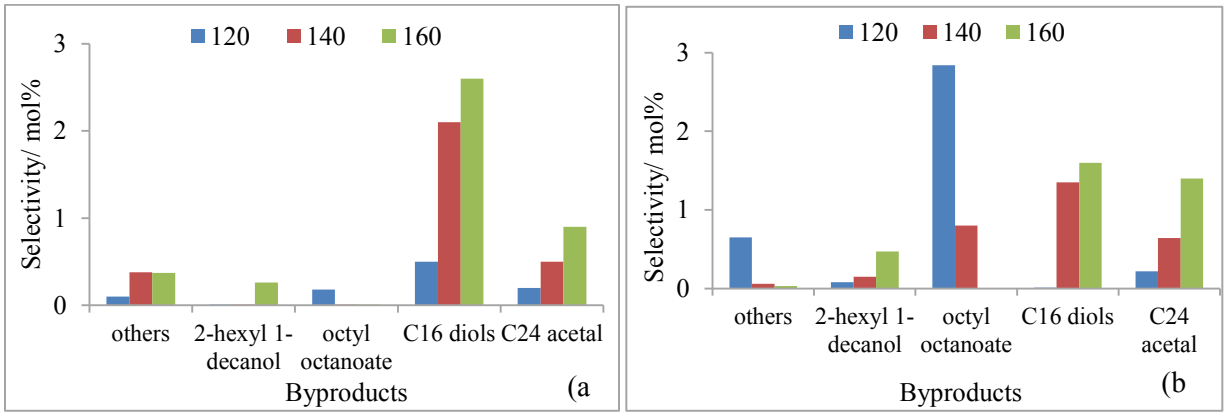

Figure 4.12. The selectivity towards byproducts for catalysts (a) 4.5Cu0.5Ag/γ-Al_2O_3 and (b) 4Cu1Ag/γ-Al_2O_3.

Figure 4.12a-b showed the selectivity towards byproduct formation for the 4.5Cu0.5Ag/γ-Al_2O_3 and 4Cu1Ag/γ-Al_2O_3 catalysts. Both catalytic systems showed similar octanol selectivities, however, the 4.5Cu0.5Ag/γ-Al_2O_3 showed a higher selectivity to C16 diols and C24 acetal with a negligible amount of octyl octanoate, while the 4Cu-1Ag/γ-Al_2O_3 shows a significant amount of

octyl octanoate at 120 °C which decreased significantly with the increase in temperature. Since octyl octanoate forms on basic sites, it can be assumed that the increase in silver content allowed for more basic sites to be available (see Table 3.8). The decrease in octyl octanoate with an increase in temperature is a result of more energy being provided to the system which causes silver to become mobile on the surface and form larger agglomerates, the acid sites become more prominent which is shown by the increase in C24 acetal over the temperature range 120 – 160 °C.

Zheng *et al.* [151] supports the results that were observed in this study for the effect of weight loadings, whereby their work on Au-Ag catalyst system for the hydrogenation of esters showed silver to have an optimum weight loading. Catalysts with weight loadings higher than the optimum Au-Ag ratio showed a decrease in conversion similar to what was observed in this work with the 4.5Cu0.5Ag/γ-Al_2O_3 and 4Cu1Ag/γ-Al_2O_3 catalysts.

4.2.4. Effect of metal impregnation sequence

It is known that the composition of bimetallic catalysts plays an important role in their catalytic activity [54, 129, 148, 154, 212, 213]. There has been sufficient work done to prepare and characterize different types of bimetallic catalysts, and to investigate their activity in various types of reactions. For this study, the effect of the impregnation sequence was investigated to determine the effect of the position of the silver, the metal-metal interaction, and its catalytic activity.

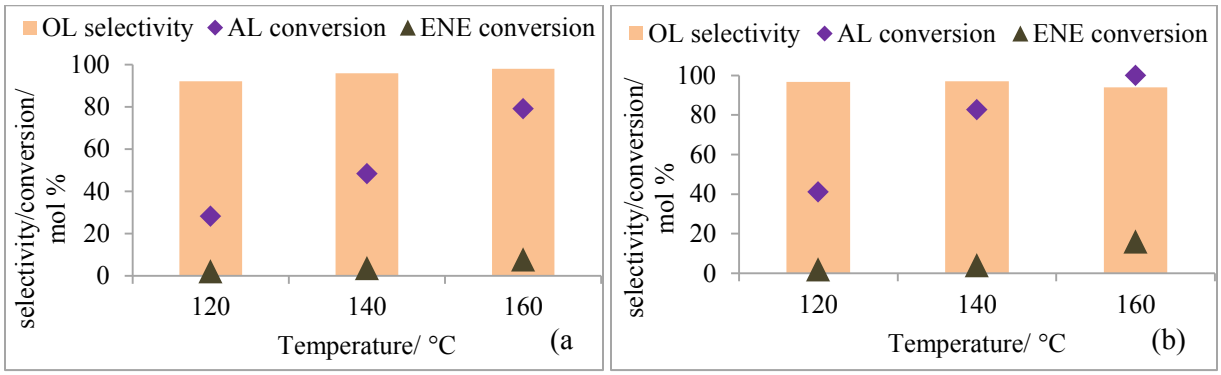

Figure 4.13. Graphs showing the conversion of octanal, and octene, and the selectivity towards octanol for (a) S-4.5Cu0.5Ag/γ-Al_2O_3, and (b) S-0.5Ag4.5Cu/γ-Al_2O_3 catalysts.

Octanal conversion: Characterization showed that sequential impregnation allows the silver to be impregnated above or below the active copper metal, which is impregnated onto the alumina support, as opposed to simultaneous impregnation where the arrangement of the metals is less controlled. When copper was impregnated first followed by silver, the silver showed a better dispersion onto the copper and bare alumina support. The S-4.5Cu0.5Ag/γ-Al_2O_3 catalyst showed a decrease in conversion (Figure 4.13a) compared to the simultaneous 4.5Cu0.5Ag/γ-Al_2O_3 catalyst (Figure 4.11a) which were 70 % and 98 % respectively. This was attributed to the silver metal limiting or hindering the availability for the active copper metal to adsorb the incoming octanal molecules. Similarly, with the S-0.5Ag4.5Cu/γ-Al_2O_3, with the silver impregnated first followed by copper, there is a decreased possibility of copper migrating into the lattice due to the weak interaction between silver ions and alumina [214]. These result in a higher metal dispersion of the active copper metal on the surface, which is consistent to the results observed in CO chemisorption (Table 3.6) and surface area measurements for both the S-0.5Ag4.5Cu/γ-Al_2O_3 and S-1Ag4Cu/γ-Al_2O_3 catalysts (Table 3.3). Figure 4.13b showed a higher conversion observed from the S-0.5Ag4.5Cu/γ-Al_2O_3 due to more active metal available on the surface, reaching a maximum of 100 %, consistent with the surface area and chemisorption measurements.

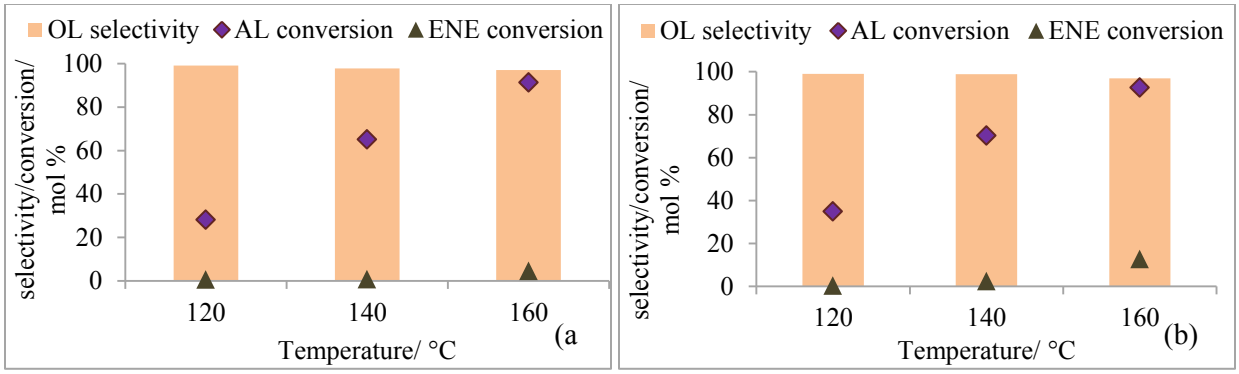

Figure 4.14. Graphs showing the conversion of octanal, octene, and the selectivity towards octanol for (a) S-4Cu1Ag/γ-Al_2O_3 (b) S-1Ag4Cu/γ-Al_2O_3.

A similar trend was obtained in the case of the S-4Cu1Ag/γ-Al_2O_3 catalyst (Figure 4.14a), whereby a lower octanal conversion is observed as compared to the simultaneous prepared 4Cu1Ag/γ-Al_2O_3 (Figure 4.11b) catalyst due to the silver limiting access to the copper sites. In the case of the S-1Ag4Cu/γ-Al_2O_3 catalyst shown in Figure 4.14b, the octanal and octene

conversion is similar to that observed with the simultaneous catalyst (Figure 4.11b) at temperatures 120 – 140 °C. A minor difference between the S-1Ag4Cu/γ-Al_2O_3 and simultaneous 4Cu1Ag/γ-Al_2O_3 catalysts was observed at 160 °C, where the S-1Ag4Cu/γ-Al_2O_3 showed a lower conversion compared to the simultaneous impregnation catalyst, unlike the result obtained with the S-0.5Ag4.5Cu/γ-Al_2O_3. This result could be attributed to the silver metal has a preferred affinity to agglomerate at higher loadings as opposed to agglomerating to the 4 % copper available, thus decreasing the synergistic effect and metal dispersion of the catalyst. When copper was impregnated first, there is an increased possibility of copper ions migrating to the alumina lattice forming copper aluminate, and this phase is not active for hydrogenation thus decreasing the quantity of active copper species available to adsorb reactants [169, 170, 198]. When silver was impregnated first, due to its larger ionic radius, silver does not migrate into the alumina lattice during calcination. The silver may also limit the interaction between the copper and alumina, which allows the copper to have a higher dispersion on the surface as well as decreasing the formation of the inactive copper aluminate phase. This is supported by characterization data obtained from the decrease in surface area observed in Chapter 3, Table 3.3 and the increase in metal dispersion and metallic surface area (Table 3.5), thus resulting in an increase in conversion. The CO chemisorption measurements support this argument where the simultaneous 4Cu1Ag/γ-Al_2O_3 and S-1Ag4Cu/γ-Al_2O_3 catalyst has a similar metallic surface area and selectivity. This observation is consistent with reports by Maity *et al.* [195], whereby the increase in alcohol selectivity was reported to correlate to higher metal dispersion as determined by CO chemisorption.

There have been a number of reports investigating the effect of the impregnation sequence such as; Shu *et al.* [213] reported on the effect of impregnation sequence using Pt-Ni catalysts for cyclohexene hydrogenation. They attributed the difference in conversion observed for the Pt-Ni catalysts prepared in different ways to the Ni^{2+} ions diffusing into the alumina lattice when the nickel was impregnated first due to its small ionic radius. As the radius increases, larger ions are unable to enter the lattice under the same conditions e.g. Pt^{2+}. The same argument could be applied in the current study by comparing the ionic radius of Cu^{2+} and Ag^{+}. When the Cu^{2+} ion (0.73 Å) is impregnated first, the copper ions are able to enter the γ-Al_2O_3 cavities. Whereas, when the Ag^{+} were deposited first, it would remain outside the γ-Al_2O_3 cavities as the Ag^{+} ionic radius is 1.26 Å, which is much larger. This is supported by studies done by Yan *et al.* [215] who

found no migration of silver ions for a 6 % Ag/Al_2O_3 catalyst due to the lack of interaction between the silver and the alumina support. Additionally, Deng *et al.* [153] reported on the effect of impregnation sequence for Cu-Co catalysts for the synthesis of alcohols. The conversion varied between 22 – 28 % with the copper catalyst, which was impregnated first, showing the highest conversion. The co-impregnated catalyst showed the highest selectivity to the desired product, alcohol; with 52 %, whereas the sequential impregnated catalyst showed selectivities lower than 44 %. On the contrary, in this study, the silver impregnated first showed the highest selectivity to octanol, while the copper impregnated first showed the highest octanal conversion.

Octene conversion: The octene conversion over both sequential catalysts consisting of $4.5Cu0.5Ag/\gamma\text{-}Al_2O_3$, shown in Figure 4.13a-b, is lower than that over the simultaneous catalysts, indicating that the synergistic effect is not as pronounced in sequential impregnation catalysts compared to the simultaneous impregnation catalysts. This observation is consistent with the results obtained with the sequential catalysts. When copper was impregnated first followed by silver, the silver is most likely above the copper and bare alumina for the $S\text{-}4.5Cu0.5Ag/\gamma\text{-}Al_2O_3$ and $S\text{-}4Cu1Ag/\gamma\text{-}Al_2O_3$ catalysts. This resulted in a lower octene conversion (shown in Figure 4.13a and 4.14a) as the active copper species may be blocked or has a limited availability to the incoming reactants. It was also shown in Figure 4.13b and 4.14b that when silver was impregnated first followed by copper, the copper is most likely on the upper layer as seen with the surface area measurements and chemisorption studies. The octene conversion is slightly lower than that of the simultaneous impregnation catalyst e.g. the $S\text{-}0.5Ag4.5Cu/\gamma\text{-}Al_2O_3$ had a 16 % octene conversion whereas the simultaneous $4.5Cu0.5Ag/\gamma\text{-}Al_2O_3$ had an octene conversion of 22 %. The difference in conversion between these two catalysts could be attributed to the decreased synergistic effect obtained from sequential impregnation synthesis. Smith *et al.* [177] made a general statement that it has been shown in a number of studies that small particles, edges and corners favour C=C hydrogenation, while larger particles and plane flat surfaces favour the adsorption and hydrogenation of C=O functional groups. It can be supported by the results observed with the $4.5Cu0.5Ag/\gamma\text{-}Al_2O_3$ catalysts, where the lower amount of silver creates small well dispersed particles which can adsorb the incoming octene reactants. The incoming reactants can then adsorbed and react with the dissociated hydrogen

adsorbed on copper. However, it was also shown from the SEM-EDX line scan (Figure 3.15) and STEM-EDX (Figure 3.12) that the simultaneous catalysts allowed for both metals to be in close contact with each other resulting in a higher octene conversion. This could be due to the synergistic effect of both metals in close contact with each other, which increases the adsorption of both octanal and octene as seen in work done by Deng *et al.* [153].

Selectivity towards octanol: S-4.5Cu0.5Ag/γ-Al_2O_3 showed an increase in selectivity with an increase in temperature (Figure 4.13a), whereas the S-0.5Ag4.5Cu/γ-Al_2O_3 catalyst (Figure 4.13b) showed a decrease at higher temperatures. This could be due to the mobility of silver atoms on the surface, which may increase the synergistic effect at higher temperatures, resulting in an increased selectivity to octanol in the case of the S-4.5Cu0.5Ag catalyst or the formation of byproducts as seen with S-0.5Ag4.5Cu/γ-Al_2O_3. The S-4Cu1Ag/γ-Al_2O_3 (Figure 4.14a) and S-1Ag4Cu/γ-Al_2O_3 (Figure 4.14b) catalysts showed a minor decrease in selectivity to octanol with increase in temperature. The highest selectivity was obtained at low temperatures of 120 °C with both catalysts showing the same selectivity at 160 °C, which is 97 %. This is consistent with work done by Maity *et al.* [195], where copper was found to increase the alcohol selectivity in the Fischer-Tropsch synthesis.

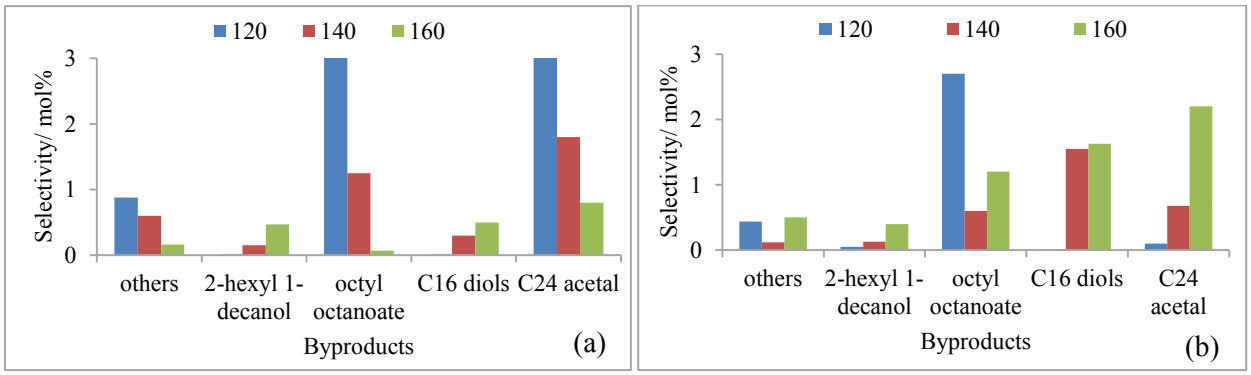

Figure 4.15. Graphs showing the selectivity towards byproducts for (a) S-4.5Cu0.5Ag/γ-Al_2O_3, and (b) S-0.5Ag4.5Cu/γ-Al_2O_3.

Selectivity towards byproducts: A significant selectivity towards acid catalyzed byproducts such as octyl octanoate and C24 acetal was observed for the S-4.5Cu0.5Ag catalyst at 120 °C (Figure 4.15a). This decreased with an increase in temperature to a negligible amount. The S-

0.5Ag4.5Cu/γ-Al_2O_3 catalyst (Figure 4.15b) showed similar behavior with the major byproduct being octyl octanoate, while C16 diol and C24 acetal showed an increase with increase in temperature. This could be due to mobility of silver as the temperature is increased, resulting in a change in the behavior of the catalyst.

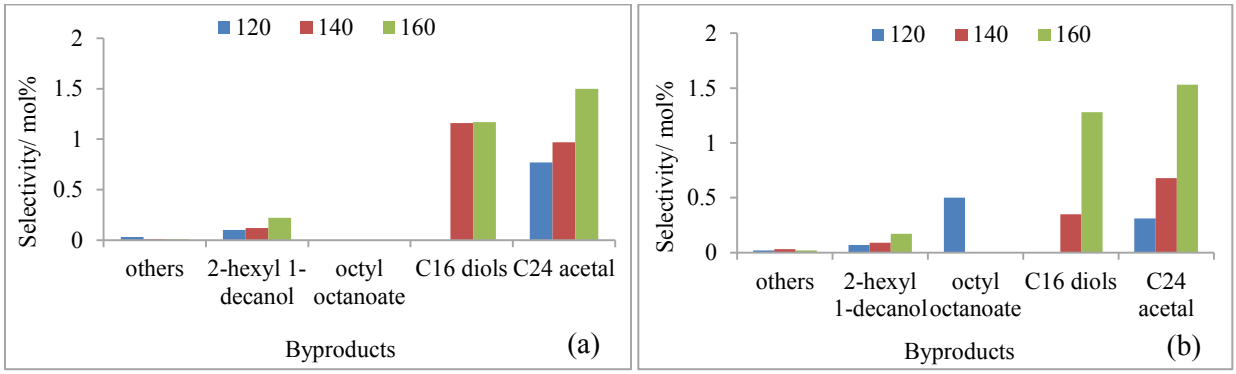

Figure 4.16. Graphs showing the selectivity towards the byproducts over the (a) S-4Cu1Ag/γ-Al_2O_3, and (b) S-1Ag4Cu/γ-Al_2O_3 catalysts.

Interestingly, when the silver loading was increased to 1 %, there is no formation of octyl octanoate for the S-4Cu1Ag/γ-Al_2O_3, as shown in Figure 4.16a. This indicates that the nature of the basic sites plays a role in which basic byproduct formation is favoured. In this study, the higher weight loading of silver promotes the formation of C16 diols. The S-1Ag4Cu/γ-Al_2O_3 showed a minor presence of octyl octanoate at 120 °C, with no formation of C16 diol (Figure 4.16b). With the increase in temperature, there was an increase in selectivity to C16 diol, reaching a maximum selectivity of approximately 1 %, while the octyl octanoate selectivity became negligible. This suggests that under reaction conditions, an increase in temperature caused a change in the surface charecteristics resulting in a change the nature of basicity, favouring octyl octanoate formation to favouring C16 diol formation. C24 acetal formation was observed for both catalysts over the temperature range 120 – 160 °C, which was increased with the increase in temperature.

4.2.5. Isoconversion between 5Cu/γ-Al_2O_3, 4.5Cu-0.5Ag/γ-Al_2O_3, and 4Cu1Ag/γ-Al_2O_3

Isoconversion studies provided information to compare the selectivities towards octanol and its byproducts using the 5Cu/γ-Al_2O_3, 4.5Cu0.5Ag/γ-Al_2O_3 and 4Cu1Ag/γ-Al_2O_3 catalysts. Figure 4.17a shows the octanol selectivity and the conversion for octanal and octene. This showed 5Cu/γ-Al_2O_3 to have the highest octanol selectivity, followed by the 4Cu1Ag/γ-Al_2O_3 with the 4.5Cu0.5Ag/γ-Al_2O_3 having the lowest selectivity to octanol.

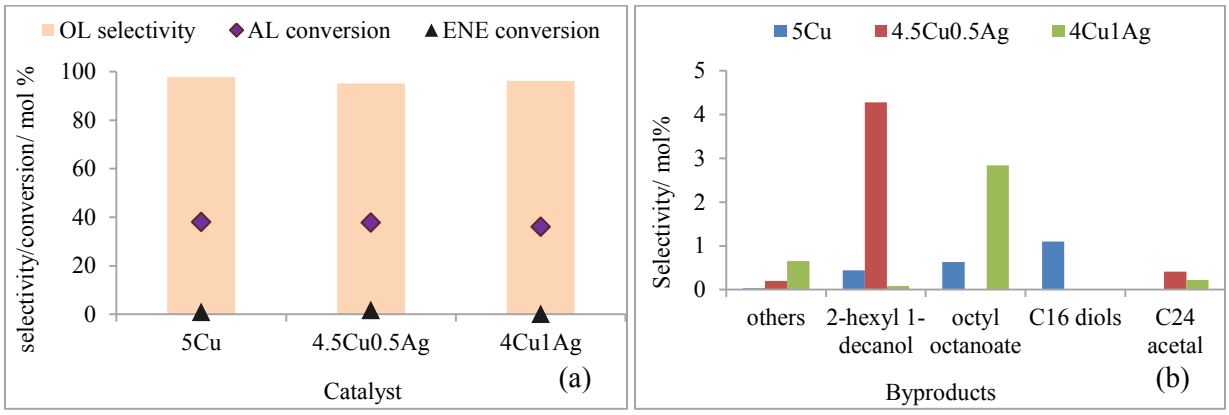

Figure 4.17. (a) Isoconversion of octanal and octene over the catalysts and octene and selectivity towards octanol over the catalysts 5Cu/γ-Al_2O_3, 4.5Cu0.5Ag/γ-Al_2O_3 and 4Cu1Ag/γ-Al_2O_3, and (b) Selectivity towards byproducts at 120 °C with a octanal:hydrogen ratio of 1:2.

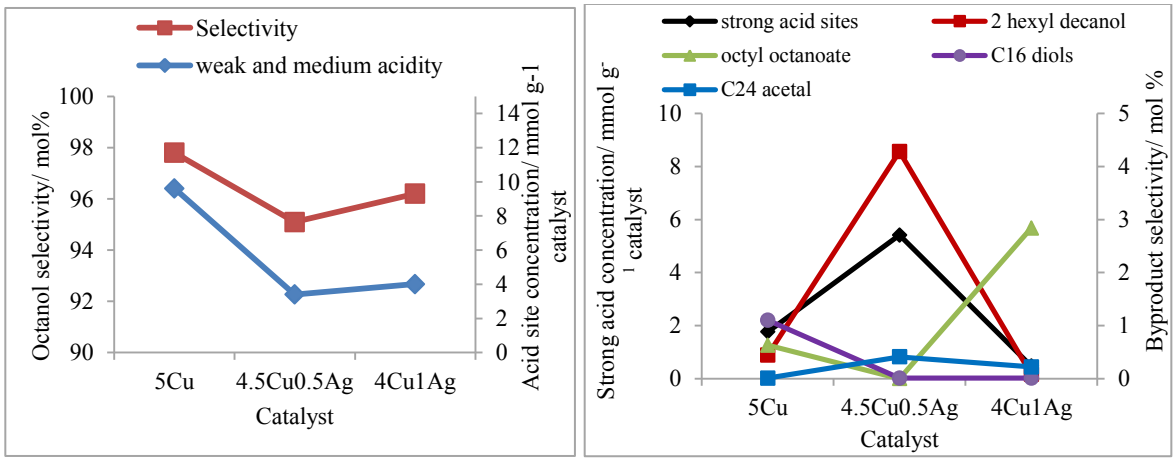

Figure 4.18. Relationship between the catalyst acidity and the catalysts investigated under isoconversion conditions with (a) depicting octanol selectivity vs. Lewis acid site concentration and (b) showing the strong acid site concentration vs. byproduct selectivity.

The difference in selectivity towards octanol and its byproducts could be attributed to the catalysts acidity and the types of acidity present. Figure 4.18a shows that the Lewis acid sites

correlates well with the octanol selectivity as in the case with the 4.5Cu0.5Ag/γ-Al_2O_3 showing the lowest Lewis acidity as well as the lowest octanol selectivity. The monometallic copper catalyst showed the highest selectivity of 98 % that is consistent with the high Lewis acidity obtained. This high selectivity could be attributed to the high concentration of Lewis acidity, which is known to favour the adsorption of the C=O functional group. This trend remained consistent with the 4Cu1Ag/γ-Al_2O_3 catalyst.

Figure 4.18b shows the relationship between the strong acid sites and the selectivity to byproducts. The 4.5Cu0.5Ag/γ-Al_2O_3 catalyst had a high concentration of strong acid sites, which increased the interaction between the octanal and catalyst surface. This interaction may decrease the desorption rate of the substrate, leading to further byproduct formation, as well as the re-adsorption of the octanol molecule leading to further reactions. The NH_3-TPD results showed 4Cu1Ag/γ-Al_2O_3 to have the lowest acidity; this would favour base catalyzed byproduct formation due to the amphoteric nature of alumina and the additional basicity introduced from the 1 % Ag on the surface (Table 3.8). This was supported by the minor formation of acid catalyzed C24 acetal.

Isoconversion studies showed that the 5Cu/γ-Al_2O_3 and 4Cu1Ag/γ-Al_2O_3 show a similar octanol selectivity and octanal conversion, however, the 4Cu1Ag/γ-Al_2O_3 provides a lower octene conversion, which is the desired effect in this study, making this catalyst the most suitable for selective hydrogenation of octanal in the presence of octene.

4.3. Kinetics

The selective hydrogenation of octanal in the presence of octene can be considered a pseudo first order reaction, following the Langmuir-Hinselwood mechanism, resulting in the hydrogen being dissociated on the catalyst surface. A few parameters were first established to determine the rate constants for the possible reaction pathways, such as the hydrogen pressure remained constant during the entire experiment, with the temperature and feed flow kept at a constant rate. In this reaction, the addition of the dissociated hydrogen to the unsaturated functional group is considered to be the rate determining step.

Much work has been done on regarding the kinetics of liquid phase hydrogenations. It was observed, by Guteirezz *et al.* [216], that the liquid phase hydrogenation of cinnamaldehyde using a copper-based catalyst, showed to have a pseudo first order rate of reaction. Additional work by Sharma *et al.* [80], showed the hydrogenation of α,β-unsaturated aldehydes followed a pseudo first order reaction. By assuming a pseudo first order reaction, one can separate the primary products from the byproducts to calculate the rate constant for octanal and octene hydrogenation as shown in Figure 4.19a-b.

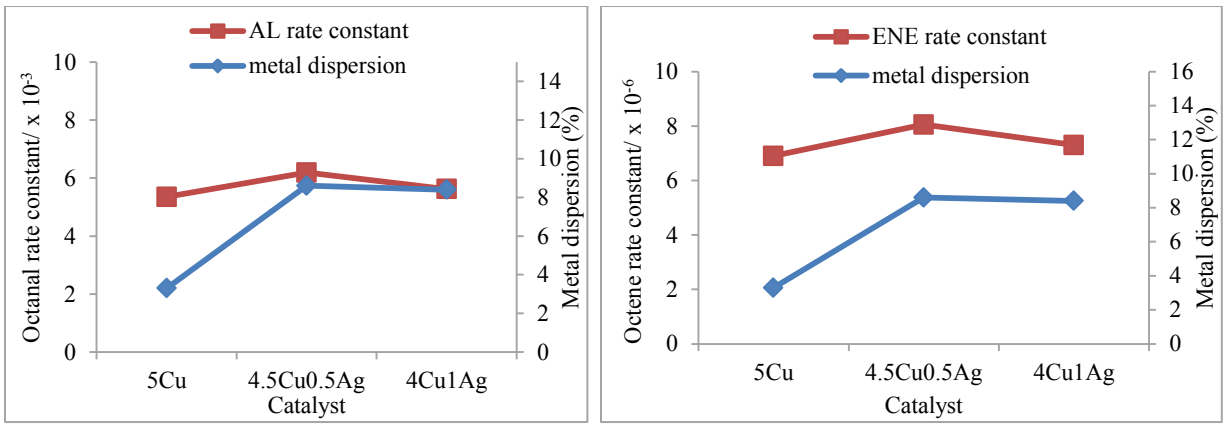

Figure 4.19. Graphs depicting the rate constant of (a) octanal and (b) octene hydrogenation vs metal dispersion for the catalysts investigated under isoconversion conditions.

Figure 4.19 shows a clear relationship between the metal dispersion and the rate constant. To summarize, Figure 4.19a-b shows that irrespective of active metal loading (copper), the higher metal dispersion results in a higher rate constant. This is due to the availability of the active copper species to adsorb the incoming reactants.

The simultaneous prepared 4.5Cu0.5Ag/γ-Al_2O_3 catalyst showed the highest octanal and octene conversion (Figure 4.2 and Figure 4.11) which is supported by the kinetics which showed the highest rate constant. The 4Cu1Ag/γ-Al_2O_3 catalyst showed the second highest rate constant for octene hydrogenation; however, catalytic testing showed this catalyst to have the lowest conversion for octene hydrogenation. The 4Cu1Ag/γ-Al_2O_3 catalyst has the lowest weight loading of copper present, however, it allows for a similar octene conversion to the 5Cu/γ-Al_2O_3 catalyst, which is due to the synergistic effect from the silver present in the bimetallic catalyst.

The turn over frequency (TOF) was calculated to determine if there were contributing factors such as mass-transfer limitations due to the catalyst system being a gas/liquid reaction. Figure 4.20 shows the TOF of the octanal and octene hydrogenation.

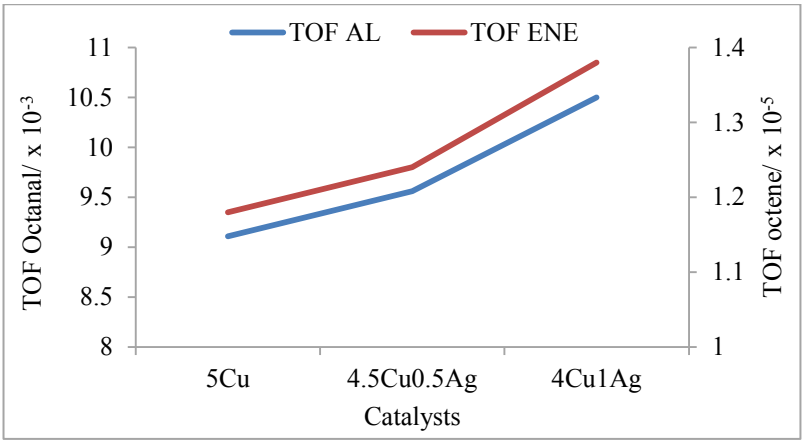

Figure 4.20. Graph depicting the TOF values of octanal (TOF AL) and octene (TOF ENE) hydrogenation for the 5Cu/γ-Al_2O_3, 4.5Cu0.5Ag/γ-Al_2O_3 and 4Cu1Ag/γ-Al_2O_3.

TOF was based on the moles of reactant converted over the moles of catalyst used over a certain period of time. It was shown in Figure 4.20 that with the decrease in copper loading, which was the active metal; there was an increase in TOF indicating a lower amount of the active metal can provide a similar or improved conversion. This relationship is attributed to the lower copper loading (4Cu1Ag/γ-Al_2O_3) showing a similar octanal and octene conversion to the 5Cu/γ-Al_2O_3 catalyst. This indicates that there are no mass-transfer limitations, as all reactions occur at 50 bar pressure with a octanal:hydrogen ratio of 1:2. The excess hydrogen and high pressure suggests the consistent hydrogen coverage on the catalyst throughout the reaction. This was supported by work done by Huerta *et al.* [217], Zhang *et al.* [218] and Chetty *et al.* [97]. The overall result showed that the addition of silver significantly improved the TOF values. This was most likely due to the interaction between the copper and silver resulting in a synergistic effect, as the copper is considered the active metal and this quantity is decreased with the increase in silver loading.

The kinetics was done at isoconversion; therefore, the most important factor to compare between the catalysts is the selectivity to the desired product, octanol. This relationship is shown in Figure 4.21.

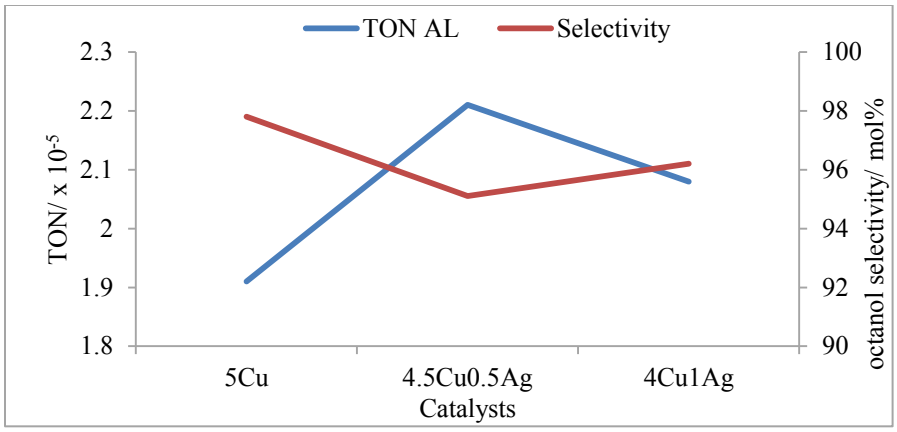

Figure 4.21. Graph depicting the TON value compared to the octanol selectivity at isoconversion using the 5Cu/γ-Al_2O_3, 4.5Cu0.5Ag/γ-Al_2O_3 and 4Cu1Ag/γ-Al_2O_3 catalysts.

The turn over number was dependent on the moles of catalyst used to adsorb a certain mole amount of reactant. The turnover number shows an inverse relationship between the TON and octanol selectivity. The 4.5Cu0.5Ag/γ-Al_2O_3 catalyst shows the highest TON value as well as the lowest octanol selectivity, while the 5Cu/γ-Al_2O_3 shows the lowest TON value and the highest octanol selectivity. This implies that the activity of the catalyst did not depend primarily on the moles of active metal, but rather on the availability and synergistic effects of the interaction between copper and silver as shown in the catalytic testing.

4.4. Used catalyst characterization

The recovery of the catalyst was obtained by drying the catalyst under 100 % Nitrogen at 200 °C for 12 hours in the reactor, thereafter the reactor was cooled to room temperature. The glass wool and carborundum was removed together with the catalyst, which was then sieved to separate the carborundum from the catalyst pellets. Used catalyst characterization was used to provide information of the catalyst thermal and mechanical stability, as well as the formation of coke on the surface. Some of the techniques used to gain insight of the catalyst surface after the reaction were Transmission Electron Microscopy (TEM), Scanning Electron Microscopy (SEM), Nitrogen Physisorption (BET), Infrared Spectroscopy (IR), Inductively Coupled Spectroscopy (ICP), and X-ray Diffraction (XRD).

4.4.1. Transmission electron microscopy (TEM) on selected catalysts

It was shown in the catalytic testing that the 5Cu/γ-Al_2O_3, there was a significant effect on the catalyst activity which was dependent on the reduction temperature. This indicated that there was a difference in their surface characteristics. TEM analysis was used to assist in characterization of the used 5Cu/γ-Al_2O_3. All used catalysts were analyzed using TEM, similarly to the fresh catalyst; there was no presence of metal or metal oxide particles. This indicates that there was limited or minimal agglomeration. Figure 4.22 showed selected images of the 5Cu/γ-Al_2O_3 used catalysts reduced at 220, 240, and 260 °C obtained from TEM analysis.

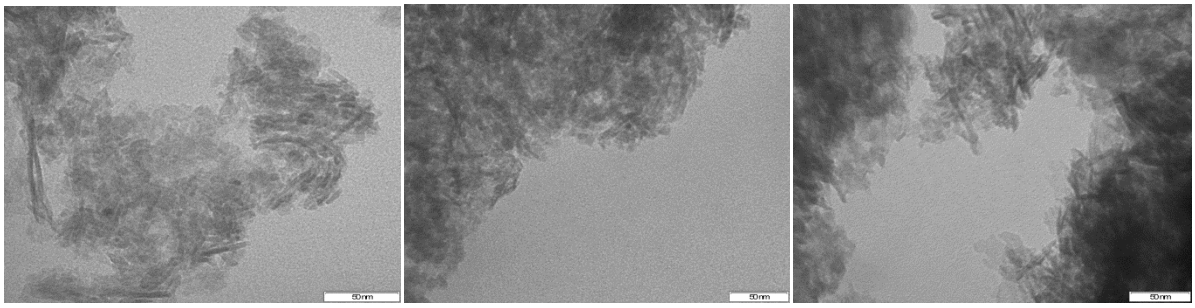

Figure 4.22. TEM Images obtained for the 5Cu/γ-Al_2O_3 catalyst reduced at temperatures (a) 220, (b) 240, and (c) 260 °C

4.4.2. Infrared spectroscopy

Infrared Spectroscopy was used to easily determine the presence on organics on the catalyst surface. Figure 4.23 shows the IR spectrum of the used 5Cu/γ-Al_2O_3 catalyst which was reduced at 220 °C.

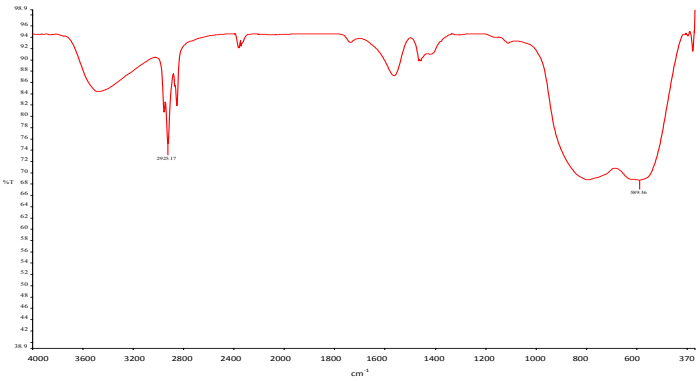

Figure 4.23. Infrared spectrum of the used 5Cu/γ-Al_2O_3 catalyst.

Further interpretation of the IR spectrum obtained indicates that within the region between 2300 -3100 cm $^{-1}$ is due to the presence of organic material. The presence of carbon/organics was observed for all used catalysts which are summarized in Table 4.5.

Table 4.3. Summary of results obtained from infrared spectroscopy of used catalysts.

Used Catalyst	O-H band (cm^{-1})	C-C (cm^{-1})	H_2O adsorbed (cm^{-1})	Al-O band (cm^{-1})	
5Cu/γ-Al_2O_3 (220)	3500	2925	1629	589	806
5Cu/γ-Al_2O_3 (240)	3502	3201, 2359	1599	543	799
5Cu/γ-Al_2O_3 (260)	3566	2924, 2360	1559	586	756
4.5Cu-0.5Ag/γ-Al_2O_3	3461	2927, 2359	1567	579	786
S-4.5Cu0.5Ag/γ-Al_2O_3	3640	2926, 2360	1558	583	783
S-0.5Ag4.5Cu/γ-Al_2O_3	3603	2932, 2440	1588	581	776
4Cu-1Ag/γ-Al_2O_3	3641	2926, 2362	1586	640	864
S-4Cu1Ag/γ-Al_2O_3	3457	2925, 2360	1554	587	820
S-1Ag4Cu/γ-Al_2O_3	3459	2965, 2345	1608	582	805
15Cu/γ-Al_2O_3	3608	2914, 2359	1614	668	811
13.5Cu-1.5Ag/γ-Al_2O_3	3633	2926, 2360	1553	552	795

Coke formation is a common by-product in catalytic reactions, which can lead to deactivation of the catalyst by blocking access of the incoming reactants to the active sites, therefore infrared spectroscopy analysis was conducted to investigate the extent of coke formation. The catalytic reactions were conducted over an 8 hour period; this showed no significant difference in conversion over time. This indicates that the formation of coke is minimal. The presence of organics obtained from infrared spectroscopy analysis could be due to insufficient drying of the

catalyst after the reaction, or heavy organics which have a boiling point greater than the drying temperature.

4.4.3. Inductively coupled plasma-optical emission spectroscopy (ICP-OES)

The use of ICP was implemented to determine the metal loading of the used catalysts; this was to investigate the possibility of leaching, as this may reduce the active metal concentration, which results in reduced activity as well as undesired catalyst stability. The ICP results obtained for all used catalysts are summarized in Table 4.6.

Table 4.4. Summary of metal loadings obtained from ICP-OES on the used catalysts.

Used Catalyst	Copper (wt %)	Silver (wt %)
5Cu/γ-Al_2O_3 (220)	4.60	-
5Cu/γ-Al_2O_3 (240)	4.75	-
5Cu/γ-Al_2O_3 (260)	4.67	-
4.5Cu-0.5Ag/γ-Al_2O_3	4.25	0.48
S-4.5Cu0.5Ag/γ-Al_2O_3	4.46	0.43
S-0.5Ag4.5Cu/γ-Al_2O_3	4.34	0.41
4Cu-1Ag/γ-Al_2O_3	3.65	1.05
S-4Cu1Ag/γ-Al_2O_3	3.87	0.93
S-1Ag4Cu/γ-Al_2O_3	4.03	0.97
15Cu/γ-Al_2O_3	14.5	-
13.5Cu-1.5Ag/γ-Al_2O_3	12.58	1.48

The metals loadings are slightly lower than for the fresh catalyst, this is a result of a minor presence of carbon deposits, which contributes towards the total mass of the sample. The amount of carbon deposits are unknown, therefore could not be subtraction from the used catalyst, resulting in a minor deviation from the actual metal loading. Keeping this into consideration, the ICP analysis did not show the possibility of metal leaching during the catalytic testing.

4.4.4. X-ray diffraction

Chapter 3 showed that due to the low weight loading of copper and silver, there were no metal oxide peaks observed for the catalysts with a total 5 wt % metal loading, metal oxides peaks were only observed with the catalysts containing a total metal loading of 15 wt %. For this reason, the used catalyst characterization was conducted for the 15Cu/γ-Al_2O_3 and the 13.5Cu1.5Ag/γ-Al_2O_3 catalysts as shown in Figure 4.24.

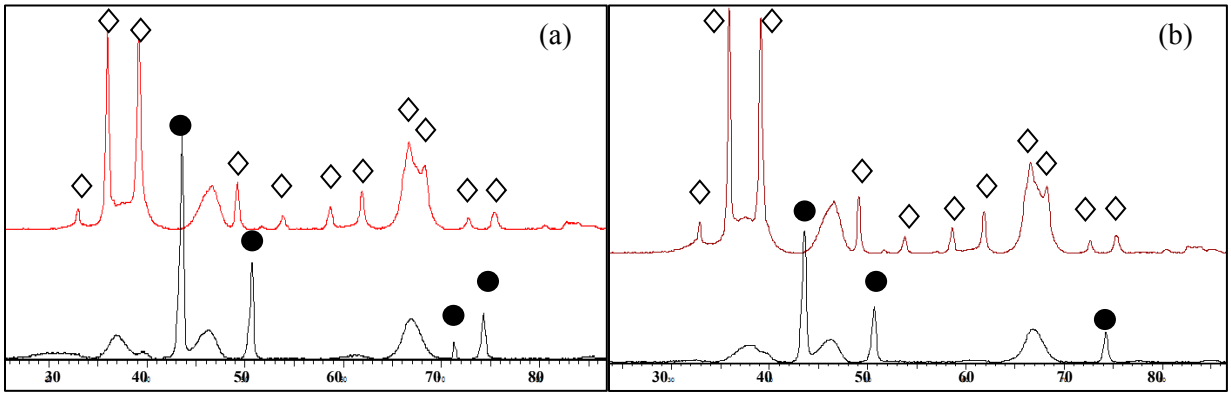

Figure 4.24. X-ray diffractogram (a) 15Cu/γ-Al_2O_3 catalyst: fresh (red) and used (black), and (b) 13.5Cu1.5Ag/γ-Al_2O_3 catalyst: fresh (red) and used (black). Peaks observed in the diffractograms are attributed to CuO (◇) and Cu (●).

Both used 15Cu/γ-Al_2O_3 and the 13.5Cu1.5Ag/γ-Al_2O_3 catalysts did not show metal oxide peaks on the diffractogram. Since copper is known to readily oxidize, while silver is stable in its metal state, suggests that the presence of carbon on the surface can minimize or inhibit the re-oxidation of copper. The CuO phase is consistent with that of ICDD 80-1268 and the used catalyst showed Cu^0 peaks consistent with JCPDS 04-0836.catalysts did not show metal oxide peaks suggesting that the presence of carbon on the surface can prevent or inhibit the re-oxidation of copper. The CuO phase is consistent with that of ICDD 80-1268 and the used catalyst showed Cu^0 peaks consistent with JCPDS 04-0836.

4.4.5. Brunauer-emmet-teller (BET) analysis

Surface area measurements using nitrogen physisorption can provide useful information on the surface area and pore size of the used catalysts. The comparison between the fresh catalyst and used catalysts can be used to investigate metal agglomeration or coke/carbon deposits on the surface or within the pores of the support. The fresh catalysts all showed a decrease in surface area of between 15-40 % depending on the metal loading and impregnation sequence shown in Chapter 3, Table 3.3.

Table 4.5. Surface measurements for all used catalysts.

Used Catalyst	Surface area/ m^2/g	Pore volume/ (cm^3/g)	Pore size/ nm
5Cu/γ-Al_2O_3 (220)	144	0.4	10.9
5Cu/γ-Al_2O_3 (240)	154	0.4	11.0
5Cu/γ-Al_2O_3 (260)	131	0.4	11.5
4.5Cu0.5Ag/γ-Al_2O_3	133	0.4	11.5
S-4.5Cu0.5Ag/γ-Al_2O_3	145	0.4	11.3
S-0.5Ag4.5Cu/γ-Al_2O_3	149	0.4	11.1
4Cu1Ag/γ-Al_2O_3	148	0.5	12.6
S-4Cu1Ag/γ-Al_2O_3	153	0.4	11.0
S-1Ag4Cu/γ-Al_2O_3	170	0.5	12.2
15Cu/γ-Al_2O_3	107	0.3	11.2
13.5Cu1.5Ag/γ-Al_2O_3	108	0.3	11.5

Table 4.5 shows a significant decrease of between 40-50 %, compared to their equivalent fresh catalysts, in surface area for all used catalysts analyzed. It can also be seen that there is a significant decrease in the pore volume of approximately 40 % while the pore size does not change significantly. This further supports that there are carbon deposits, which were adsorbed onto the catalyst surface and within the pores of the catalyst. There was no significant decrease

in the pore size which indicated that the carbon deposits form a relatively thin layer over the surface, which remains consistent with the results obtained from Infrared spectroscopy and ICP analysis.

4.4.6. Scanning electron microscopy

SEM analysis was conducted to selected used catalysts to provide information on the surface morphology of the catalyst surface after the reaction. Transmission Electron Microscopy (TEM), was used to analyze the used 5Cu/γ-Al_2O_3 which was reduced at different temperatures, did not provide sufficient information on the catalysts which could be used to correlate the catalyst surface and the catalytic activity. SEM analyses were implemented to obtain further information on the surface of the catalysts, which are shown in Figures 4.32 and 4.33.

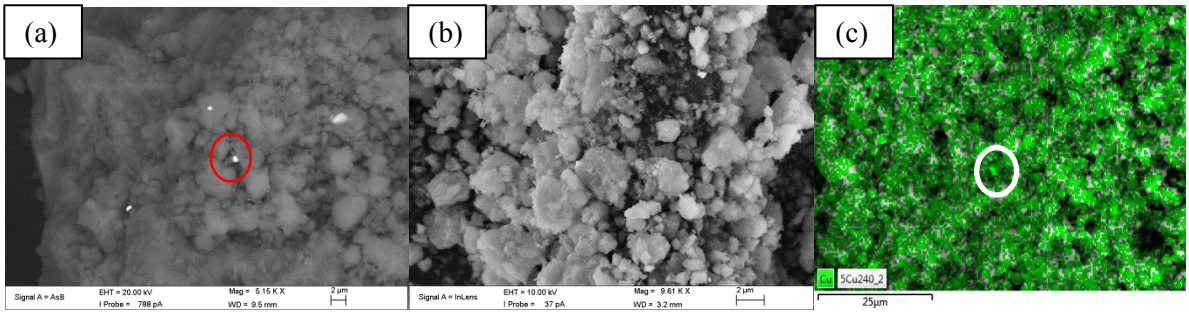

Figure 4.25. Used 5Cu/γ-Al_2O_3 catalyst reduced at 240 °C showing (a) Backscattered, (b) SEM, and (c) Backscattered Map with copper (green).

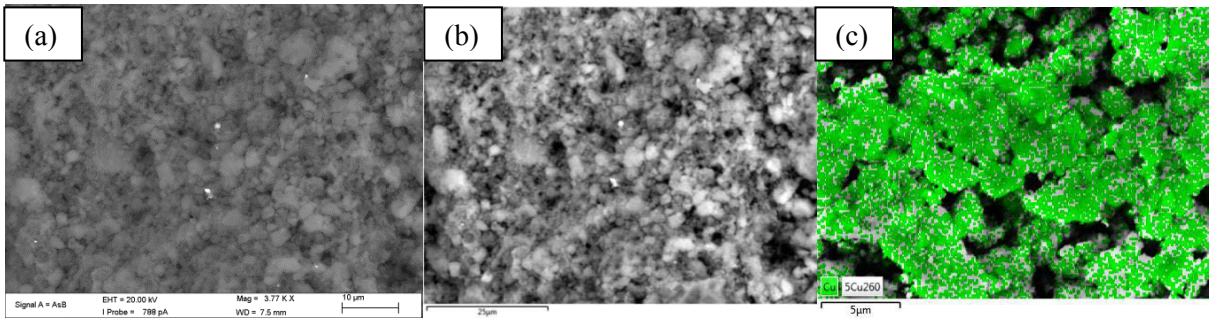

Figure 4.26. Used 5Cu/γ-Al_2O_3 catalyst reduced at 260 °C showing (a) Backscattered, (b) SEM, and (c) Backscattered Map with copper (green).

The catalytic results showed that with an increase in reduction temperature, there was an increase in the catalytic activity. Characterization using SEM-EDX mapping was conducted on the 5Cu/γ-Al_2O_3 used catalysts, which were reduced at 240 and 260 °C (Figure 4.25 and 4.26). The results showed minimal signs of agglomeration of copper. The EDX mapping (Figure 4.25c and Figure 4.26c) showed that the copper maintained a good dispersion across the support. The higher reduction temperature may cause an increase in the metal dispersion, which results in more available sites to adsorb the incoming reactants. The results obtained were also supported by hydrogen chemisorption analysis (Table 3.5), which showed an increase in metal dispersion with an increase in reduction temperature. A line scan analysis was conducted for the used 5Cu/γ-Al_2O_3 catalyst reduced at 260 °C to confirm if the copper was well dispersed across the support. This is shown in Figure 4.27a-b. The line scan shows that the copper profile follows the same trend as the aluminium line scan. This confirms that the copper is well dispersed with minimal agglomeration.

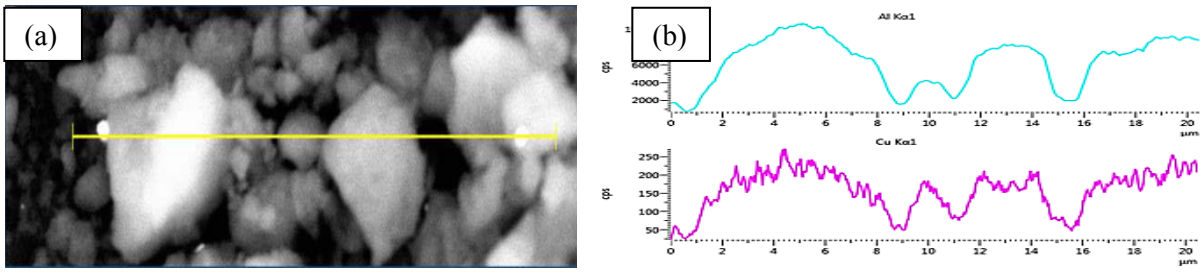

Figure 4.27. Line scan of used 5Cu/γ-Al_2O_3 catalyst reduced at 260 °C showing (a) SEM, and (c) Line scan spectra for copper (pink) and aluminium (blue).

Used 15Cu/γ-Al_2O_3

The analysis of the fresh 15Cu/γ-Al_2O_3 catalyst showed the metal to be clustered in some regions, with an overall good dispersion of metal across the support. The results of the SEM analysis done on the used 15Cu/γ-Al_2O_3 catalyst, to compare the surface characteristics of the catalyst surface after the reduction and catalytic testing, the SEM results are shown in Figure 4.28.

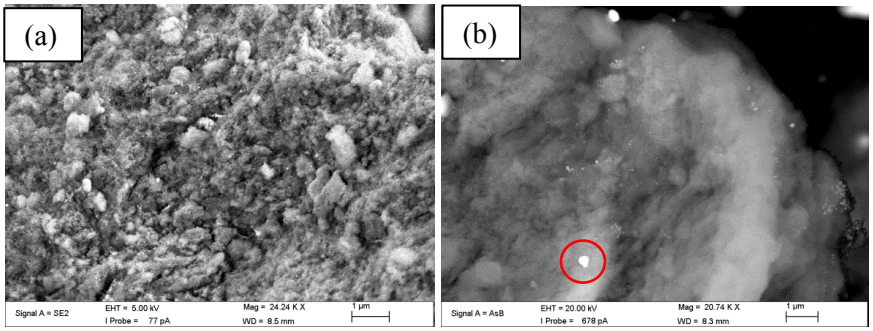

Figure 4.28. The used 15Cu/γ-Al_2O_3 catalyst reduced at 220 °C showing (a) SEM, and (b) Backscattered SEM.

SEM analysis off the used 15Cu/γ-Al_2O_3 showed an irregular morphology, and the presence of copper agglomerates was visible using backscattered SEM. The copper agglomerates were due to the high metal loading, and this is consistent with the results obtained of the fresh 15Cu/γ-Al_2O_3 catalyst shown in Chapter 3, Figure 3.23. The Fresh 15Cu/γ-Al_2O_3 catalyst showed a higher amount of copper oxide particles, suggesting that during the reduction, the metal dispersion of the reduced metal increased. This increase in metal dispersion and the smaller copper particles could result in higher catalytic activity, as there are more metal particles available to react. The used catalyst SEM analysis provided supporting information to the catalytic testing results obtained, where the 15Cu/γ-Al_2O_3 catalyst showed higher octene and octanal conversions compared to the 5Cu/γ-Al_2O_3 catalyst (Table 4.1).

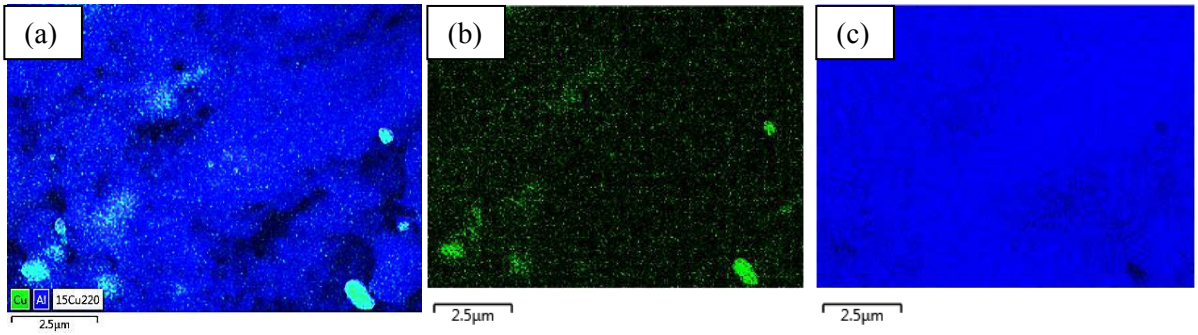

Figure 4.29. Used 15Cu/γ-Al_2O_3 catalyst reduced at 220 °C showing (a) SEM Map for copper and aluminium, (b) Copper (green) and (c) aluminium (blue).

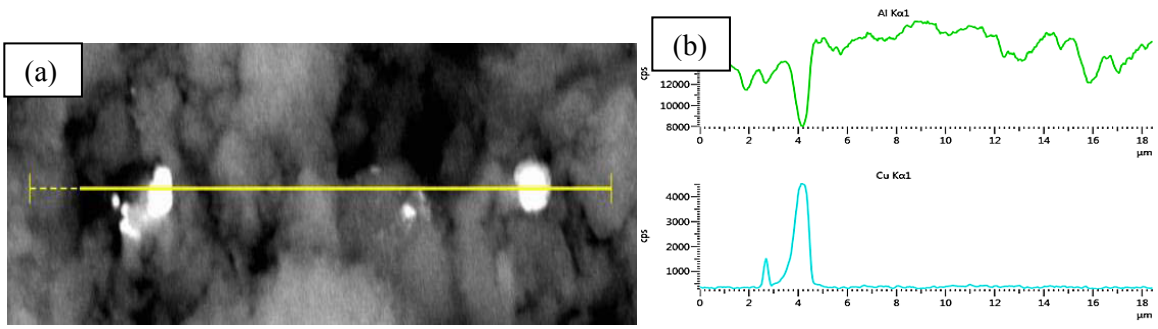

Figure 4.30. Used 15Cu/γ-Al_2O_3 catalyst reduced at 220 °C showing (a) Backscattered, (b) Line scan for aluminium (green) and copper (blue).

Figure 4.29 showed the results from EDX-Mapping of the used 15Cu/γ-Al_2O_3 catalyst. This technique confirmed the bright spots to be made up of copper, which correlates to the results obtained from the fresh catalysts. The line scan shown in Figure 4.30 conducted across a bright spot can also show that the bright particles may not be due to copper. There were two bright regions, which were analyzed; the first region was made up of copper, while the second bright spot could be due to carbon deposits causing the surface to charge in certain regions on the catalyst surface. This was supported by the presence of organic material on the catalyst surface, as shown by infrared spectroscopy and BET analysis.

Used 4.5Cu0.5Ag/γ-Al_2O_3 (simultaneous)

The SEM-EDX analysis of the fresh 4.5Cu0.5Ag/γ-Al_2O_3 catalyst showed agglomeration of silver in certain regions on the catalyst surface. Due to the low reduction temperature of silver (below 100 °C), there is a possibility the silver may agglomerate at higher reaction temperatures. Therefore, SEM and backscattered SEM were implemented for analysis of the used 4.5Cu0.5Ag/γ-Al_2O_3 catalyst to determine if there was a change in the surface morphology of the catalyst, which are shown in Figure 4.31.

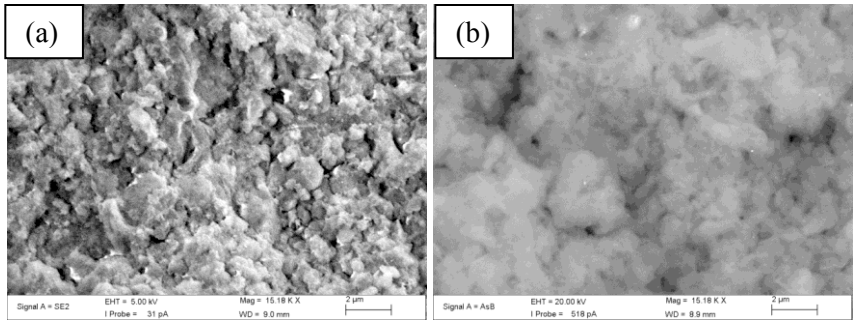

Figure 4.31. Used 4.5Cu0.5Ag/γ-Al_2O_3 catalyst reduced at 220 °C showing (a) SEM and (b) Backscattered SEM image.

Contradictory to the results for the fresh catalysts, the SEM and backscattered SEM results obtained did not show large agglomerated particles. This indicates that in a reducing environment, the metals have a higher metal dispersion than their metal oxide counterparts. This result was similar to the results observed with the used 15Cu/γ-Al_2O_3 catalyst.

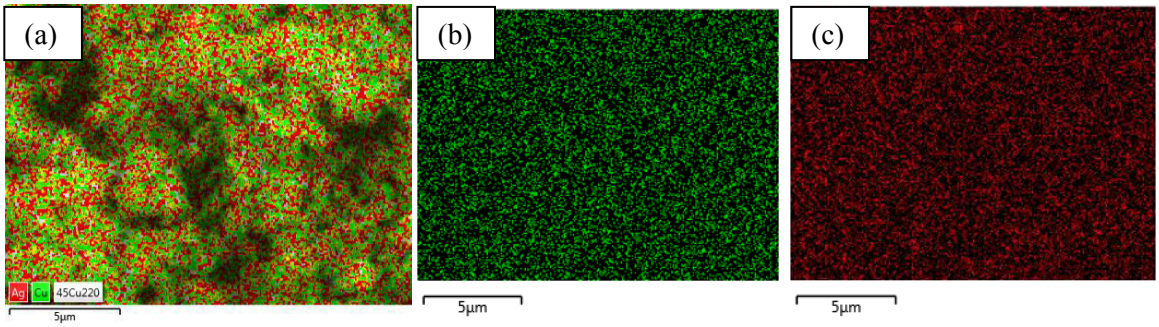

Figure 4.32. Used 4.5Cu0.5Ag/γ-Al_2O_3 catalyst reduced at 220 °C showing (a) SEM and (b) copper map (green) and (c) silver map (red).

Figure 4.32 showed the EDX mapping results of the 4.5Cu0.5Ag/γ-Al_2O_3, which was prepared via simultaneous impregnation. The SEM-EDX mapping showed an even distribution of both metals on the surface. Similar, to the fresh catalyst, the used 4.5Cu0.5Ag/γ-Al_2O_3 catalyst after catalytic testing showed a minor degree of silver agglomeration, consistent with results obtained for the fresh catalyst. This indicated that the surface morphology of the catalyst does not differentiate much from the freshly prepared catalyst, most likely due to the high thermal stability of the alumina-supported catalysts which may limit the extent of migration of the metals on the surface.

4.5. Summary of catalytic results and used catalyst characterization

The optimization experiments show that copper supported on γ-alumina is effective in selective hydrogenation of octanal in the presence of octene, with conversion being favoured with a higher metal weight loading, temperature and pressure. The optimum LHSV was found to be 18 h^{-1}, which allowed a good balance between high octanal conversion and low octene conversion to be obtained. The optimum temperature was chosen to be 160 °C as it provided maximum octanal conversion, while maintaining a high selectivity. At 160 °C, the octanal:hydrogen ratio of 1:2 was chosen due to the higher octanal conversion compared to the 1:1.5 ratio.

Bimetallic studies showed that there are a few key factors to consider when introducing an additional metal into the catalyst system. This includes weight loading and impregnation sequence. The increase in weight loading from 0.5 % Ag to 1 % Ag showed a decrease in octanal and octene conversion, with the S-4.5Cu0.5Ag/γ-Al_2O_3 and S-4Cu1Ag/γ-Al_2O_3 catalysts showing a lower conversion than the simultaneous impregnation catalysts (4.5Cu0.5Ag/γ-Al_2O_3). The S-0.5Ag4.5Cu/γ-Al_2O_3 catalyst showed a higher conversion compared to the simultaneous catalyst, while S-1Ag4Cu/γ-Al_2O_3 showed similar results to the simultaneous impregnation catalyst (4Cu1Ag/γ-Al_2O_3).

A main objective of this study was to obtain a low octene conversion to allow for the selective hydrogenation of octanal. The activity of all catalysts in terms of octene conversion under optimum conditions, with the conversion (%) shown in italics, is shown as:

13.5Cu1.5Ag/γ-Al_2O_3 *(40)* > 4.5Cu0.5Ag/γ-Al_2O_3 *(22)* >15Cu/γ-Al_2O_3 *(22)* > S-0.5Ag4.5Cu/γ-Al_2O_3 *(16)* > 4Cu1Ag/γ-Al_2O_3 *(13)* > S-1Ag4Cu/γ-Al_2O_3 *(13)* > 5Cu/γ-Al_2O_3 *(12)* > S-4.5Cu0.5Ag/γ-Al_2O_3 *(8)* > S-4Cu1Ag/γ-Al_2O_3 *(5)*

These results correlate with the characterization data obtained for the fresh and used catalysts. The larger the particle size, present with higher metal loaded catalysts, promoted the octene conversion, while the sequence of impregnation showed the simultaneous impregnation had a stronger synergistic effect resulting in higher activity. The presence of silver proved useful in decreasing the octene conversion at higher temperatures, with the lowest conversion obtained over the S-4Cu1Ag/γ-Al_2O_3 catalyst.

A summary of the octanal conversion under optimum conditions, shown in italics, showed the following trend.

S-0.5Ag4.5Cu/γ-Al_2O_3 *(100)* > 15Cu/γ-Al_2O_3 *(100)* > 4.5Cu0.5Ag/γ-Al_2O_3 *(98)* > 13.5Cu1.5Ag/γ-Al_2O_3 *(96)* > 4Cu1Ag/γ-Al_2O_3 *(96)* > S-1Ag4Cu/γ-Al_2O_3 *(93)* > S-4Cu1Ag/γ-Al_2O_3 g *(91)* > 5Cu/γ-Al_2O_3 *(90)* > S-4.5Cu0.5Ag/γ-Al_2O_3 *(79)*

This was consistent with results obtained from chemisorption studies where the higher metal dispersion had more available active sites for adsorption and hydrogenation of the incoming octanal and octene reactants. With the sequential catalysts, when copper was impregnated first, the silver on the upper layer minimized or inhibited the access and availability of the active copper sites, which decreased conversion of both reactants. The S-4.5Cu0.5Ag/γ-Al_2O_3 showed the lowest octanal conversion due to the silver on the upper layer having a higher dispersion over the copper compared to the S-4Cu1Ag/γ-Al_2O_3, where silver would tend to agglomerate to other silver atoms, exposing more copper.

All catalysts showed selectivities greater than 95 % towards octanol. It was shown that when silver was impregnated first, the copper migration into the alumina lattice was inhibited, thus increasing the copper dispersion allowing for a higher amount of available active sites. The most suitable catalyst was concluded to be the S-4Cu1Ag catalyst, as this catalyst showed the lowest octene conversion, while maintaining a good conversion of octanal of approximately 91 % and a high selectivity towards octanol.

Used catalysts were characterized using IR, ICP, BET, XRD, SEM, and TEM analysis. These techniques showed a minor presence of carbon deposits/organics on the surface, with no signs of metal leaching, and no significant changes in morphology indicating that all catalysts were thermal stable and recyclable.

Chapter 5
Conclusions and Future Work

Conclusions

Selective hydrogenation of C=O functional groups in the presence of C=C functional groups has been considered difficult due to the C=C bond being more thermodynamically favoured to hydrogenate. Extensive studies have been conducted over a wide range of catalytic systems, and new catalysts, are constantly investigated to determine the most efficient system for this reaction. Copper has been established in previous work to be active in the selective hydrogenation for unsaturated carbonyl molecules. This research effort showed γ-Al_2O_3 supported CuAg catalysts, which were used for the selective hydrogenation of octanal in the presence of octene in a competitive reaction environment. The optimum conditions were chosen to be 160 °C, 50 bar pressure, 18 h^{-1} LHSV, and 1:2 octanal:hydrogen ratio.

Nine catalysts were prepared using wet impregnation and were characterized using various techniques to obtain an insight into the surface composition and interaction between the copper and silver impregnated on the alumina support. SEM-EDX, TPR and H_2/CO chemisorption studies showed key differences between the simultaneous and sequential impregnation catalysts. This was used to understand and correlate the results, obtained from catalytic testing. Notable difference showed with the 5 % Cu and 15 % Cu catalysts was that an increase in weight loading resulted in clustering and agglomeration of the copper oxide on the surface in the higher loaded catalyst. This was confirmed using XRD, SEM-EDX and TPR. TPR also showed a decrease in reduction temperature for the bimetallic catalysts, with the copper and silver having a good dispersion on the support. STEM-EDX provided useful information in determining the surface composition and metal-metal interaction. Other techniques such as BET, TGA, and TPD all served as supporting techniques in establishing surface characteristics.

The 5 wt % catalysts were further investigated for the effect of silver and impregnation sequence, this resulted in the higher loading of silver increasing the selectivity towards octanal conversion,

while allowing for minimal octene conversion making a suitable catalyst. It was observed that a low loading of silver (0.5 % Ag) causes an increase in defect sites, resulting in a strong synergistic effect. At a silver loading of 1 %, the silver has a higher preference to agglomerate with other silver particles present rather than the copper particles, therefore the synergistic effect between these two metals were not as strong as with the 4.5Cu0.5Ag/γ-Al_2O_3 catalysts.

The effect of silver was established by preparing and testing a wide range of 5 wt % bimetallic catalyst. A few key factors were established; namely a suitable total weight loading, the weight loading of silver, and the impregnation technique. Catalytic results showed, with monometallic catalysts, a higher weight loading showed higher activity, which in some cases may not be a desired result due to the increased octene conversion. Under optimum conditions, the higher weight loadings of the bimetallic catalysts showed the formation of silver agglomerates which resulted in a decrease the activity.

The results obtained indicated a lower weight loading of 5 % for bimetallic catalyst system was more suitable compared to the 15 wt % catalysts. The 5 wt % bimetallic catalysts provided low octene conversion and high octanal conversion under optimum conditions. The octanol selectivity across all catalysts was higher than 95%, with the major byproducts being octyl octanoate, C16 diol and C24 acetal, which varied depending on the acidity of the catalysts and the temperature of the reaction. From the seven 5 wt % bimetallic catalysts investigated, the S-4Cu1Ag showed a lowest octene conversion of 5 % under optimum conditions, indicating that this catalyst system was most suitable, while maintaining a good conversion and octanol selectivity comparable to that of a monometallic copper catalyst system.

This work showed that within bimetallic systems investigated, their activity was dependent on a few key factors such as total weight loading of the catalyst, intermetallic weight loading and the impregnation sequence (simultaneous and sequential). It can be concluded that the presence of silver proved beneficial for the selective hydrogenation of octanal in the presence of octene, which allowed for minimal octene conversion while maintaining high octanal conversion and octanol selectivity as in the case of the 4Cu1Ag/γ-Al_2O_3 catalyst.

Kinetic calculations was implemented understand the rates of reaction towards the octanol formation and relates the surface characteristics (acidity and metal dispersion) contribution towards the selectivity of the desired and undesired products and byproducts.

Future work

The results obtained in this study provided sufficient information for a strong foundation into the use of copper-silver bimetallic catalysts for selective hydrogenation. Further investigation of these bimetallic catalysts must be extended to establish their effectiveness in selective hydrogenation with reactant feeds containing a higher concentration of octene in the presence of octanal. The application of these catalysts can also be extended into different mixed feeds such as an alkyne:alkene system, as this is a well-known industrial process which requires selective hydrogenation of alkyne to alkenes.

It was stated in this work that the alumina support contributed to the by-product formation and the migration of copper into the lattice forming a copper aluminate phase which was inactive for hydrogenation. It is important to change the support to provide supporting information on observations presented in this work. It is expected that the change in support would vary the metal-support interaction and its contribution towards byproduct formation, however, the extent of the support effect must be established to prove that the copper and silver are the active components responsible for selective hydrogenation. This can further be extended by looking at the effect of the impregnation sequence, as shown in this study, as this showed significant effect on the catalyst activity.

Lastly, a general overview on the results obtained in this work showed that the bimetallic catalysts showed a changed catalytic behavior due to metal-metal interaction. In this work, copper was presented as the active metal, while silver allowed for synergistic effects and a change in the metal dispersion. Therefore, a different second metal could be added to the copper/alumina system to determine the preferred or most efficient bimetallic system. Additionally, a monometallic silver/alumina catalyst must also be investigated to provide further information on the contribution to silver in the bimetallic catalyst system. The incorporation of

additional promoters or additives can be introduced to the catalytic system, such as ionic liquids, which will alter the surface properties, thus changing the behavior of the catalyst.

References

1. D. Astruc, *Introduction to catalysis*, in *Organometallic chemistry and catalysis* J. Perez, Editor. 2007.Springer Berlin Heidelberg,14. p. 351-355.
2. I. Chorkendorff and J. W. Niemantsverdriet, *Introduction to catalysis*, in *Concepts of modern catalysis and kinetics*, VCH-Wiley, Editor. 2003. Germany,1. p. 1-12.
3. J. H. Sinfelt,AIChE Journal,(1979).25(4):p. 734-734.
4. M. V. Twigg and M. S. Spencer,App. Cat.A: Gen.,(2001).212(1–2):p. 161-174.
5. J. A. Moulijn, A. E. van Diepen, and F. Kapteijn,App.Cat. A: Gen.,(2001).212(1–2):p. 3-16.
6. D. P. Secondary.*Collision theory*.2013 [cited 2013 14 Jan]; Available from: http://duch.sd57.bc.ca/~rmcleod/Chemists_Corner/PE_Diagram_Multi.html.
7. J. N. Armor,Catal. Today,(2011).163(1):p. 3-9.
8. F. E. Kühn, *Catalysis. From principles to applications.* , in *Angewandte chemie international edition*, Matthias Beller, Albert Renken, and Rutger A. van Santen, Editors. 2013.WILEY-VCH Verlag,1. p. 2650-2680.
9. B. Lindström and L. Pettersson,CATTECH,(2003).7(4):p. 130-138.
10. A. J. B. Robertson,Platinum Metals Rev.,(1975).19(2):p. 64-69.
11. H. Schulz,App. Cat. A: Gen.,(1999).186(1–2):p. 3-12.
12. A. V. Sapre, *Conversion of methanol to olefins in a tubular reactor with light olefin co-feeding*, 1986, Google Patents.
13. I. A. Cody, d. Glen P. Hamner, W. H. Sawyer, and J. J. Schorfheide, *Method for producing a wax isomerization catalyst*, 1990, Google Patents.
14. W. S. Frederick and W. R. Frank, *Hydrocarbon conversion by contact with active catalyst and inert solid heat carryingmaterial*, 1948, Google Patents.
15. K. E. Holt,ChemInform,(2005).36(42):p. 1-3.
16. T. Johannes, M. R. Simurdiak, and H. Zhao, *Biocatalysis*, in *Encyclopedia of chemical processing*. 2006. 101-110.
17. P. Wanner and R. Tressl,Eur. J.Biochem.,(1998).255(1):p. 271-278.
18. M. A. Swiderska and J. D. Stewart,J.Mol. Catal.B: Enzym.,(2006).42(1–2):p. 52-54.
19. T. Hirata, A. Matsushima, Y. Sato, T. Iwasaki, H. Nomura, T. Watanabe, S. Toyoda, and S. Izumi,J Mol Catal B Enzym,(2009).59(1-3):p. 5-5.
20. H. Zhang, X. Gao, J. Ren, J. Feng, T. Zhang, Q. Wu, and D. Zhu,J.Mol. Catal. B: Enzym.,(2014).105(0):p. 118-125.
21. M. K. Lam, K. T. Lee, and A. R. Mohamed,Biotechnology Adv.,(2010).28(4):p. 500-518.
22. B. Cornils and W. A. Herrmann,J.Catal.,(2003).216(1–2):p. 23-31.
23. D. Morzin and T. Salmi, *Catalysis*, in *Catalytic kinetics*, Elsevier B. V, Editor. 2005. The Netherlands,2. p. 27-43.
24. *Introduction to hydroformylation*, in *Rhodium catalyzed hydroformylation*, P. W. N. M. van Leeuvan and Carmen Claver, Editors. 2001.Kluwer Academic Publishers: The Netherlands,1. p. 1-13.
25. I. Choinopoulos, I. Papageorgiou, S. Coco, E. Simandiras, and S. Koinis,Polyhedron,(2012).45(1):p. 255-261.
26. J. Zakzeski, H. R. Lee, Y. L. Leung, and A. T. Bell,App. Cat. A: Gen.,(2010).374:p. 201-212.
27. M. L. Clarke,Polyhedron,(2001).20(3–4):p. 151-164.

28. M. Beller, *Homogeneous catalysis for fine chemical synthesiss — new trends and perspectives —*, in *Heterogeneous catalysis and fine chemicals iv*, H.U. Blaser, A. Baiker, and R. Prins, Editors. 1997.Elsevier,1. p. 1-16.
29. P. W. N. M. van Leeuwen, *Introduction*, in *Homogeneous catalysis: Understanding the art*, Kluwer Academic Publishers, Editor. 2006. The Netherlands,1. p. 1-10.
30. C. Perego and P. Villa,Catalysis Today,(1997).34(3–4):p. 281-305.
31. K. W. Kolaninski, *Surface science, foundation of catalysis and surface science*, John Wiley & sons, Editor. 2012. West Sussex, United Kingdom,1. p. 3-10.
32. S. Nishimura, *Hydrogenation of aldehydes and ketones*, in *Handbook of heterogeneous catalytic hydrogenation for organic synthesis*, John Wiley & Sons, Editor. 2001. United States of America,5. p. 170-218.
33. M. Sankar, N. Dimitratos, P. J. Miedziak, P. P. Wells, C. J. Kiely, and G. J. Hutchings,Chem. Soc. Rev.,(2012).41(24):p. 8099-8139.
34. S. Nanda.*Reactors and fundamentals of reactors design for chemical design,*Maharshi Dayanand University,Delhi,PhD,p.2-22
35. V. K. Jayaraman and B. D. Kulkarni, *Catalytic reactors: A review*, in *Encyclopedia of Life Support Systems*: India. p. 1-9.
36. K. R. Westerterp, E. J. Molga, and K. B. van Gelder,Chem. Eng. and Processing: Process Intensification,(1997).36(1):p. 17-27.
37. T. E. C. Industry.*Chemical reactors*.2013 26 March]; Available from: http://www.essentialchemicalindustry.org/processes/chemical-reactors.html.
38. G. Biardi and G. Baldi,Catal. Today,(1999).52(2–3):p. 223-234.
39. D. Mousko.*Heterogeneous catalysis in the different reactor types on the examples of ethyl benzene to styrene, methane dehydroaromatization, and propylene carbonate/methanol transesterification,*Rhine Westphalia University of Technology,Aachen,PhD,p.3-14
40. N. Gounden.*The oxidative activation of n-octane over titania supported cobalt,*University of KwaZulu-Natal,South Africa,MSc,p.1-10
41. F. A. N. Fernandes and L. M. F. Lona,Brazilian J.Chem.Eng.,(2000).17:p. 163-170.
42. B. Bachiller-Baeza, I. Rodr guez-Ramos, and A. Guerrero-Ruiz,App. Cat. A: Gen.,(2001).205(1–2):p. 227-237.
43. Wikipedia.*James. F. Boyce, sr*.2014 [cited 2014 7 Jan]; Available from: http://en.wikipedia.org/wiki/James_F._Boyce,_Sr.
44. V. Ponec,App. Cat. A: Gen.,(1997).149(1):p. 27-48.
45. Sanfilippo. D, *Catalytic industrial process*, in *Catalysis*2009, EOLSS. p. 1-9.
46. G. Scrinis,World Nutrition,(2014).5(1).
47. *Reactions*, in *Hydrogen: An overview*, E.P.Muljadi, Editor. 1979.CRC Press,3. p. 72-82.
48. BASF.*Make the right move with nanoselect catalysts*.2009 [cited 2014 1 August]; Available from: https://www.basf.de/basf2/img/pharma/2009-01/BASF_NanoSelect.pdf.
49. B. Yang, R. Burch, C. Hardacre, G. Headdock, and P. Hu,ACS Catal.,(2013).4(1):p. 182-186.
50. A. Andoni and R. A. van Santen,Chem. Eng. Trans.,(2013).34:p. 19-24.
51. M. Lenarda, M. Casagrande, E. Moretti, L. Storaro, R. Frattini, and S. Polizzi,Catal. Letters,(2007).114(1-2):p. 79-84.
52. A. A. Nikolopoulos, B. W. L. Jang, and J. J. Spivey,App. Cat. A: Gen,(2005).296(1):p. 128-136.
53. S. K. Sharma, P. A. Parikh, and R. V. Jasra,J.Mol.Catal. A: Chem.,(2010).316(1–2):p. 153-162.
54. A. B. da Silva, E. Jordão, M. J. Mendes, and P. Fouilloux,App. Cat. A: Gen.,(1997).148(2):p. 253-264.
55. A. Mori, T. Mizusaki, Y. Miyakawa, E. Ohashi, T. Haga, T. Maegawa, Y. Monguchi, and H. Sajiki,Tetrahedron,(2006).62(51):p. 11925-11932.
56. J. Hong, W. Chu, M. Chen, X. Wang, and T. Zhang,Catal.Comm.,(2007).8(3):p. 593-597.

57. M. B. Smith and March. J, *March's advanced organic chemistry: Reactions, mechanisms and structure,* , Inc Wiley & Sons, Editor. 2007.Wiley & Sons, Inc, : Hoboken, New Jersey,15. p. 1792-1793.
58. B. Wu, H. Huang, J. Yang, N. Zheng, and G. Fu,Ang. Chem. Int. Ed.,(2012).51(14):p. 3440-3443.
59. J. M. Winterbottom, H. Marwan, J. Viladevall, S. Sharma, and S. Raymahasay, *Selective catalytic hydrogenation of 2-butyne-1,4-diol to cis-2-butene-1,4-diol in mass transfer efficient slurry reactors*, in *Heterogeneous catalysis and fine chemicals iv*, A. Baiker H.U. Blaser and R. Prins, Editors. 1997.Elsevier: The Netherlands,7. p. 59-66.
60. X. Wang, R. Y. Saleh, and U. S. Ozkan,J.Catal.,(2005).231(1):p. 20-32.
61. G. M. R. van Druten and V. Ponec,App.Cat. A: Gen.,(2000).191(1–2):p. 153-162.
62. A. Stolle, T. Gallert, C. Schmoger, and B. Ondruschka,RSC Adv.,(2013).3(7):p. 2112-2153.
63. R. L. Augustine and J. V. Peppen,Annals of the New York Academy of Sciences,(1969).158(2):p. 482-491.
64. B. Mattson, W. Foster, J. Greimann, T. Hoette, N. Le, A. Mirich, S. Wankum, A. Cabri, C. Reichenbacher, and E. Schwanke,J.Chem. Ed.,(2013).90(5):p. 613-619.
65. R. J. Baxter and P. Hu, J.Chem. Phys.,(2002).116(11):p. 4379-4381.
66. E. E. Gonzo, J. C. Gottifredi, and L. C. Romero,Chem. Eng. Sci.,(1988).43(6):p. 1410-1413.
67. B. Yang, X.-Q. Gong, H.-F. Wang, X.-M. Cao, J. J. Rooney, and P. Hu,J.Am.Chem. Soc.,(2013).135(40):p. 15244-15250.
68. B. Bridier, N. López, and J. Pérez-Ramírez,J.Catal.,(2010).269(1):p. 80-92.
69. C. Ando, H. Kurokawa, and H. Miura,App.Cat. A: Gen.,(1999).185(2):p. L181-L183.
70. P. Gallezot and D. Richard,Catal.Revi.sci. and Eng.,(1998).40(1-2):p. 81-126.
71. A. Govender.*Supported copper oxide catalysts for octanal hydrogenation: The influence of water,*University of KwaZulu-Natal,South Africa,MSc,p.1-162
72. S. Sitthisa, T. Sooknoi, Y. Ma, P. B. Balbuena, and D. E. Resasco,J. Catal.,(2011).277(1):p. 1-13.
73. J. D. Roberts and M. C. Caserio, *Alkenes and alkynes ii. Oxidation and reduction reaction, acidity or alkynes* in *Basic principles of organic chemistry*, W. A. Benjamin, Editor. 1977. Canada,16. p. 405-437.
74. C. S. Karaiskos, D. Matiadis, O. Igglessi-Markopoulou, and J. Markopoulos, *Homogeneous chemoselective hydrogenation of heterocyclic compounds – the case of 1,4 addition on conjugated c-c and c-o double bonds of arylidene tetramic acids*, in *Hydrogenation*, Iyad Karame, Editor. 2012.InTech,4. p. 91-120.
75. A. K. Ghosh and K. Krishnan,Tetrahedron Letters,(1998).39(9):p. 947-948.
76. H. Donkervoot,Focus on Catalysts,(2009).2009(5):p. 6.
77. H. Sajiki, S. Mori, T. Ohkubo, T. Ikawa, A. Kume, T. Maegawa, and Y. Monguchi,Chemistry – A Eur. Journal,(2008).14(17):p. 5109-5111.
78. I. T. Duncanson, I. W. Sutherland, B. Cullen, S. D. Jackson, and D. Lennon,Catal. Letters,(2005).103:p. 3-4.
79. C. V. Rode, P. R. Tayae, J. M. Nadgeri, R. Jaganathan, and R. V. Chaudari,Org. Process Research and Development,(2006).10:p. 278-284.
80. R. V. Sharma, U. Das, R. Sammynaiken, and A. K. Dalai,App. Cat.A: Gen.,(2013).454(0):p. 127-136.
81. M. M. Villaverde, N. M. Bertero, T. F. Garetto, and A. J. Marchi,Catal. Today,(2013).213(0):p. 87-92.
82. P. Sangeetha, B. M. Nagaraja, K. Shanthi, K. S. Rama Rao, and S. Narayanan,Bulletin of the Catalyis Society of India,(2009).8:p. 52-63.
83. J. P. Dath, F. Genin, K. Hortmann, and G. Vulpescu,*Catalyst and process for hydrogenation of hydrocarbon feedstocks*,(2010),Total Petrochemicals Research Feluy,EP20080172308
84. S. J. Stanley and C. Sumner,*Catalytic distillation and hydrogenation of heavy unsaturates in an olefins plant*,(1999),US 08/914,712

85. R. R. Whetstone,*Preparation of acrolein acetal*,(1953),US2626283
86. M. Foral, L. Satek, and D. Ventura,*Process for recovery of diene-free feedstocks from olefinic process streams*,(2003),BP Corp North America Inc.,PCT/US2002/034929
87. B. M. Bhanage, S. S. Divekar, R. M. Deshpande, and R. V. Chaudhari,J.Mol.Catal. A: Chem.,(1997).115(2):p. 247-257.
88. A. R. Tadd, A. Marteel, M. R. Mason, J. A. Davies, and M. A. Abraham, J.Supercritical Fluids,(2003).25(2):p. 183-196.
89. A. B. Rivas, J. J. Pérez-Torrente, A. J. Pardey, A. M. Masdeu-Bultó, M. Diéguez, and L. A. Oro,J.Mol.Catal. A: Chem.,(2009).300(1–2):p. 121-131.
90. L. c. Ropartz, R. E. Morris, D. F. Foster, and D. J. Cole-Hamilton,J.Mol.Catal. A: Chem.(2002).182–183(0):p. 99-105.
91. J. Qiu, H. Zhang, X. Wang, and B. Yin,Preprints of Papers-Am.Chem.Soc., Division of Fuels and Chemicals,(2004).49(2):p. 940-941.
92. S.-Y. Yun, M. J. Seong, J.-H. Yim, Y. S. Ko, Y.-K. Park, and J.-K. Jeon,Rev. Adv. Materials Science,(2011).28(2):p. 154-157.
93. M. Benaissa, U. J. Jáuregui-Haza, I. Nikov, A. M. Wilhelm, and H. Delmas,Catal. Today,(2003).79–80(0):p. 419-425.
94. U. J. Jáuregui-Haza, E. Pardillo-Fontdevila, P. Kalck, A. M. Wilhelm, and H. Delmas,Catal. Today,(2003).79–80(0):p. 409-417.
95. A. Riisager, K. M. Eriksen, P. Wasserscheid, and R. Fehrmann,Catal. Letters,(2003).90(3-4):p. 149-153.
96. D. T. Johnson Mattey.*Sasol heptene to 1-octanol*.2014 [cited 2014 16 Jan]; Available from: http://www.davyprotech.com/default.aspx?cid=500.
97. T. Chetty, H. B. Friedrich, V. D. B. C. Dasireddy, A. Govender, P. J. Mohlala, and W. Barnard,ChemCatChem,(2014).6(8):p. 2384-2393.
98. P. Gallezot and D. Richard,Catal. Reviews,(1998).40(1-2):p. 81-126.
99. R. Bruckner, *Additions of heteroatom nucleophiles to carbonyl compounds and subsequent reactions—condensations of heteroatom nucleophiles with carbonyl compounds*, in *Organic mechanisms: Reactions, stereochemistry and synthesis*, Micheal Harmata, Editor. 2010.Springer,6. p. 359-395.
100. A. Burrows, J. Holman, A. Parsons, G. Pilling, and G. Price, *Aldehydes and ketones,: Nucleophillic addition and α--substitution reactions*, in *Chemistry: Introducing inorganic, organic and physical chemistry*, OUP Oxford, Editor. 2013. United States,23. p. 1050-1088.
101. K. G. Bothara, *Nucleophilic addition of a carbonyl function*, in *Organic pharmaceutical chemistry*, Nirali Prakashan, Editor. 2008. Pune,9. p. 119-132.
102. S. Veibel and J. I. Nielsen,Tetrahedron,(1967).23(4):p. 1723-1733.
103. M. N. Dvornikoff and M. W. Farrar, J.Org.Chem.,(1957).22(5):p. 540-542.
104. B. C. Gates and F. C. Jentoft, *Advances in catalysis*, ed. Elsevier Science. Vol. 56. 2013, USA.
105. B. A. Tschaen, J. R. Schmink, and G. A. Molander,Org.Letters,(2013).15(3):p. 500-503.
106. V. Bethmont, C. Montassier, and P. Marecot,J. Mol.Catal.A: Chem.,(2000).152(1–2):p. 133-140.
107. J. M. Bell, D. G. Kubler, P. Sartwell, and R. G. Zepp, J. Org. Chem.,(1965).30(12):p. 4284-4292.
108. W. S. Millman and G. V. Smith, *Role of acetal formation in metal catalyzed hydrogenation and exchange of cinnamaldehyde* in *Catalysis in organic syntheses 1977*, Gerard V. Smith, Editor. 1977.Academic Press: United States of America,1. p. 33-65.
109. F. Delbecq and P. Sautet,J.Catal.,(1995).152(2):p. 217-236.
110. W. Q. Du, Z. M. Rong, Y. Liang, Y. Wang, X. Y. Lu, Y. F. Wang, and L. H. Lu,Chinese Chem. Letters,(2012).23(7):p. 773-776.
111. S. Valange, A. Derouault, J. Barrault, and Z. Gabelica,J. Mol.Catal.A: Chem.,(2005).228(1–2):p. 255-266.
112. J. Joubert and F. Delbecq,Organometallics,(2006).25:p. 854-861.

113. K. H. Lim, A. B. Mohammad, I. V. Yudanov, K. M. Neyman, M. Bron, P. Claus, and N. R sc h,The Journal of Physical Chemistry C,(2009).113(30):p. 13231-13240.
114. V. N. Ipatieff and V. Haensel,J.Am. Chem.Soc.,(1942).64(3):p. 520-521.
115. F. Zaccheria, N. Ravasio, R. Psaro, and A. Fusi,Tetrahedron Letters,(2005).46(21):p. 3695-3697.
116. R. Hubaut, M. Daage, and J. P. Bonnelle,App. Cat.,(1986).22(2):p. 243-255.
117. R. Hubaut, M. Daage, and J. P. Bonnelle,App.Cat.,(1986).22(2):p. 231-241.
118. R. Hubaut, M. Daage, and J. P. Bonnelle, *Role of electronic effects and steric hindrance in hydrogenation of unsaturated compounds on copper chromite catalysts*, in *Studies in surface science and catalysis*, J. Barrault C. Bouchoule D. Duprez C. Montassier M. Guisnet and G. Pérot, Editors. 1988.Elsevier,3. p. 131-138.
119. A. Chambers, S. David Jackson, D. Stirling, and G. Webb,J.Catal.,(1997).168(2):p. 301-314.
120. A. J. Marchi, D. A. Gordo, A. F. Trasarti, and C. R. Apestegu a,App.Cat. A: Gen.,(2003).249(1):p. 53-67.
121. E. Sayah, C. La Fontaine, V. Briois, D. Brouri, and P. Massiani,Catal. Today,(2012).189(1):p. 55-59.
122. N. Bogdanchikova, F. C. Meunier, M. Avalos-Borja, J. P. Breen, and A. Pestryakov,App. Cat. B: Environ.,(2002).36(4):p. 287-297.
123. R. Crook, J. Deering, S. J. Fussell, A. M. Happe, and S. Mulvihill,Tetrahedron Letters,(2010).51(39):p. 5181-5184.
124. M. Bron, D. Teschner, A. Knop-Gericke, F. C. Jentoft, J. Krohnert, J. Hohmeyer, C. Volckmar, B. Steinhauer, R. Schlogl, and P. Claus,Phys. Chem.Chem. Phys.,(2007).9(27):p. 3559-3569.
125. K. Brandt, M. E. Chiu, D. J. Watson, M. S. Tikhov, and R. M. Lambert,J.Am. Chem.Soc.,(2009).131(47):p. 17286-17290.
126. D. Diesing, G. Kritzler, and A. Otto. *Electron and ion transfer in condensed media: Theoretical physics for reaction kinectics*. 1997. Italy: World Scientific.
127. Y. Nagase, H. Hattori, and K. Tanabe,Chem.Letters,(1983).12(10):p. 1615-1618.
128. Y. Chen, C. Wang, H. Liu, J. Qiu, and X. Bao,Chem.Communications,(2005)(42):p. 5298-5300.
129. P. Claus, P. Kraak, and R. Schödel,Studies in Sur. Sci.Catal.,(1997).108:p. 281-288.
130. W. Grünert, A. Brückner, H. Hofmeister, and P. Claus,J.Phys.Chem. B,(2004).108(18):p. 5709-5717.
131. M. Bron, D. Teschner, A. Knop-Gericke, B. Steinhauer, A. Scheybal, M. Hävecker, D. Wang, R. Födisch, D. Hönicke, A. Wootsch, R. Schlögl, and P. Claus,J.Catal.,(2005).234(1):p. 37-47.
132. H. Wei, C. Gomez, J. Liu, N. Guo, T. Wu, R. Lobo-Lapidus, C. L. Marshall, J. T. Miller, and R. J. Meyer,J.Catal.,(2013).298(0):p. 18-26.
133. R. Ferullo, M. M. Branda, and F. Illas,J.Phys.Chem.Letters,(2010).1(17):p. 2546-2549.
134. P. Claus and H. Hofmeister, J.Phys.Chem.B,(1999).103(14):p. 2766-2775.
135. C. E. Volckmar, M. Bron, U. Bentrup, A. Martin, and P. Claus,J. Catal.,(2009).261(1):p. 1-8.
136. C. Baatz, N. Decker, and U. Prüße,J.Catal.,(2008).258(1):p. 165-169.
137. S. Ivanova, V. Pitchon, Y. Zimmermann, and C. Petit,App. Cat. A: Gen.,(2006).298(0):p. 57-64.
138. M. Bowker, A. Nuhu, and J. Soares,Catal. Today,(2007).122(3–4):p. 245-247.
139. A.-F. An, A.-H. Lu, Q. Sun, J. Wang, and W.-C. Li,Gold Bulletin,(2011).44(4):p. 217-222.
140. G. C. Bond and P. A. Sermon,Gold Bulletin,(1973).6(4):p. 102-105.
141. A. Sanchez, S. Abbet, U. Heiz, W. D. Schneider, H. Häkkinen, R. N. Barnett, and U. Landman,J Phys.Chem.A,(1999).103(48):p. 9573-9578.
142. N. Perret, F. Cárdenas-Lizana, and M. A. Keane,Catal.Comm.,(2011).16(1):p. 159-164.
143. V. R. Choudhary, P. A. Chaudhari, and V. S. Narkhede,Catal. Comm.,(2003).4(4):p. 171-175.
144. A. Hugon, L. Delannoy, J.-M. Krafft, and C. Louis, J.Phys. Chem. C,(2010).114(24):p. 10823-10835.
145. R. Ferrando, J. Jellinek, and R. Johnston,Chem. Rev.,(2008).108(3):p. 845-910.
146. H. Wei.*Selective hydrogenation of acrolein over supported silver and silver alloy catalysts,*University of Illinois,Chicago, Illinois,PhD,p.7-15

147. M. Cazayous, C. Langlois, T. Oikawa, C. Ricolleau, and A. Sacuto,Phys.Rev.B,(2006).73(113402):p. 1-4.
148. L. E. Murillo, A. M. Goda, and J. G. Chen,J.Am. Chem.Soc.,(2007).129(22):p. 7101-7105.
149. M. Simionato and E. M. Assaf,Mat.Research,(2003).6:p. 535-539.
150. D. Sun, Y. Yamada, and S. Sato,App. Cat.A: Gen.,(2014).475(0):p. 63-68.
151. J. Zheng, H. Lin, Y.-n. Wang, X. Zheng, X. Duan, and Y. Yuan,J. Catal.,(2013).297:p. 110-118.
152. S.-Y. Zhu, R.-J. Hou, and T.-F. Wang, Chinese J.Process Eng.,(2012).12(3):p. 489 -496.
153. S. Deng, W. Chu, H. Xu, L. Shi, and L. Huang,J. Natural Gas Chem.,(2008).17(4):p. 369-373.
154. S. Jongpatiwut, Z. Li, D. E. Resasco, W. E. Alvarez, E. L. Sughrue, and G. W. Dodwell,App.Cat. A: Gen.,(2004).262(2):p. 241-253.
155. R. V. Malyala, C. V. Rode, M. Arai, S. G. Hegde, and R. V. Chaudhari,App.Cat. A: Gen.(2000).193(1–2):p. 71-86.
156. O. S. Alexeev, G. W. Graham, M. Shelef, and B. C. Gates,J.Catal.,(2000).190(1):p. 157-172.
157. B. Bachiller-Baeza, A. Guerrero-Ruiz, P. Wang, and I. Rodr guez-Ramos,J.Catal.,(2001).204(2):p. 450-459.
158. P. Reyes, G. Pecchi, and J. L. G. Fierro,Langmuir,(2000).17(2):p. 522-527.
159. S. S. Ashour, J. E. Bailie, C. H. Rochester, J. Thomson, and G. J. Hutchings,J.Mol.Catal.A: Chem.,(1997).123(1):p. 65-74.
160. M. Lucas and P. Claus,Chem. Eng. Tech.,(2005).28(8):p. 867-870.
161. W.-P. Dow, Y.-P. Wang, and T.-J. Huang,J.Catal.,(1996).160(2):p. 155-170.
162. A. M. Turek, I. E. Wachs, and E. DeCanio, J.Phys. Chem.,(1992).96(12):p. 5000-5007.
163. H. Knözinger and P. Ratnasamy,Catal.Rev.,(1978).17(1):p. 31-70.
164. M. Trueba and S. P. Trasatti,Eur.J.Inorg.Chem.,(2005).2005(17):p. 3393-3403.
165. H. A. Al-Abadleh and V. H. Grassian,Langmuir,(2002).19(2):p. 341-347.
166. C. Mo, Z. Yuan, L. Zhang, and C. Xie,Nanostructured Materials,(1993).2(1):p. 47-54.
167. S. Ramesh, E. Sominska, B. Cina, R. Chaim, and A. Gedanken,J.Am.Ceramic Soc.,(2000).83(1):p. 89-94.
168. H.-K. Wang, C.-Y. Yi, L. Tian, W.-J. Wang, J. Fang, J.-H. Zhao, and W.-G. Shen,J.Nanomater.,(2011).2012:p. 1-8.
169. M.-F. Luo, P. Fang, M. He, and Y.-L. Xie,J.Mol.Catal.A: Chem.,(2005).239(1–2):p. 243-248.
170. L. Kundakovic and M. Flytzani-Stephanopoulos,App.Catal.A: Gen.(1998).171(1):p. 13-29.
171. R. M. Friedman, J. J. Freeman, and F. W. Lytle,J.Catal.,(1978).55(1):p. 10-28.
172. B. Aysİn.*Photocatalytic properties of silver loaded titanium dioxide powders produced by mechanical ball milling,*Middle East Technical University,M.Sc,p.29-37
173. X. Wang, S. Li, H. Yu, J. Yu, and S. Liu,Chemistry – A Eur.J.,(2011).17(28):p. 7777-7780.
174. K. Page, R. G. Palgrave, I. P. Parkin, M. Wilson, S. L. P. Savin, and A. V. Chadwick,J.Mater. Chem.,(2007).17(1):p. 95-104.
175. M. N. H. Hamed,J.App.Sci.Research,(2010).6(8):p. 1247-1264.
176. A. Alouche,Jordan J.Mech. Ind.Eng.,(2008).
177. G. V. Smith and F. Notheisz, *Heterogeneous catalysis in organic chemistry*. 1999, United States of America: Elsevier Science.
178. D. P. VanderWiel, M. Pruski, and T. S. King,J.Catal.,(1999).188(1):p. 186-202.
179. K. Nakai and K. Nakamura, *Pulse chemisorption measurement: Metal dispersion measurement*, 2003. p. 1-4.
180. M. A. Nygren and P. E. M. Siebahn,J. Phys. Chem,(1992).96:p. 7579-7584.
181. G. H. Guvelioglu, P. Ma, X. He, R. C. Forrey, and H. Cheng,Phys Rev Lett,(2005).94(2):p. 026103.
182. R. C. Forrey,Physi.Rev.B,(2006).73(15):p. 1-9.
183. A. Dandekar and M. A. Vannice,App. Catal. B: Environ.,(1999).22(3):p. 179-200.
184. A. Dandekar and M. A. Vannice,J.Catal.,(1998).178(2):p. 621-639.

185. R. Knapp, S. A. Wyrzgol, A. Jentys, and J. A. Lercher,Journal of Catalysis,(2010).276(2):p. 280-291.
186. J. Ma, C. Park, N. M. Rodriguez, and R. T. K. Baker,The Journal of Physical Chemistry B,(2001).105(48):p. 11994-12002.
187. A. Yin, X. Guo, W.-L. Dai, and K. Fan,The Journal of Physical Chemistry C,(2009).113(25):p. 11003-11013.
188. M. Fadoni and L. Lucarelli,Studies in Surface Science and Catalysis,(1999).120-A:p. 177-225.
189. J. L. Contreras and G. A. Fuentes,ChemInform,(2013).44(41):p. no-no.
190. G. J. Hutchings, F. King, I. P. Okoye, M. B. Padley, and C. H. Rochester,Journal of Catalysis,(1994).148(2):p. 464-469.
191. G. J. Hutchings, F. King, I. P. Okoye, and C. H. Rochester,Applied Catalysis A: General,(1992).83(2):p. L7-L13.
192. J. Czaplinska, I. Sobczak, and M. Ziolek,The Journal of Physical Chemistry C,(2014).118(24):p. 12796-12810.
193. D. A. King, *The chemical physics of solid surfaces*. 1993, The Netherlands: Elsevier Science.
194. C.-F. Mao and M. A. s. Vannice,Applied Catalysis A: General,(1994).111(2):p. 151-173.
195. S. Maity, O. O. James, B. Chowdury, and A. Auroux,Current Science,(2014).106(11):p. 1538-1548.
196. A. Rachel, V. D. Kumari, R. Subramanian, K. V. R. Chary, and P. K. Rao,Indian Journal of Chemistry,(2004).43A:p. 1172-1180.
197. Chetty. T.*'Coinage metals" for the preferential hydrogenation of octanal in a mixture of octene,*University of KwaZulu-Natal,Durban, South Africa,Ph.D p.1-110
198. C. Liang, X. Li, Z. Qu, M. Tade, and S. Liu,Applied Surface Science,(2012).258(8):p. 3738-3743.
199. G. A. El-Shobaky, G. A. Fagal, and N. H. Amin,Thermochimica Acta,(1989).141(0):p. 205-216.
200. Z. H. Zhu, H. Y. Zhu, S. B. Wang, and M. G. Lu,Catalysis Letters,(2003).91(1-2):p. 73-81.
201. E. Garbowski and M. Primet,Journal of the Chemical Society, Chemical Communications,(1991)(1):p. 11-12.
202. G. Kiss, E. J. Mozeleski, K. C. Nadler, E. Van Driessche, and C. De Roover,Journal of Molecular Catalysis A: Chemical,(1999).138(2–3):p. 155-176.
203. P. G. Menon and J. Prasad,Journal of Catalysis,(1970).17(2):p. 238-244.
204. H. Kusama, K. K. Bando, K. Okabe, and H. Arakawa,Applied Catalysis A: General,(2000).197(2):p. 255-268.
205. B. Zhang, S. Hui, S. Zhang, Y. Ji, W. Li, and D. Fang,Journal of Natural Gas Chemistry,(2012).21(5):p. 563-570.
206. K. Zhang, F. Li , H. Zhang, M. Hongfang, W. Ying, and D. Fang,World Academy of Science, Engineering and Technology,(2013).76(International Science Index):p. 486-490.
207. N. M. Bertero, C. R. Apesteguía, and A. J. Marchi,Applied Catalysis A: General,(2008).349(1–2):p. 100-109.
208. E. Sayah, D. Brouri, Y. Wu, A. Musi, P. Da Costa, and P. Massiani,Applied Catalysis A: General,(2011).406(1–2):p. 94-101.
209. M. H. Yamukyan, K. V. Manukyan, and S. L. Kharatyan,Journal of Alloys and Compounds,(2009).473(1–2):p. 546-549.
210. B. R. Strohmeier, D. E. Levden, R. S. Field, and D. M. Hercules,Journal of Catalysis,(1985).94(2):p. 514-530.
211. M. Lo Jacono, A. Cimino, and M. Inversi,Journal of Catalysis,(1982).76(2):p. 320-332.
212. L. E. Murillo.*Controlling hydrogenation activity and selectivity of bimetallic surfaces and catalysts,*University of Delaware,Ann Arbor,PhD,p.1-212
213. Y. Shu, L. E. Murillo, J. P. Bosco, W. Huang, A. I. Frenkel, and J. G. Chen,Applied Catalysis A: General,(2008).339(2):p. 169-179.

214. J. Yan, M. C. Kung, W. M. H. Sachtler, and H. H. Kung,Journal of Catalysis,(1997).172(1):p. 178-186.
215. J. Y. Yan, H. H. Kung, W. M. H. Sachtler, and M. C. Kung,Journal of Catalysis,(1998).175(2):p. 294-301.
216. V. Gutierrez, M. Alvarez, and M. A. Volpe,Applied Catalysis A: General,(2012).413–414(0):p. 358-365.
217. I. Huerta, J. García-Serna, and M. J. Cocero,The Journal of Supercritical Fluids,(2013).74(0):p. 80-88.
218. J. Zhang, X.-Z. Sun, M. Poliakoff, and M. W. George,Journal of Organometallic Chemistry,(2003).678(1–2):p. 128-133.

Appendix

1. Infrared Spectroscopy

1.1. Fresh catalysts

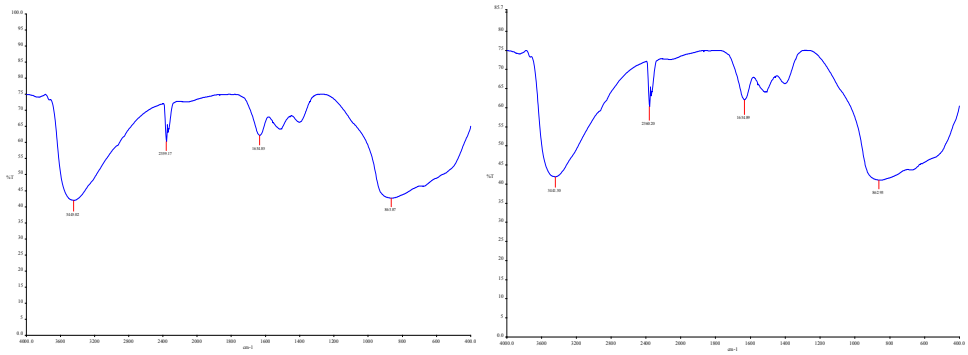

Figure A1. IR spectra of γ-Al_2O_3 supported (a) 15Cu and (b) 13.5Cu1.5Ag catalysts.

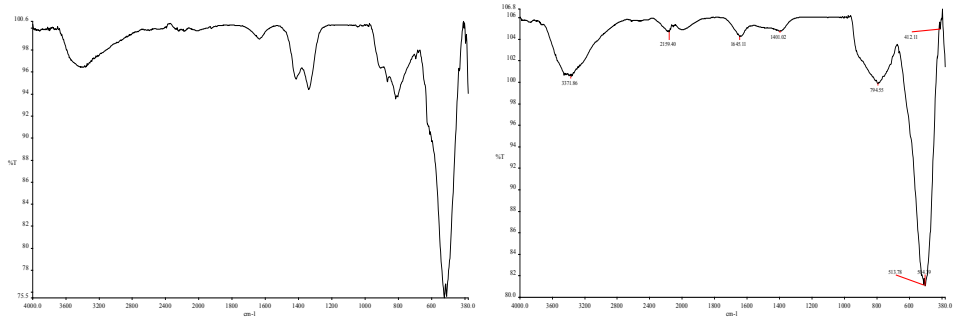

Figure A2. IR spectra of γ-Al_2O_3 supported (a) 4.5Cu0.5Ag and (b) 4Cu1Ag catalysts.

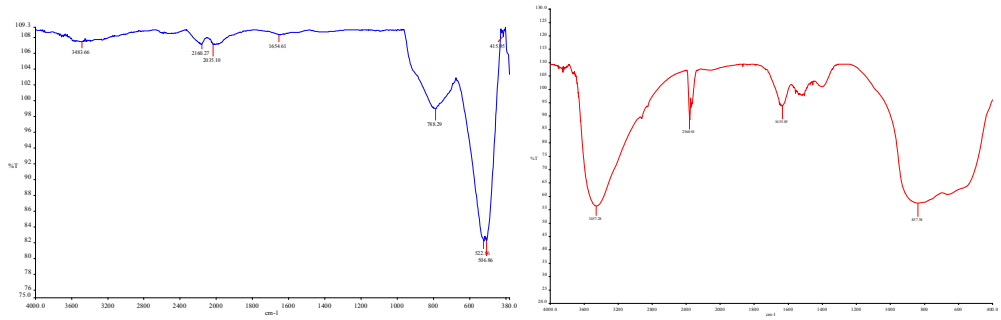

Figure A3. IR spectra of γ-Al_2O_3 supported (a) S-4.5Cu0.5Ag and (b) S-0.5Ag4.5Cu catalysts.

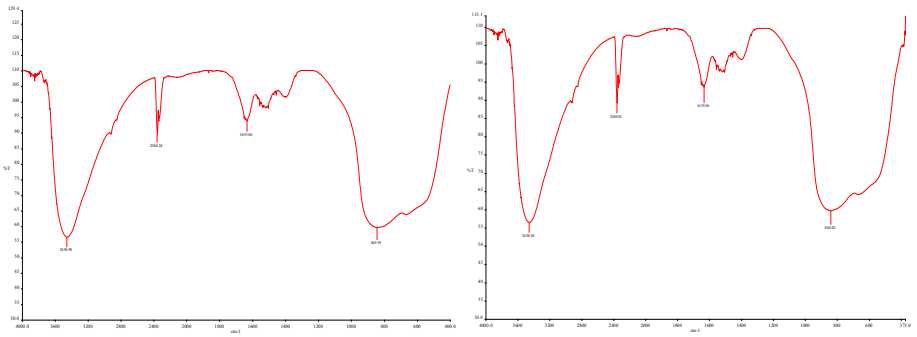

Figure A4. IR spectra of γ-Al_2O_3 supported (a) S-4Cu1Ag and (b) S-1Ag4Cu catalysts.

1.2. Used Catalysts

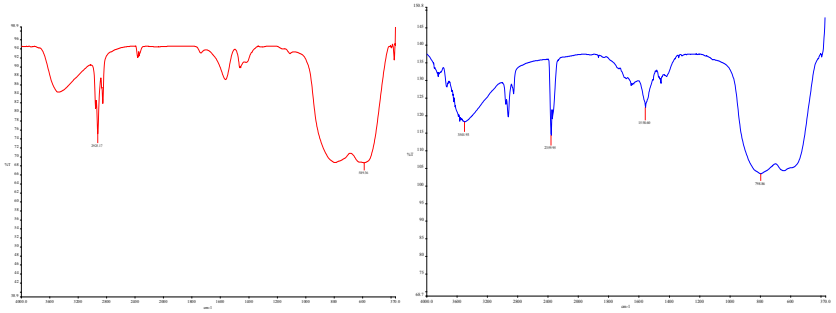

Figure A5. IR spectra of γ-Al_2O_3 supported (a) 5Cu/γ-Al_2O_3 -220 and (b) 5Cu/γ-Al_2O_3 -240 catalysts.

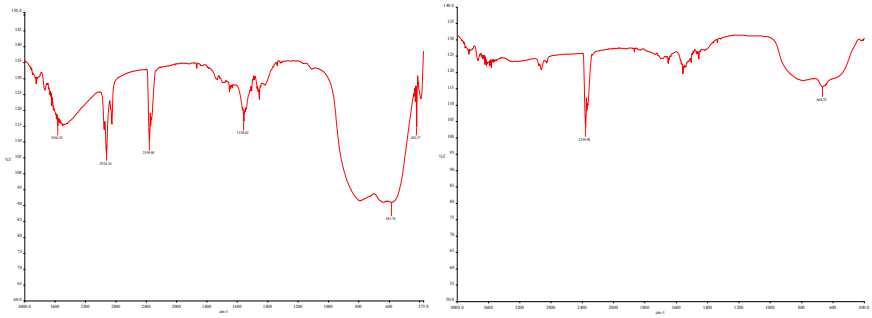

Figure A6. IR spectra of γ-Al_2O_3 supported (a) 5Cu/γ-Al_2O_3 -260 and (b) 15Cu/γ-Al_2O_3 catalysts.

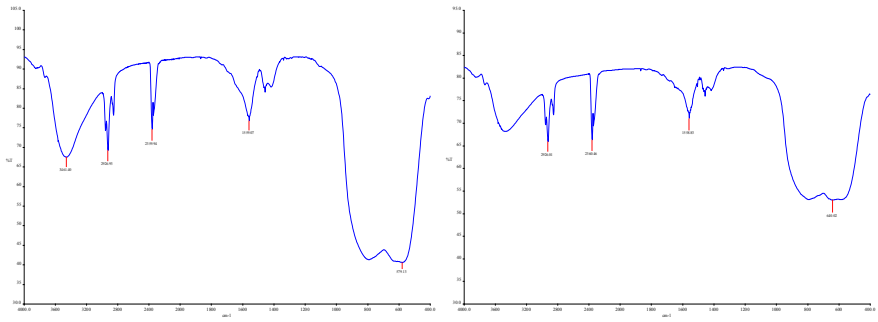

Figure A7. IR spectra of γ-Al_2O_3 supported (a) 4.5Cu0.5Ag-220 and (b) 4Cu1Ag-220 catalysts.

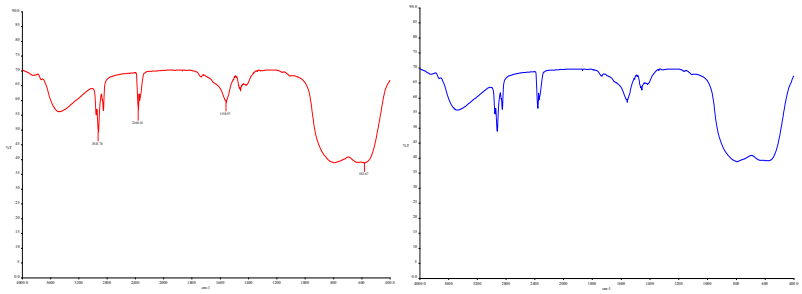

Figure A8. IR spectra of γ-Al_2O_3 supported (a) S-4.5Cu0.5Ag and (b) S-0.5Ag4.5Cu catalysts.

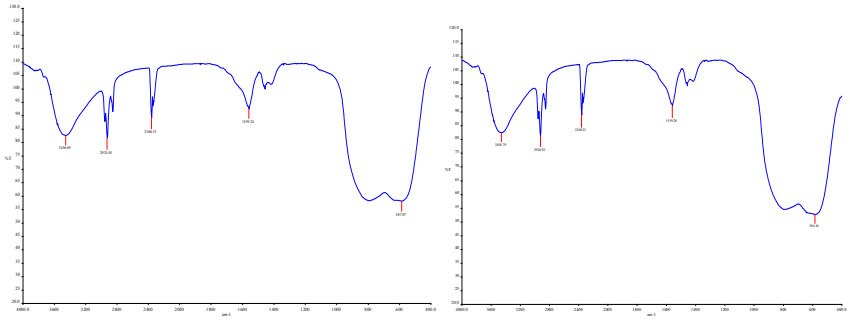

Figure A9. IR spectra of γ-Al_2O_3 supported (a) S-4Cu1Ag and (b) S-1Ag4Cu catalysts.

2. Scanning electron microscopy (SEM)

15Cu/ γ-Al_2O_3

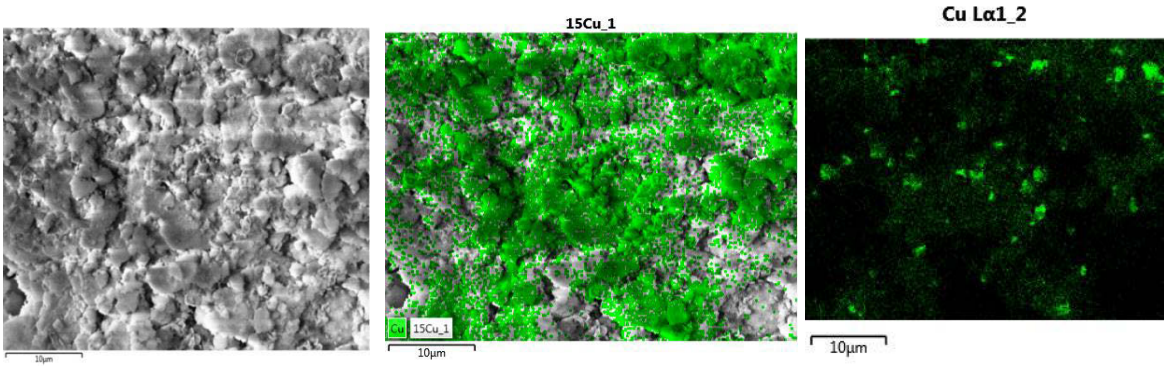

Figure A10. Images for15Cu/ γ-Al_2O_3 (a) SEM, (b) SEM-EDX mapping with copper (green), and (c) copper only map (green).

3. GC spectrum

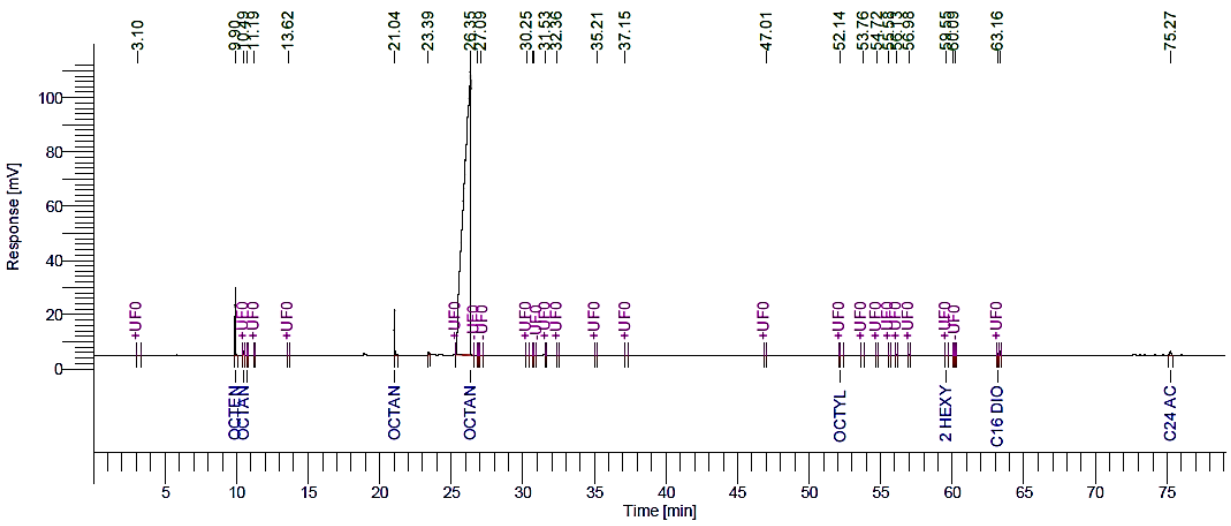

Figure A11. Example of a GC chromatogram of the products obtained.

4. GC-MS for the main reactants and products

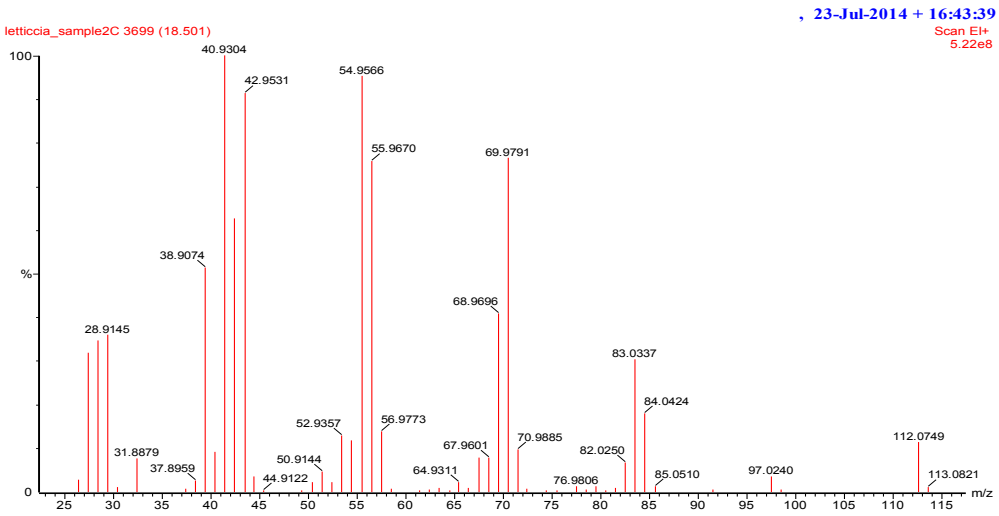

Figure A12. GC-MS spectrum of octene.

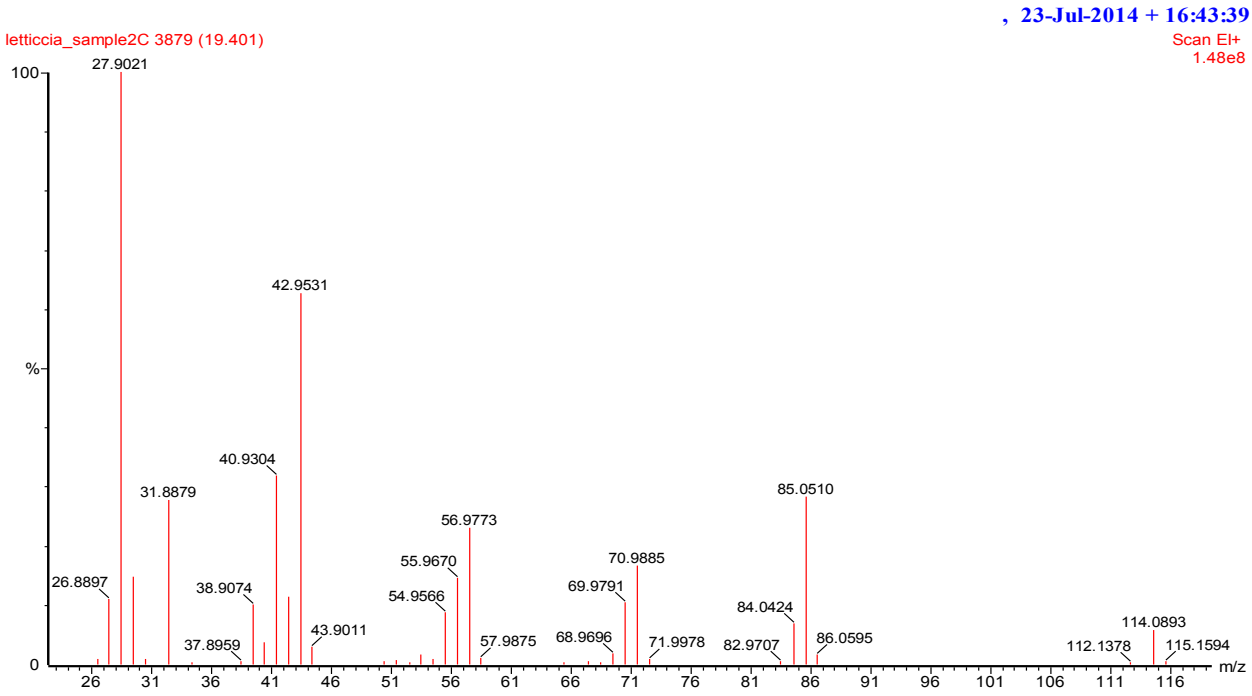

Figure A13. GC-MS spectrum of octane.

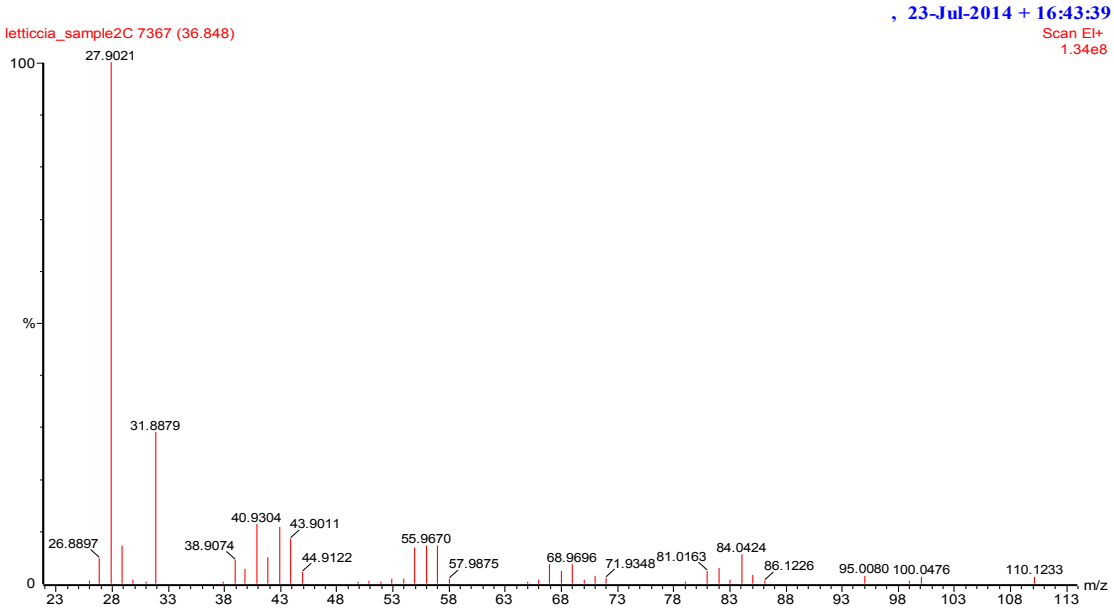

Figure A14. GC-MS spectrum of octanal.

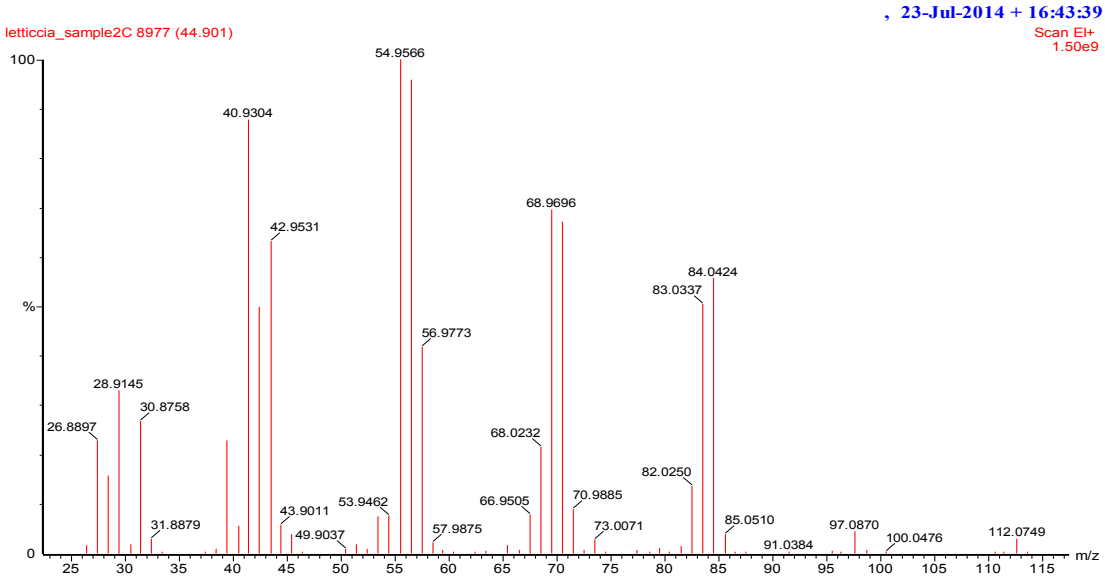

Figure A15. GC-MS spectrum of octanol.

5. GC-MS for selected byproducts

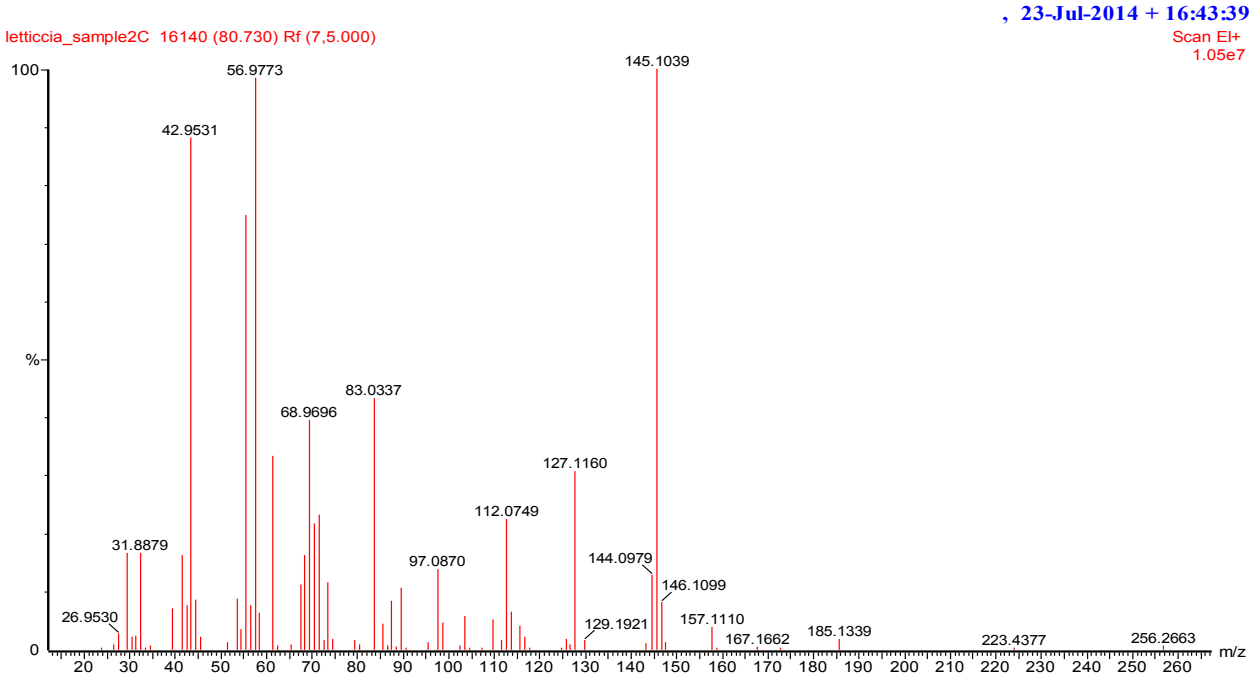

Figure A16. GC-MS spectrum of Octyl octanoate.

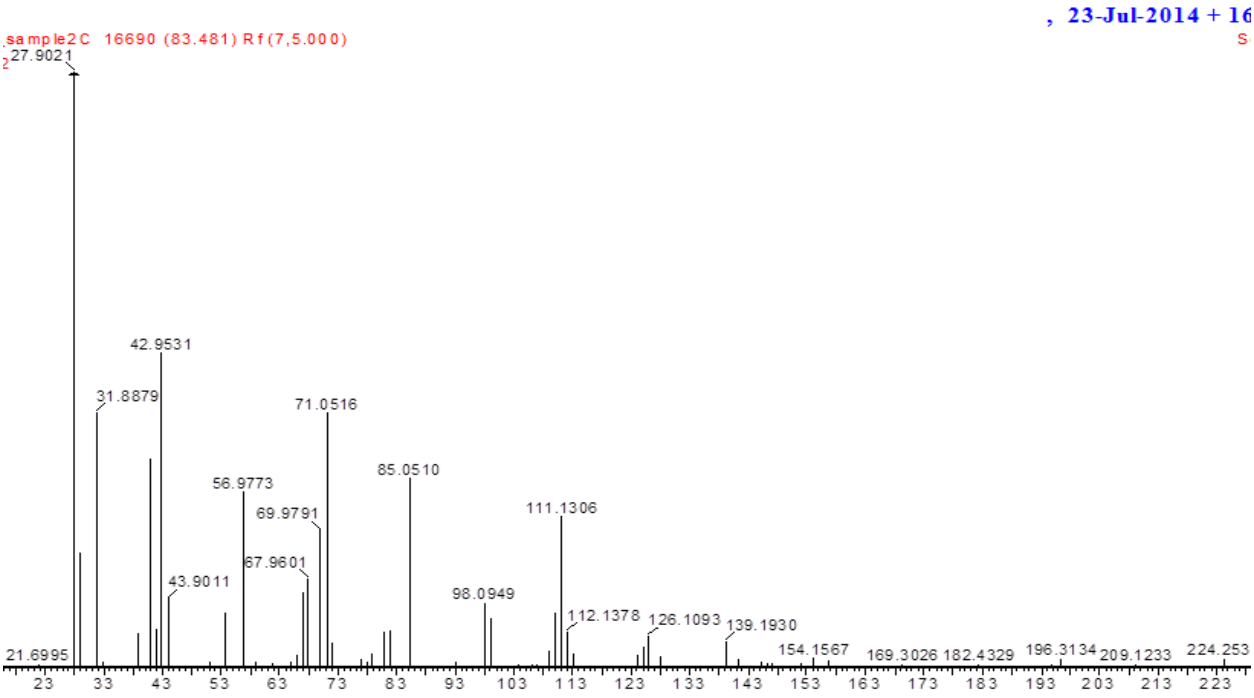

Figure A17. GC-MS spectrum of C16 diol.

6. Reactor set up

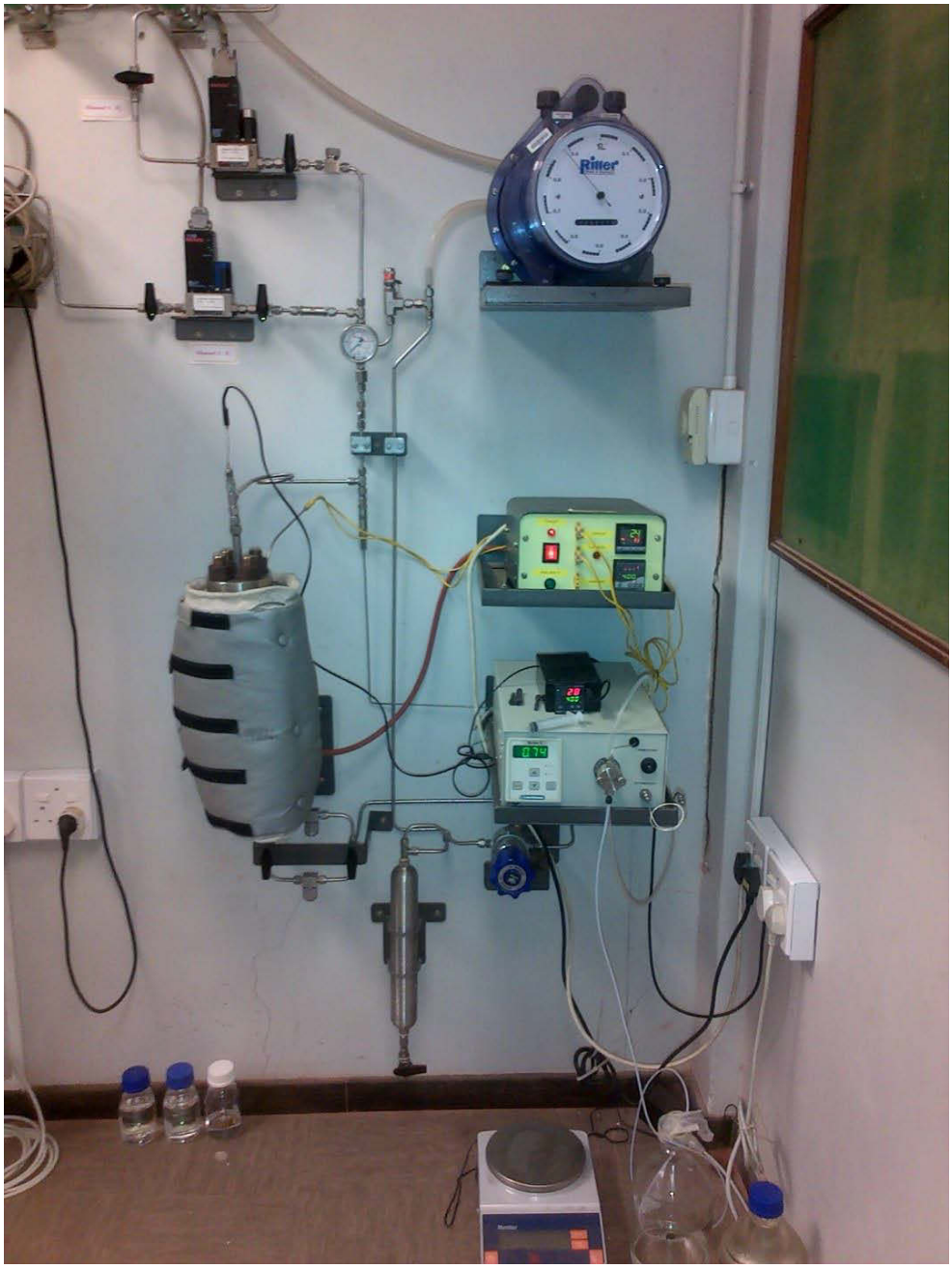

Figure A**18**. Image of the reactor.